Gamma ray astronomy and the origin of galactic cosmic rays

Stefano Gabici

GAMMA RAY ASTRONOMY AND THE ORIGIN OF GALACTIC COSMIC RAYS

STEFANO GABICI

Laboratoire AstroParticule et Cosmologie (APC) – Paris, France

---

Habilitation à diriger des recherches presentée à l'Université Paris 7 – Denis Diderot

Soutenue le 30 Juin 2011 devant le jury composé par:

Pierre Binetruy – President

Catherine Cesarsky – Rapporteur

Angela Olinto – Rapporteur

Catherine Boisson – Rapporteur (interne)

Fiorenza Donato – Examinateur

Etienne Parizot – Examinateur

Elisa Resconi – Examinateur

Contents

Acknowledgements

I have learned how to do research from Felix Aharonian, Pasquale Blasi, and Gianfranco Brunetti, so the first *thank you* is for them.

I would like to thank the members of the jury of this HDR: Pierre Binetruy, Catherine Boisson, Catherine Cesarsky, Fiorenza Donato, Angela Olinto, Etienne Parizot, and Elisa Resconi.

Most of the work presented here has been carried out in collaboration with many colleagues. Many thanks in particular to Sabrina Casanova and Giulia Vannoni for a day-to-day collaboration over many years and then thanks to (alphabetical!): Elena Amato, Don Ellison, Yasuo Fukui, Stanislav Kelner, Denis Malyshev, Gavin Rowell, Andrew Taylor, and Richard White.

Thanks to Alexandre Marcowith, Vladimir Ptuskin, and Pierre Cristofari with whom I am collaborating at the moment.

It is a pleasure to thank the colleagues I had the occasion to meet and with whom I had many enlightening discussions over the past years. The list includes (but it is for sure incomplete ...): Paolo Coppi, Luigi Costamante, Eveline Helder, Tom Jones, Dmitry Khangulyan, Kumiko Kotera, Thierry Montmerle, Olaf Reimer, Vincent Tatischeff, Regis Terrier, Jacco Vink, Malcolm Walmsley, Vladimir Zirakashvili.

Thanks to Denis Allard and Veronique Van Elewyck for their comments on some of the chapters of this thesis.

And then thanks to (in strict chronological order): Istituto di Radioastronomia di Bologna (in particular G. Setti and L. Feretti), Dipartimento di Astronomia e Scienza dello Spazio dell'Università di Firenze, Osservatorio Astrofisico di Arcetri (in particular Franco Pacini), Alexander von Humboldt Foundation (in particular Sven Baszio), Max-Planck-Institut für Kernphysik (in particular Heinz Völk), the European Commission, Dublin Institute for Advanced Studies (in particular Luke Drury), and Laboratoire APC for paying me a salary and/or hosting and supporting me during all these years.

Finally, thanks to my father Franco to whom this work is dedicated.

Abstract

Diffusive shock acceleration operating at expanding supernova remnant shells is by far the most popular model for the origin of galactic cosmic rays. Despite the general consensus received by the model, an unambiguous and conclusive proof of the supernova remnant hypothesis is still missing. In this context, the recent developments in gamma ray astronomy provide us with precious insights into the problem of the origin of galactic cosmic rays, since production of gamma rays is expected both during the acceleration of cosmic rays at supernova remnant shocks and during their subsequent propagation in the interstellar medium. In particular, the recent detection of a number of supernova remnants at TeV energies nicely fits with the model, but it still does not constitute a conclusive proof of it, mainly due to the difficulty of disentangling the hadronic and leptonic contributions to the observed gamma ray emission. The main goal of my research is to search for an unambiguous and conclusive observational test for proving (or disproving) the idea that supernova remnants are the sources of galactic cosmic rays with energies up to (at least) the cosmic-ray-knee ($\sim 4 \times 10^{15}$eV). Our present comprehension of the mechanisms of particle acceleration at shocks and of the propagation of cosmic rays in turbulent magnetic fields encourages beliefs that such a conclusive test might come from future observations of supernova remnants and of the Galaxy in the almost unexplored domain of multi-TeV gamma rays.

Chapter 1

Introduction

Cosmic rays (CRs) are relativistic particles (mainly protons, but also heavier nuclei and electrons) that reach the Earth with the same intensity from any direction in the sky. Since their discovery by Victor Hess in 1912, cosmic rays have been studied by means of constantly improving direct and indirect detection techniques (see e.g. Berezinskii et al. 1990; Gaisser 1990). Despite exciting experimental results and extensive theoretical efforts over the past decades, the origin of these particles is still debated. The problem is that, unlike photons, CRs are deflected and isotropized by the galactic magnetic field and thus their arrival direction does not point back to the actual position of their accelerators (e.g. Wentzel 1974; Cesarsky 1980; Strong et al. 2007). Revealing the mystery of their origin is of fundamental importance, since CRs can provide unique information about the physical conditions of the extreme astrophysical objects in which they are likely to be accelerated. Moreover, the energy density of CRs, largely dominated by the hadronic component, is comparable with the pressure of the galactic magnetic field as well as to that of the interstellar medium. This makes CRs an essential ingredient for studies of the dynamical balance of the Galaxy (e.g. Parker 1969). Finally, CRs also play a key role in the process of star formation, since they are the dominant source of ionization and heating in dense proto-stellar regions, where ionizing radiation cannot penetrate (e.g. Stahler & Palla 2005; Padovani et al. 2009).

The belief that one single class of sources is responsible for the acceleration of the bulk of the CRs is suggested by the fact that the observed CR spectrum is almost featureless. It is in fact a single power law in energy with slope $\propto E^{-2.7}$ until a particle energy of ≈ 4 PeV, where the spectrum slightly steepens to $\propto E^{-3}$. This feature is called the CR *knee* and candidate CR sources are required to accelerate particles *at least* until this energy [1] (Berezinskii et al. 1990; Gaisser 1990).

Diffusive shock acceleration operating at expanding supernova remnant (SNR) shells is by far the most popular model for the origin of galactic CRs (see Hillas 2005, for a recent review). However, despite the general consensus received by the

[1] The existence of such a class of sources is of course not guaranteed, but seems likely given that fitting a featureless power law by adding the contributions from different classes of sources would probably require excessive fine tuning.

model, an unambiguous and conclusive proof of the SNR hypothesis is still missing. The main (but, still, not conclusive) arguments supporting this idea are the fact that SNRs can provide the total power required to maintain the galactic CR population, and the belief that an efficient acceleration mechanism, diffusive shock acceleration, operates in these objects (Krymskii 1977; Axford et al. 1977; Bell 1978; Blandford & Ostriker 1978). The detection of some SNRs in TeV gamma rays (Aharonian et al. 2008b), expected if they indeed are the sources of CRs (Drury et al. 1994), also supports this scenario, though the emission might have a leptonic origin (namely, inverse Compton scattering) and not be related to the acceleration of the bulk of CRs (e.g. Ellison et al. 2010).

In this thesis, the connections between gamma ray astronomy and CR physics will be investigated, within the framework of the SNR hypothesis for CR origin. In particular, it will be shown how future observations in the gamma ray domain of SNRs and of dense molecular clouds (MCs) located in their vicinity might contribute in solving the problem of CR origin (Gabici et al. 2009; Gabici 2010). Remarkably, observations in the currently almost unexplored domain of multi-TeV gamma rays (up to ~ 100 TeV) might provide us with a conclusive test for the validity of the SNR hypothesis (Gabici & Aharonian 2007b; Gabici 2008). This is because in this energy range, unlike at TeV energies, there is no ambiguity in the interpretation of the emission. In fact, due to the Klein-Nishina effect, the efficiency of inverse Compton scattering in the 100 TeV region is dramatically reduced, leaving as the only viable interpretation the hadronic emission of CRs with energies in the PeV range. Thus, detecting SNRs in gamma rays with a spectrum extending up to ~ 100 TeV without significant attenuation, would unambiguously tell us that these objects can indeed accelerate CRs up to the energies of the knee.

This energy region will be probed in the near future by the Cherenkov Telescope Array (www.cta-observatory.org).

1.1 A very brief overview of observational facts on cosmic rays

The energy density of CRs measured at Earth is ≈ 1 eV/cm^3 (e.g. Berezinskii et al. 1990). As said above, this energy density is comparable to the energy density of thermal gas and magnetic field in the Galaxy. Such energy equipartition might not be a mere coincidence, but indicate some kind of coupling between thermal and non-thermal constituents of the Galaxy (Parker 1969). Remarkably, also the energy density of the radiation field in the Galaxy is comparable to the CR energy density, though in this case a direct connection between the two quantities might be less obvious. The steepness of the CR spectrum (see Fig. 1.1 and discussion below) implies that $\sim$ GeV particles carry the bulk of the CR energy.

Another crucial piece of information comes from spallation measurements of CRs. These measurements tell us that CRs with an energy of $\sim 1-10$ GeV remain confined about ten million years in the Galaxy, and that this confinement time decreases as the energy of the particles increases (e.g. Berezinskii et al. 1990; Gaisser 1990). Since

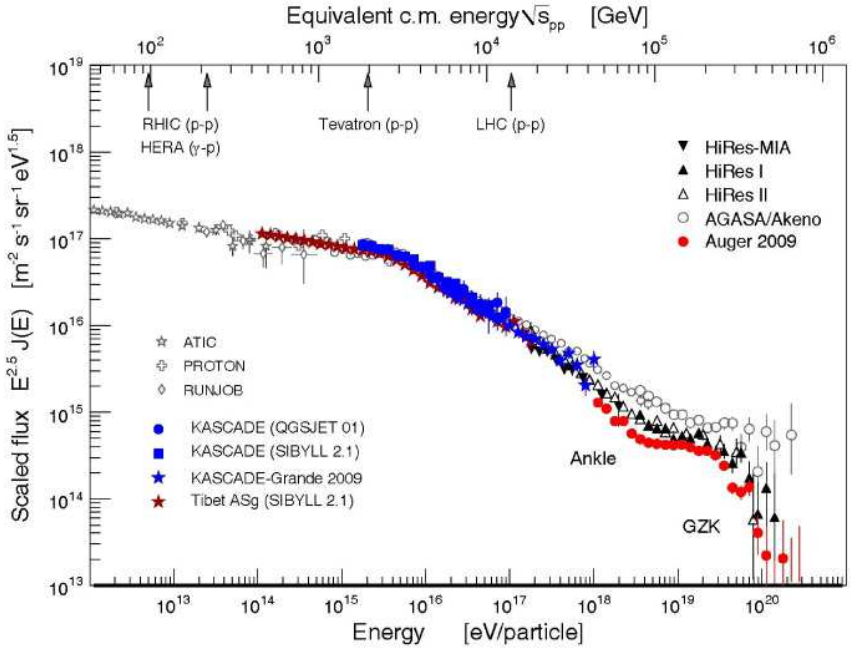

Figure 1.1: The observed cosmic ray spectrum (figure from Matthiae 2010). The *knee* is clearly visible at an energy of $E \approx 4 \times 10^{15}$eV.

the confinement time is orders of magnitude longer than the light crossing time of the Galaxy, we can infer that CRs must follow non-rectilinear paths while travelling through the interstellar medium. This diffusive behaviour of CRs is the result of their propagation in the turbulent magnetic field of the Galaxy, which provides the strong source of scattering required both to confine CRs and to explain their isotropy in the sky. Moreover, the fact that the escape time from the Galaxy is energy dependent tells us that the CR spectrum that we observe at the Earth (proportional to $E^{-2.7}$) must be steeper than the spectrum that CR sources, whichever they are, inject in the interstellar medium. In order to be consistent with observations, CR sources need to inject a spectrum which is close to (slightly steeper than) E^{-2} (e.g. Strong & Moskalenko 1998; Maurin et al. 2001; Ptuskin et al. 2010).

The third crucial observational fact is the almost total absence of features in the observed CR spectrum up to $\sim$ PeV energies, see Fig. 1.1. The spectrum extends up to extremely high energies ($\approx 10^{20}$eV) and can be described as a pure power law in energy ($\propto E^{-2.7}$) up to $E \sim 4$ PeV (1 PeV $= 10^{15}$eV). At this energy, the spectrum slightly steepens (to E^{-3}), originating the feature called *knee*. Below the knee the CR chemical composition is strongly dominated by protons, while at higher energies the contribution from heavier elements becomes relevant (Berezinskii et al. 1990; Gaisser 1990). The absence of features in the spectrum suggests that a single class of galactic sources is likely to be responsible for the whole observed CRs at least up to the energies of the knee (for protons), and probably well above it (for heavier nuclei). In other words, the sources of galactic CRs must be able to

accelerate protons up to at least several PeVs, and thus to act as CR PeVatrons.

Conversely, the highest energy end of the spectrum ($E \gtrsim 4 \times 10^{17}$ or 10^{19}eV [2]) is believed to have an extragalactic origin, since particles with such extreme energies cannot be easily confined within the Galaxy. This thesis is focused onto the galactic part of the spectrum, with the exception of Chapter 8 which is devoted to the extragalactic component.

Summarizing, a good theory for the origin of *galactic* CRs must explain the following facts:

1. the CR intensity in the Galaxy;
2. the observed spectrum of CRs and their isotropy in the sky;
3. the fact that the galactic component must extend at least up to the knee (for protons) and most likely above it (for heavier nuclei).

Remarkably, point 2 tells us that, in order to solve the problem of CR origin, we have to study not only the nature of the sources and of particle acceleration mechanisms, but also the way in which CRs propagate from the sources to us.

1.2 The supernova remnant paradigm for cosmic ray origin and its connection with gamma ray astronomy

In 1934, Baade and Zwicky first proposed that supernovae are the sources of galactic CRs (Baade & Zwicky 1934). To support their idea, they used a simple argument: the observed CR population can be maintained at the present level if a small fraction (some 10%) of the galactic supernovae kinetic energy is somehow converted into CRs. This argument is strengthened by the fact that it is commonly believed that CRs can be efficiently accelerated via Fermi mechanism at shock waves that form during the expansion of supernova remnants (SNRs) in the interstellar medium (see Drury 1983; Blandford & Eichler 1987; Jones & Ellison 1991; Malkov & O'C Drury 2001, for reviews).

In order to be proven (or disproven), the SNR hypothesis for the origin of CRs needs to confront observational tests. A natural connection exists between CR studies and gamma ray astronomy, since gamma rays are produced in hadronic interactions between CRs and the interstellar medium. In this context, a fundamental test has been proposed in 1994 by Drury, Aharonian, and Voelk. The rationale of their approach was the following: from the (measured) CR power of the Galaxy and from the (measured) supernova rate in the Galaxy, it is possible to infer what is the typical fraction of energy that each SNR has to convert into CRs in order to sustain the CR intensity at the observed level. This can be done because the total

[2] These are the positions of the features in the CR spectrum called *second knee* and *ankle*, respectively. Whether the extragalactic component becomes dominant above the former or the latter feature is still a matter of debate (see Allard et al. 2007; Aloisio et al. 2008, for details).

energy released in each supernova explosion is remarkably close to a constant value of $\sim 10^{51}$ erg. This fraction happens to be rougly $\approx 10\%$. Then, from the knowledge of the average density of the interstellar medium ($\approx 0.1 - 1$ cm^{-3}), one can compute the average gamma ray luminosity of individual SNRs due to proton-proton interactions of CRs in the interstellar gas. The gamma ray fluxes estimated in this way fall within the capabilities of currently operating Cherenkov telescopes (such as *H.E.S.S.*, *VERITAS*, and *MAGIC*).

To date, several SNRs have been detected at TeV energies by the major currently operating Cherenkov telescopes (e.g. Aharonian et al. 2004, 2008b; Hinton & Hofmann 2009), whose flux level matches very well the above mentioned predictions. Though these results undoubtedly constitute one of the most important advancements in the field, they still do not provide us with a definite and direct evidence of proton acceleration at SNRs. In fact, competing leptonic processes can also explain the observed TeV gamma ray emission, provided that the average magnetic field does not exceed ≈ 10 μG (e.g. Ellison et al. 2010), and thus accurate modeling is needed in order to disentangle the different contributions.

1.2.1 Hadronic or leptonic?

The question about the hadronic or leptonic nature of the TeV emission from SNRs constitutes one of the most discussed issues in gamma ray astronomy. If, from the one side, hadronic TeV gamma rays are expected if SNRs are the sources of galactic CRs, it is also true that most of the SNRs are sources of non-thermal X-rays, commonly interpreted as synchrotron radiation from multi-TeV electrons (see e.g. Koyama et al. 1995; Reynolds 2008). Such electrons can also emit TeV gamma rays via inverse Compton scattering off photons of the cosmic microwave background, thus providing a competing emission process that might explain the observed TeV fluxes. If the magnetic field at the SNR is significantly stronger than ≈ 10 μG, then the observed synchrotron X-rays can be explained by a relatively meagre number of electrons, which would produce unappreciable TeV inverse Compton emission. Conversely, if the value of the magnetic field is ≈ 10 μG the electrons needed to explain the X-ray emission will also suffice to explain the whole observed TeV emission, thus implying inefficient (or at least less efficient) acceleration of CR protons. Thus, the value of the magnetic field at the shock is a crucial parameter of the problem, and its determination would allow us to unveil the nature of the gamma ray emission.

The observation of thin (down to a few arcseconds scale) synchrotron X-ray filaments surrounding a number of SNRs has been interpreted as an evidence for the presence of a strong (≈ 100 μG or more) magnetic field at the shock (see e.g. Bamba et al. 2003; Vink & Laming 2003). According to this interpretation, the formation of such filaments is due to the fact that, in such a strong magnetic field, the synchrotron cooling time of X-ray emitting electrons is very short. Thus electrons radiate X-ray synchrotron photons before being significantly advected or diffuse away downstream of the shock (e.g. Völk et al. 2005; Ellison & Cassam-Chenaï 2005; Parizot et al. 2006; Morlino et al. 2010). The value of the magnetic field is estimated by comparing the observed width of the filament with the expected one, which is roughly $\approx \sqrt{k_d \tau_d}$,

where k_d and τ_d are the diffusion coefficient and synchrotron loss time of the emitting electrons, both quantities depending on the value of the magnetic field (e.g. Berezhko et al. 2003). The derived value of the magnetic field relies on the (plausible, but not at all proven[3]) assumption that diffusion is proceeding at the Bohm rate.

The presence of a high magnetic field at the shock indirectly supports the hadronic origin of the TeV emission for two main reasons. First, according to theoretical studies, magnetic field amplification due to non-resonant CR driven instability is expected to take place at shocks which are accelerating efficiently CR protons (Bell 2004). The predicted value of the amplified field is compatible with the values inferred from X-ray observations and it is also the value needed to allow acceleration to proceed up to the energy of the CR knee or even above (Bell 2004). This fact solves the old standing issue, first pointed out by Lagage & Cesarsky (1983b), of the effective capability of SNRs to accelerate particles up to the PeV energy range. Second, as said above, if the magnetic field is stronger than ~ 10 μG the inverse Compton scattering contribution to the TeV emission is negligible, leaving the hadronic channel as the only viable mechanism for gamma ray production.

However, a high value of the magnetic field is not the only possible interpretation for the observed narrow X-ray synchrotron filaments. Filaments can also be formed due to damping of magnetic turbulence downstream of the shock (Pohl et al. 2005). In this scenario, though magnetic field amplification can still operate at the shock, the width of filaments can not be used to estimate the value of the magnetic field, instead it simply reflects the spatial structure of the magnetic field. An important difference between the magnetically limited filaments and the energy loss limited filaments is that in the former case filamentary structures, though broader and of less amplitude, should be observed also at lower (e.g. radio) frequencies (Pohl et al. 2005), while in the latter case no filaments are expected at radio frequencies since low energy electrons are unaffected by synchrotron losses (Ellison & Cassam-Chenaï 2005; Cassam-Chenaï et al. 2005). In the case of the SNR SN 1006 the profile of the radio emission is quite broad, with only shallow bumps, when compared to the narrow peak in the X-ray emission (Rothenflug et al. 2004). However, an accurate comparison between observation and theory is needed in order to draw firm conclusions. Similarly, a comparison between the X-ray and radio morphology of the Tycho SNR has been attempted, but results still remain inconclusive (Cassam-Chenaï et al. 2007).

Further evidence for the presence of a strong magnetic field at SNR shocks comes from the recently discovered fast variability of synchrotron X-rays hot spots in the shell of RX J1713.7-3946 (Uchiyama et al. 2007) and Cas A (Uchiyama & Aharonian 2008). An extremely strong magnetic field of ≈ 1 mG has been inferred by comparing the decay time of the X-ray flux, of the order of a year, with the synchrotron cooling time. Though the estimate of the magnetic fields refers only to the sub-parsec scale hot spot regions which are seen to vary in X-rays, it suggests that significant

[3]Attempts to use X-ray data to derive the diffusion coefficient have been made (Parizot et al. 2006; Stage et al. 2006). However, such estimates are seriously affected by the uncertainty in the determination of supernova parameters such as the shock speed and the cutoff energy in the synchrotron spectra.

amplification of the field can possibly happen throughout the whole SNR shell [4].

Another way to discriminate between hadronic or leptonic origin of the TeV emission consists in comparing model predictions with the observed X-ray and TeV gamma ray spectra. While hadronic models based on predictions of non-linear shock acceleration theory generally fit quite satisfactorily both X-ray and gamma ray data (for RX J1713.7-3946 see e.g. Berezhko & Völk 2006; Morlino et al. 2009; Zirakashvili & Aharonian 2010), leptonic models seem to provide somewhat worse fits. High quality *SUZAKU* data have been obtained over two decades in energy ($\approx 0.5 \div 50$ keV) for the SNR RX J1713.7-3946 (Tanaka et al. 2008). Such data allow us to constrain the spectrum of the synchrotron emitting electrons with unprecedented accuracy and over a wide energy range. Remarkably, the resulting electron spectrum is very close to that expected from electrons accelerated via diffusive shock acceleration in presence of synchrotron losses (Zirakashvili & Aharonian 2007; Tanaka et al. 2008). The electron spectrum derived in this way can be used to calculate the TeV spectrum due to inverse Compton emission off photons of the cosmic microwave background and of the galactic optical and infrared background. Such an inverse Compton spectrum fails to fit the lowest energy part of the measured TeV spectrum. The fit can be improved only at the expense of enhancing the infrared background of a factor of $\approx 20 \div 100$ with respect to the adopted value or by adding a second electron component. Both these possibilities seems quite artificial and thus an hadronic origin of the TeV emission seems favored over the pure leptonic one based on spectral information only (Tanaka et al. 2008; Morlino et al. 2009). However, mixed models in which the TeV emission is produced in comparable amount by hadronic and leptonic interactions can also fit well the data (Zirakashvili & Aharonian 2010).

Finally, evidence for efficient CR acceleration can also be searched by means of observations of the thermal emission of SNRs. This is because if supernova remnants do accelerate efficiently cosmic rays, this is done at the expenses of gas heating. In other words, if a non negligible fraction of the supernova remnant kinetic energy is used to accelerate cosmic rays, there is less energy available to heat the gas and thus the thermal (as well as the dynamical) properties of SNRs are affected (e.g. Ellison 2000).

One effect of efficient CR acceleration is an increase of the shock compression factor (e.g. Malkov & O'C Drury 2001). In part this is due to the softer equation of state associated with relativistic particles, but the more significant reason is the need to constantly pump energy into particles near the maximum energy of the spectrum (see Drury et al. 2009, for a discussion and Chapter 2 for a description of shock acceleraiton). An higher compression factor would increase the density downstream of the shock and this would in turn make the contact discontinuity closer to the SNR forward shock with respect to the case of negligible particle acceleration. Evidence for this has been claimed for the Tycho (Warren et al. 2005) and the SN 1006 (Cassam-Chenaï et al. 2007) SNRs, which supports the idea that in these objects efficient CR acceleration occurs.

The other major effect of CR acceleration on the thermal properties of SNRs is a

[4] For a different interpretation see Bykov et al. (2008).

significant suppression of gas heating. As said above, if a significant fraction of the total SNR energy is channeled into relativistic particles, there is less energy that can be converted into gas heating. Remarkably, in the idealized case of extremely efficient ($\lesssim 100\%$) CR acceleration, the downstream shock temperature T_2 is suppressed so much to be simply reduced to a multiple of the upstream temperature[5]: $T_2 \approx 6 - 10 \times T_1$ (Drury et al. 2009). This clearly shows how this situation is radically different to the standard (i.e. no CR acceleration) picture for shock heating, where the downstream temperature is, for a strong shock, independent on the upstream one, but depends only on the shock speed v_s as:

$$kT_2 = \frac{3}{16} m_p v_s^2 \tag{1.1}$$

where k is the Boltzmann constant and m_p is the proton mass. It is important to remind here that the shock heating of the plasma is relevant for protons only (or, more generally, for ions), which carry the inertia of the flow. Electrons can be heated downstream of the shock via Coulomb collisions with hot ions, but the characteristic time scale of the process is much too long to establish electron-ions temperature equilibrium (Rakowski 2005; Malyshev et al. 2010). Other processes, possibly mediated by plasma waves, might heat electrons and facilitate the equipartition (e.g. Rakowski et al. 2008), but since the nature of such processes is uncertain, it is not possible to draw any firm conclusion. In summary, low electron temperatures are expected in SNRs which accelerate CRs, and this would substantially reduce the thermal X-ray emission, since the peak of the emission would be shifted towards the UV energy range (Dorfi & Bohringer 1993). This seems to fit with the fact that the SNRs which are most prominent in TeV gamma rays, such as for example RX J1713.7-3946 or Vela Junior do not exhibit X-ray thermal emission. Moreover, very low proton temperatures have been measured from thermal broadening of Hα optical lines from the SNRs RCW 86 (Helder et al. 2009) (also detected in TeV gamma rays) and SNR 0509-67.5 (Helder et al. 2010), which strongly supports the idea that these SNRs are currently accelerating CRs. However, the CR-induced suppression of the shock temperature would lead also to an enhancement of the line emission in the X-ray band, a fact which has been claimed to be in contradiction with the observations of RX J1713.7-3946 that do not show any line emission, thus indirectly supporting a leptonic origin for the TeV gamma ray emission (Ellison et al. 2010).

Summarizing, to date there is still no conclusive evidence for the fact that SNRs are, as a class of sources, responsible for the acceleration of galactic CRs. Further investigations and observational tests are thus required in order to finally solve this issue. The current developments of gamma ray astronomy both in the GeV and TeV energy range encourage beliefs that future observations in this domain of the electromagnetic spectrum might finally provide us with such conclusive evidence in favour or against the SNR hypothesis for CR origin.

[5]Indexes 1 and 2 refer to the upstream and downstream side of the shock, respectively.

1.2.2 The role of *Fermi* and of the Cherenkov Telescope Array

The *Fermi* gamma ray space telescope is currently surveying the sky in the GeV energy range with unprecedented sensitivity and angular resolution. The simultaneous operation of gamma ray detectors both from space (the above mentioned *Fermi* but also *AGILE*) and from the ground (the Cherenkov telescopes *HESS*, *MAGIC* and *VERITAS*), provides a full coverage of the gamma ray domain of the electromagnetic spectrum in the broad interval of photon energies spanning from few tens of MeVs to few tens of TeVs. Of greatest relevance here is the fact that combined GeV and TeV observations of SNRs can constrain emission models and possibly break the degeneracy of leptonic or hadronic origin of the gamma ray emission. This is because the GeV gamma ray emission from relatively young (i.e. few thousand years) SNRs is expected to have a remarkably different spectrum if the emission has a hadronic or leptonic origin. Very roughly, a spectrum proportional to $\approx E^{-2}$ is expected in the former case, while a much harder one ($\approx E^{-1.5}$) is predicted in the latter case. Even though *Fermi* detected the SNR RX J1713.7-3946, deeper observations ($\sim$ 5 yrs) are needed for this purpose (Funk 2007). However, *Fermi* observations will allow us to study CRs with energy in the GeV range only, and will not provide us with any direct information about the efficiency of SNRs in accelerating CRs up to the energies of the knee.

To probe the acceleration of CRs up to $\sim$ PeV energies gamma ray observations in the $\sim$ 100 TeV range are needed, since this is the energy of the photons produced in hadronic interactions of PeV CRs. This region of the electromagnetic spectrum is, to date, almost unexplored. In the near future (i.e. from 2015 on) the Cherenkov Telescope Array will extend the observed photon energy range up to the region of interest. As already said, observations of SNRs in this energy region would be of fundamental importance since, unlike at TeV energies, there is no ambiguity in the interpretation of the emission. This is because, due to the Klein-Nishina effect, the inverse Compton scattering emission in the 100 TeV region is strongly suppressed, and this would make hadronic emission of PeV CRs the only viable explanation. Thus, detecting SNRs in gamma rays up to $\sim$ 100 TeV, would unambiguously tell us that these objects can accelerate CRs up to the energies of the knee. The main problem in detecting such emission is the fact that SNRs are believed to be capable of accelerating PeV CRs for a very short time only, namely, at the transition between the free expansion and the Sedov phase of their evolution. This happens a few hundred years after the supernova explosion. After that the SNR enters the Sedov phase, the shock velocity gradually decreases and PeV CRs cannot be confined any more within the remnant and escape in the interstellar medium (Ptuskin & Zirakashvili 2005). Thus, assuming a duration of the PeV-phase equal to few hundred years and remembering that about 3 supernovae explode per century in the Galaxy, we can infer that the number of the SNRs in the Galaxy which might be currently accelerating PeV CRs (and thus potentially visible in 100 TeV gamma rays) is of the order of 10. This is of course an over optimistic number, since the actual detection of these remnants will depend on the distance from us, on the density of the surrounding medium that provides the target for hadronic interactions and on the details of

particle acceleration (e.g. the exact duration of the PeV-phase). It is clear from these figures that the number of SNRs in the PeV-phase that will be detected by the Cherenkov Telescope Array will be at most a few. However, even a single detection will be extremely important in order to assess the capability of SNRs in accelerating CRs up to the energies of the knee.

1.3 Molecular clouds as cosmic ray barometers and the diffusion of cosmic rays in the Galaxy

As said above, the problem of the origin of galactic cosmic rays cannot be solved without understanding the way in which cosmic rays propagate in the interstellar medium. This is because the (energy dependent) mode of propagation and escape of cosmic rays from the Galaxy is a major contributor in shaping the spectrum of cosmic rays that we observe at the Earth. In other words, we can deduce what is the spectrum of cosmic rays which is injected in the interstellar medium by their sources only if we know how cosmic rays propagate in the Galaxy. The observed isotropy of cosmic rays in the sky and their spatial homogeneity inferred by observations of the Galaxy in the GeV energy range hint for a diffusive behavior of cosmic rays in the galactic magnetic field. Unfortunately, it is very difficult to obtain constraints or estimates of the cosmic ray diffusion coefficient, both from observations and theory.

A solid constrain on the average diffusion coefficient comes from the measurements of the amount of spallation suffered by cosmic rays while propagating in the Galaxy. These measurements allow us to infer the average residence time of a cosmic ray of energy E_p in the Galaxy as $t_{res} \propto E_p^{-\delta}$, with $\delta \sim 0.3 - 0.7$. If h is the length a cosmic ray has to move away from its source before escaping the Galaxy (i.e. the Galaxy's thickness), then the diffusion coefficient reads: $D_{gal} \approx h^2/t_{res} \approx 10^{28}(E_p/10 \text{ GeV})^{\delta}$ cm^2/s (Berezinskii et al. 1990). However, this has to be intended as the average diffusion coefficient in the Galaxy, and local variations (both in time and space) might exist.

In particular, the diffusion coefficient might be suppressed close to CR sources. This is because CRs can excite magnetic turbulence while streaming away from their acceleration site. This would enhance the scattering rate of CR themselves and thus reduce the diffusion coefficient (Kulsrud & Pearce 1969; Kulsrud & Cesarsky 1971). The problem of estimating, on theoretical grounds, the diffusion coefficient around CR sources is far from being solved, mainly because of its intrinsic non-linearity and because various mechanisms might damp the CR–generated waves and thus affect the way in which CRs diffuse (see e.g. Farmer & Goldreich 2004; Ptuskin et al. 2008).

In principle, gamma ray observations can provide us with constraints on the diffusion coefficient close to cosmic ray sources. This is because, once escaped from their sources, cosmic rays undergo hadronic interactions with the surrounding gas and produce gamma rays. The characteristics of such radiation (in particular its spectrum and intensity as a function of the time elapsed since cosmic rays escaped the source) depend on the value of the diffusion coefficient that can thus be constrained, if a reliable model for cosmic ray acceleration at the source is available.

The presence of massive molecular clouds close to the source would enhance the gamma ray emission, making its detection more probable. Studying such radiation is of great importance not only in order to reach a better understanding of how cosmic rays diffuse, but also because its detection can provide an indirect way to identify the sources of galactic cosmic rays (e.g. Montmerle 1979; Casse & Paul 1980; Aharonian & Atoyan 1996; Gabici & Aharonian 2007b). Since molecular clouds and their gamma ray emission will be extensively studied in the following chapters, it is worth reminding how we can use them to probe the cosmic ray intensity at specific locations in the Galaxy.

Consider a molecular cloud with mass M_{cl} at a distance d, located in a region in the Galaxy where the cosmic ray (protons) intensity is J_{CR}. For illustrative purpose, we set here $J_{CR} = K_{CR} E_p^{-\alpha}$. We further assume that the high energy CRs (the ones with energy above the threshold for π^0-production) can freely penetrate the cloud (for a discussion on cosmic ray exclusion from massive and dense clouds see Cesarsky & Volk 1978; Skilling & Strong 1976; Gabici et al. 2007; Protheroe et al. 2008 or Chapter 6). Under these assumptions the expected gamma ray flux from the molecular cloud due to proton-proton interactions is given by:

$$F_\gamma(E_\gamma) \sim Y_\gamma \, \frac{\sigma_{pp}}{m_p} \, J_{CR}(E_\gamma) \, \left(\frac{M_{cl}}{d^2} \right) \propto E_\gamma^{-\alpha} \tag{1.2}$$

where $\sigma_{pp} \approx 34$ mb is the interaction cross section [6] , m_p is the proton mass, and Y_γ depends on α and is tabulated in Table 1.1. Equation 1.2 is valid at high energies only ($E_\gamma \gtrsim 10$ GeV), while at lower energies the spectrum (in log-log scale) is symmetric with respect to the energy $E_\gamma = m_{\pi^0}/2 \sim 70$ MeV.

Assume now that the cosmic ray intensity in the region under exam differs by a factor $\delta(E_p) = J_{CR}(E_p)/J_{bg}(E_p)$ from the one measured at the Earth, which is (Nakamura & Particle Data Group 2010):

$$\frac{4\pi}{c} \, E_p^2 \, J_{bg}(E_p) \sim 6 \times 10^{-3} \left(\frac{E_p}{\mathrm{TeV}} \right)^{-0.7} \mathrm{eV \ cm^{-3}}, \tag{1.3}$$

so that Equation 1.2 can be rewritten as:

$$E_\gamma^2 F_\gamma(E_\gamma) \sim 2.5 \times 10^{-13} \left(\frac{Y_\gamma f_{0.1}^{2.7-\alpha}}{0.0275} \right) \left(\frac{M_5}{d_{kpc}^2} \right) \delta(E_p) E_\gamma^{-0.7} \mathrm{TeV/cm^2/s} \tag{1.4}$$

where M_5 is the mass of the molecular cloud in units of $10^5 M_\odot$, d_{kpc} is the distance in kpc, and $f_{0.1} = (f/0.1) \approx 1$ takes into account the fact that on average CRs with energy E_p produce gamma rays with energy $E_\gamma \approx f \times E_p$. Moreover, following Casanova et al. (2010b), a multiplicative factor of 1.5 has been applied to account for the contribution to the emission from nuclei heavier than H both in CRs and in the gas that constitute the molecular cloud (Mori 1997, 2009).

[6] Due to its weak energy dependence, the cross section is taken here as a constant. For a detailed treatment of proton-proton interactions see Kelner et al. (2006) or Kamae et al. (2006). These accurate approaches will be used in the following chapters.

α	2.1	2.2	2.3	2.4	2.5	2.6
Y_γ	116	88.8	69.0	54.2	43.0	34.5

Table 1.1: Coefficients Y_γ (multiplied by 1000) for Eq. 1.4 are taken from Berezinskii et al. (1990).

Thus, if gamma rays are detected from a molecular cloud, and its mass and distance are known from its CO emission (e.g. Dame et al. 1987), then Equation 1.4 allows one to measure both the spectrum and intensity of cosmic rays at the molecular cloud's location, and thus the quantity $\delta(E_p)$. It follows that molecular clouds can be effectively used as probes of the energy density of cosmic rays at different locations in the Galaxy, and for this reason have been sometimes referred to as *CR barometers* (Issa & Wolfendale 1981; Aharonian 1991; Casanova et al. 2010a). Since observations in the GeV range of the Galaxy suggest that, on large spatial scales, CR variations are not very large (Strong et al. 1988; Hunter et al. 1997; Abdo et al. 2010b), $\delta(E_p)$ is normally interpreted as the excess above the galactic CR background and is expected to be significantly larger than 1 only in the vicinity of cosmic ray sources. Some examples of how to use this fact to estimate the cosmic ray diffusion coefficient will be given in the following Chapters.

1.4 Outline of the thesis

The aim of this thesis is to show how gamma ray observations can be used to test the supernova remnant hypothesis for the origin of galactic cosmic rays. The two main points will be to extend the region of interest to the multi-TeV domain ($\approx$ 100 TeV, currently almost unexplored) and to use the gamma ray emission from molecular clouds to both identify the sources of cosmic rays and constrain the propagation of cosmic rays themselves.

The thesis is structured as follows: in Chapter 2 a review of the mechanism of diffusive shock acceleration is given. In Chapter 3 this will be applied to supernova remnants to predict the gamma ray fluxes expected in the multi-TeV domain of the electromagnetic spectrum. Predictions will be made both for supernova remnants themselves and for nearby molecular clouds that might be illuminated by cosmic rays that escaped from the remnants. In Chapter 4 the scenario of a cosmic ray illuminated molecular cloud will be developed in details, and the expected broad band (from radio waves to multi-TeV photons) non-thermal emission from a molecular cloud will be estimated. The model developed in this chapter will be applied in Chapter 5 to two test-cases, namely, the supernova remnants RX J1713.7-3946 and W28. The assumption of free cosmic ray penetration into clouds made throughout all the thesis will be checked in Chapter 6. Conclusions and future perspectives in the field will be summarized in Chapter 7.

This Introduction summarizes the content of the following reviews:

- S. Gabici, *Gamma ray astronomy and the origin of cosmic rays*, Proc. XXI European Cosmic Ray Symposium, p. 66 (2008) – arXiv:0811.0836
- S. Gabici, *How to use molecular clouds to study the propagation of cosmic rays in the Galaxy*, Proc. ICATPP Conference on Cosmic Rays for Particle and Astroparticle Physics (2010) – arXiv:1011.2029

Some of the results on gamma ray emission from molecular clouds and their role as cosmic ray barometers have been presented in:

- S. Casanova, F.A. Aharonian, Y. Fukui, S. Gabici, D.I. Jones, A. Kawamura, T. Onishi, G. Rowell, H. Sano, K. Torii, H. Yamamoto, PASJ **62**, 769 (2010)

Some of the results on gas heating at SNR shocks briefly described in this Introduction have been published in:

- L. O'C. Drury, F. A. Aharonian, D. Malyshev, S. Gabici, A&A **496**, 1 (2009)
- D. Malyshev, S. Gabici, L. O'C. Drury, F. A. Aharonian, A&A **521**, A14 (2010)

Chapter 2

The theory of diffusive shock acceleration

Diffusive shock acceleration is very often invoked as the mechanism responsible for the acceleration of CRs in a large number of astrophysical contexts, going from galactic supernova remnants, to large scale cosmological shocks, or to shocks in the solar system, just to name a few examples. The mechanism has been proposed in its modern formulation about 35 years ago in a number of seminal papers (Krymskii 1977; Axford et al. 1977; Blandford & Ostriker 1978; Bell 1978). To have an efficient acceleration, a turbulent magnetic field is required to exist on both sides of the shock, which is here assumed to move at a non relativistic speed. The field is assumed to provide enough scattering to isotropize the (relativistic) particles involved in the acceleration, which can thus cross repeatedly the shock from up to down-stream and back, performing cycles. After each cycle, a particle gains a small amount of energy. This implies that many of these cycles are required before a particle can be accelerated up to the ultra relativistic energies observed in the CR spectrum. The beauty of the mechanism resides in the fact that, provided that the isotropy of particles is preserved (and that particles can be somehow injected into the acceleration process[1]), particles *must* undergo these cycles and the acceleration is limited only by geometric factors (i.e. the particle's Larmor radius being larger than the size of the system) or by the lifetime of the accelerator itself.

Soon after its introduction, the mechanism was found to be non-linear in many ways. First of all, the magnetic turbulence required to scatter and isotropize the accelerated particles is believed to be generated by the particles themselves (Bell 1978; Lagage & Cesarsky 1983a). Moreover, the mechanism is expected to be so efficient that the pressure in form of CRs cannot be neglected in the equation of momentum conservation across the shock (as it is done in the test-particle approach), and this additional pressure term modifies the structure of the shock itself, and in turn also the spectrum of accelerated particles (Eichler 1979; Blandford 1980; Drury

[1]The injection problem is one of the most obscure issues in shock acceleration theory and discussing it in details goes well beyond the scope of this thesis. A discussion can be found, for example, in Malkov & Voelk (1995).

& Voelk 1981).

Most of the efforts made to develop the theory of particle acceleration at non-relativistic shocks have been carried out in order to demonstrate whether or not diffusive acceleration operating at SNR shocks could be responsible for the acceleration of galactic CRs. As said in the previous chapter, this issue is still open. In particular, the CR-induced modification of the hydro-dynamical structure of the shock is influencing the spectrum of the accelerated particles itself, while the level of CR-generated turbulence determines the maximum energy that a particle can attain at a shock.

For a long time, SNRs were believed to be unable to accelerate particles up to the energy of the CR knee. This crucial issue was first pointed out by Lagage & Cesarsky (1983b), who computed the expected level of turbulence due to the resonant CR streaming instability. This issue has been recently solved (at least from a theoretical point of view) by Bell (2004), who suggested that a non resonant CR current driven instability, previously overlooked, can indeed operate at shocks and amplify the turbulent magnetic field up to the level required to accelerate particles up to the knee and above.

Given that most of this thesis will deal with the acceleration of particles at SNR shocks and the subsequent escape in the interstellar medium, it seems appropriate to review here the theory of diffusive shock acceleration. This brief review will be focused on the aspects of the theory which are the most relevant for the topic treated in the following chapters. Namely, the dynamical reaction of CRs onto the shock structure and the way in which particles are released from SNRs will be treated in detail. For a comprehensive description of the non resonant CR streaming instability the reader is referred to the excellent paper by Bell (2004).

2.1 Diffusive shock acceleration: linear theory

In this section we solve the transport equation for CRs at a shock in the case in which the CRs have no dynamical effect onto the shock structure and can be treated as test–particles. It is convenient to solve the problem in the shock rest frame (i.e. the rest frame in which the shock is at rest). Since we consider here shocks moving at constant speed only, this can always be done through a Galilean transformation. The steady state equation describing the transport of CRs at a shock is:

$$\frac{\partial}{\partial x}\left(D\,\frac{\partial f}{\partial x}\right) - u\,\frac{\partial f}{\partial x} + \frac{p}{3}\,\frac{du}{dx}\,\frac{\partial f}{\partial p} + Q = 0 \tag{2.1}$$

where $f \equiv f(p,x)$ is the particle distribution function which depends on particle momentum p and position x, $u > 0$ is the fluid velocity, $D \equiv D(p)$ is the CR diffusion coefficient, assumed here to be homogeneous in space, and Q is a particle injection term. The shock is located at $x = 0$ and the upstream (downstream) region corresponds to $x < 0$ ($x > 0$) and the fluid speed there is constant and equal to $u = u_1$ ($u = u_2$). We set $\partial f/\partial t = 0$, since we are interested in the steady state solution of the equation.

The first term in the equation describes the diffusive behavior of CRs in the turbulent magnetic field. The second term represents the advection of CRs with the fluid. The third term represents the acceleration of particles, is non vanishing at $x = 0$ only, and can be rewritten as:

$$\frac{p}{3}\,\frac{du}{dx} = -\,\frac{p}{3}\,(u_1 - u_2)\,\delta(x)\ . \tag{2.2}$$

The forth term represents the injection of particles in the acceleration process. Particle injection is very often assumed to take place at the shock surface, so that also this term can be written as a delta function in x:

$$Q(p,x) = Q_0(p)\,\delta(x)\delta(p - p_{inj})\ , \tag{2.3}$$

where p_{inj} is the momentum at which particles are injected into the acceleration mechanism[2]. As boundary conditions we set both f and its spatial derivative equal to zero at upstream infinity ($x = -\infty$), and $\partial f/\partial x = 0$ downstream of the shock. The latter condition is a consequence of the assumption of isotropy of the particle distribution function. At the shock, the particle distribution function (but not its spatial derivative), must be continuous, i.e. $f(0^+) = f(0^-) = f_0$.

Under these conditions Eq. 2.1 can be solved in the following way. First, take the integral between $x = -\infty$ to $x = 0^-$ to get:

$$\left| D\,\frac{\partial f}{\partial x}\right|_{x=0^-} \;=\; u_1\ f_0\ . \tag{2.4}$$

Repeating the integration between $x = 0^-$ and $x = 0^+$ gives:

$$-\left| D\,\frac{\partial f}{\partial x}\right|_{x=0^-} \;-\; \frac{p}{3}\,(u_1 - u_2)\,\frac{\partial f_0}{\partial p} \;+\; Q_0\ \delta(p - p_{inj}) \;=\; 0\ . \tag{2.5}$$

By combining the two expressions above, and considering momenta above the injection one, it is easy to recover the very well known result:

$$\alpha \;=\; -\;\frac{p}{f_0}\,\frac{\partial f_0}{\partial p} \;=\; \frac{3\ u_1}{u_1 - u_2} \tag{2.6}$$

that can also be expressed as a function of the shock compression factor $r = u_1/u_2$ as:

$$\alpha \;=\; \frac{3\ r}{r-1}\ . \tag{2.7}$$

This is a very remarkable results which tells us that:

1. the spectrum of accelerated particles at the shock is a power law: $f_0(p) \propto p^{-\alpha}$;
2. for strong shocks the compression factor is $r = 4$ and thus the spectrum of particles is independent on the shock Mach number and has the universal shape $f_0(p) \propto p^{-4}$;

[2] A more detailed discussion on the value of the injection momentum will be provided in the following.

3. the spectral shape does not depend on the diffusion coefficient, which is a quantity very poorly constrained since it depends on the (virtually unknown) power spectrum of the magnetic field on both sides of the shock.

As said above, as a consequence of the assumed isotropy of particles, the solution of Eq. 2.1 downstream of the shock is constant at any given momentum and equal to: $f_2(x,p) = f_0(p)$. On the other hand, the solution upstream of the shoc depends on the particle diffusion coefficient and can be found after a simple integration:

$$f_1(x,p) \;=\; f_0 \exp\left[\frac{u_1}{D}\; x\right] \;. \tag{2.8}$$

This equation tells us that particles can diffuse ahead of the shock up to a distance $x_d \sim D/u_1$. At distances from the shock smaller than x_d the spatial distribution of particles (at a given momentum) is almost constant, while at larger distances it falls down exponentially. Since the diffusion coefficient is an increasing function of particle momentum (e.g. for the Bohm diffusion, which seems a reasonable assumption in very turbulent media, the scaling is $D \propto p$), particles with higher energy can diffuse further away upstream of the shock than low energy particles.

Another important issue concerns the maximum energy attainable by particles accelerated at a shock. A dimensional argument suggests that the acceleration time needed for a particle to reach an energy E is given by:

$$t_{acc} \approx \frac{D(E)}{u_1^2} \;. \tag{2.9}$$

Thus, for Bohm diffusion ($D \propto E/B$, where B is the magnetic field strength at the shock), and for constant shock speed, this corresponds to a linear scaling of the maximum particle energy with time:

$$E_{MAX} \propto B\; u_1^2\; t \;. \tag{2.10}$$

This tells us that, provided that particles remain confined within the accelerator, the maximum energy is determined by the age of the accelerator.

Formally, if a plane and infinite shock moving at constant speed is considered, particles cannot leave the system, and the expression above for the maximum energy remains always valid. However, in realistic situations the shock size is finite and particle escape can become the most relevant factor in determining the particles maximum energy. Using again a dimensional argument, one can see that the maximum distance that a particle of energy E can travel ahead of the shock while performing a cycle down $\rightarrow$ up $\rightarrow$ down-stream of the shock is given by:

$$L_{diff} \approx \frac{D(E)}{u_1} \;. \tag{2.11}$$

When this length becomes larger than the size of the shock R_s, particles leave the system. If we consider the case of a spherical SNR shock, than R_s (i.e. the SNR radius) is an increasing function of time, and its velocity is $u_1 = dR_s/dt \approx R_s/t$. If

we further assume, as done above, that diffusion proceeds in the Bohm regime we can write:

$$E_{MAX} \propto R_s \; u_1 \; B \; . \tag{2.12}$$

According to Bell (2004), the magnetic field at the shock is amplified due to CR streaming instability and the level of the amplification depends on the shock velocity. Observations of X-ray filaments in SNRs allow us to infer the magnetic field strength there and, though with quite high uncertainty, suggest that $B \propto u_1$ (Völk et al. 2005). We can thus rewrite the expression for the maximum energy as: $E_{MAX} \propto u_1^3 \; t$. For a SNR in its adiabatic phase of evolution (the Sedov-Taylor phase, see Sedov 1959) the velocity scales as $u_1 \propto t^{-3/5}$, leading to:

$$E_{MAX} \propto t^{-4/5} \; . \tag{2.13}$$

Just after the explosion, i.e. before the Sedov-Taylor phase, a SNR shock expands freely at constant velocity (for this reason this phase is called the free expansion phase). Thus, during this time, Eq. 2.10 holds and the maximum energy of accelerated particles increases with time. When the mass of the swept up gas becomes comparable to the mass of the supernova ejecta, the SNR shock enters the Sedov phase and decelerates. At this point, the maximum energy is determined by Eq. 2.13, and it decreases with time. This allows particles with lower and lower energy to leave gradually the SNR as the shock speed slows down.

2.2 Particle acceleration at modified shocks: non linear theory

As seen in the Introduction, if we want SNRs to be the sources of galactic CRs, they have to convert a significant fraction ($\sim 10\%$ or so) of their explosion energy into CRs. This energy conversion is believed to happen at the shock via diffusive acceleration. The detection of some SNRs in TeV gamma rays fits with this picture since, at least in the hadronic scenario, a significant fraction of the total energy needs to be in form of CR protons in order to explain the observed emission. It seems thus appropriate to investigate the effects of CR pressure onto the shock structure.

If a substantial fraction of the shock energy is converted into CRs, then the structure of the shock itself is modified, due to an additional pressure term (i.e. the pressure P_{CR} is form of CRs) that has to be added to the momentum conservation equation. The shock modification manifests itself upstream of the shock, where the CR pressure acts against the fluid ram pressure and slows it down. As a consequence, the shock is no longer a sharp transition, but develops an extended precursor upstream, where the fluid slows down before entering a weak shock, called *subshock*.

Several different approaches exists to solve the problem of CR modified shocks, including analytic or semi-analytic kinetic studies (e.g. Eichler 1979; Malkov 1999; Berezhko & Ellison 1999; Blasi 2002; Amato & Blasi 2005), two fluid models (e.g. Drury & Voelk 1981), finite difference numerical schemes (e.g. Kang & Jones 1991;

Duffy 1992; Berezhko et al. 1994; Ferrand et al. 2008), and montecarlo approaches (see Ellison & Eichler 1984, and follow up papers).

Here we describe in detail the semi-analytic model proposed by Blasi (2002) and subsequently developed by e.g. Blasi et al. (2005); Amato et al. (2008). Let us start with the transport equation (Eq. 2.1). The main difference with respect to the test-particle case treated in the previous section is that the upstream velocity is no longer constant. It is thus convenient to define the quantities u_0 and u_1, which represent the fluid velocity at upstream infinity and just upstream of the subshock ($x = 0^-$), respectively. Upstream of the shock ($x < 0$) the velocity will not be constant, but a decreasing function of position $u(x)$. Downstream ($x > 0$) all the physical quantities are expected to be constant as in the test-particle case, and the fluid velocity is u_2.

Keeping in mind all these differences, one can perform exactly the same integrations of Eq. 2.1 as done in the previous section, to get:

$$\frac{1}{3}p\frac{df_0}{dp}(u_2-u_1)-u_1 f_0+Q_0\delta(p-p_{inj})+\int_{-\infty}^{0^-}dx f\frac{du}{dx}+\frac{1}{3}\int_{-\infty}^{0^-}dx\frac{du}{dx}p\frac{\partial f}{\partial p}=0. \quad (2.14)$$

We introduce the quantity u_p defined as

$$u_p = u_1 - \frac{1}{f_0}\int_{-\infty}^{0^-}dx\frac{du}{dx}f(x,p), \quad (2.15)$$

whose physical meaning is instrumental to understand the nonlinear reaction of particles. The function u_p is the average fluid velocity experienced by particles with momentum p while diffusing upstream away from the shock surface. In other words, the effect of the average is that, instead of a constant speed u_1 upstream, a particle with momentum p experiences a spatially variable speed, due to the pressure of the accelerated particles. Since the diffusion coefficient is in general p-dependent, particles with different energies *feel* a different compression factor, higher at higher energies if, as expected, the diffusion coefficient is an increasing function of momentum (see Blasi 2002 for further details on the meaning of the quantity u_p).

With the introduction of u_p, Eq. 2.14 becomes:

$$\frac{1}{3}p\frac{df_0}{dp}(u_2-u_p)-f_0\left[u_p+\frac{1}{3}p\frac{du_p}{dp}\right]+Q_0\delta(p-p_{inj})=0, \quad (2.16)$$

where we used the fact that:

$$p\frac{d}{dp}\int_{-\infty}^{0^-}dx\frac{du}{dx}f = p\left[\frac{df_0}{dp}(u_1-u_p)-f_0\frac{du_p}{dp}\right].$$

The solution of Eq. 2.16 is:

$$f_0(p)=\frac{3R_{sub}}{R_{sub}-1}\frac{\eta n_{gas,1}}{4\pi p_{inj}^3}\exp\left\{-\int_{p_{inj}}^{p}\frac{dp'}{p'}\frac{3}{u_{p'}-u_2}\left[u_{p'}+\frac{1}{3}p'\frac{du_{p'}}{dp'}\right]\right\}. \quad (2.17)$$

Here we used $Q_0 = \frac{\eta n_{gas,1} u_1}{4\pi p_{inj}^2}$, with $n_{gas,1}$ the gas density immediately upstream ($x = 0^-$) and η the fraction of the particles crossing the shock which takes part in the acceleration process.

Here we introduced the two quantities $R_{sub} = u_1/u_2$ and $R_{tot} = u_0/u_2$, which are respectively the compression factor at the gas subshock and the total compression factor between upstream infinity and downstream. For a modified shock, R_{tot} can attain values much larger than R_{sub} and more in general, much larger than 4, which is the maximum value achievable for an ordinary strong non-relativistic shock. The increase of the total compression factor compared with the prediction for an ordinary shock is responsible for the peculiar flattening of the spectra of accelerated particles that represents a feature of nonlinear effects in shock acceleration. In terms of R_{sub} and R_{tot} the density immediately upstream is $n_{gas,1} = (\rho_0/m_p)R_{tot}/R_{sub}$.

In Eq. 2.17 we can introduce a dimensionless quantity $U(p) = u_p/u_0$ so that

$$f_0(p) = \left(\frac{3R_{sub}}{R_{tot}U(p) - 1}\right) \frac{\eta n_{gas,1}}{4\pi p_{inj}^3} \exp\left\{ - \int_{p_{inj}}^{p} \frac{dp'}{p'} \frac{3R_{tot}U(p')}{R_{tot}U(p') - 1} \right\}. \tag{2.18}$$

The nonlinearity of the problem reflects in the fact that $U(p)$ is in turn a function of f_0 as it is clear from the definition of u_p. In order to solve the problem we need to write the equations for the thermodynamics of the system including the gas, the cosmic rays accelerated from the thermal pool and the shock itself.

The velocity, density and thermodynamic properties of the fluid can be determined by the mass and momentum conservation equations, with the inclusion of the pressure of the accelerated particles. We write these equations between a point far upstream ($x = -\infty$), where the fluid velocity is u_0 and the density is $\rho_0 = m n_{gas,0}$, and the point where the fluid velocity is u_p (density ρ_p). The index p denotes quantities measured at the point where the fluid velocity is u_p, namely at the point x_p that can be reached only by particles with momentum $\geq p$ (this is clearly an approximation, but as shown in Blasi et al. 2005 it provides a good agreement with other calculations where this approximation is not used).

The mass conservation implies:

$$\rho_0 u_0 = \rho_p u_p. \tag{2.19}$$

Conservation of momentum reads:

$$\rho_0 u_0^2 + P_{g,0} = \rho_p u_p^2 + P_{g,p} + P_{CR,p}, \tag{2.20}$$

where $P_{g,p}$ is the gas pressure at the point $x = x_p$ and $P_{CR,p}$ is the pressure of accelerated particles at the same point (we use the symbol CR to mean *cosmic rays*, in the sense of *accelerated particles*). The mass and momentum escaping fluxes in the form of accelerated particles have reasonably been neglected (see following section for an extensive discussion of this issue). Note that at this point the equation for energy conservation has not been used.

Our basic assumption, similar to that used by Eichler (1984), is that the diffusion is p-dependent and more specifically that the diffusion coefficient $D(p)$ is an

increasing function of p. Therefore the typical distance that a particle with momentum p travels away from the shock is approximately $\Delta x \sim D(p)/u_p$, larger for high energy particles than for lower energy particles[3]. As a consequence, at each given point x_p only particles with momentum larger than p are able to affect appreciably the fluid. Strictly speaking the validity of the assumption depends on how strongly the diffusion coefficient depends on the momentum p.

Since only particles with momentum $\geq p$ can reach the point $x = x_p$, we can write

$$P_{CR,p} \simeq \frac{4\pi}{3} \int_p^{p_{max}} dp p^3 v(p) f_0(p), \tag{2.21}$$

where $v(p)$ is the velocity of particles with momentum p, p_{max} is the maximum momentum achievable in the specific situation under investigation.

From Eq. 2.20 we can see that there is a maximum distance, corresponding to the propagation of particles with momentum p_{max} such that at larger distances the fluid is unaffected by the accelerated particles and $u_p = u_0$.

The equation for momentum conservation is:

$$\frac{dU}{dp}\left[1 - \frac{1}{M_0^2} U^{-(\gamma_g+1)}\right] + \frac{1}{\rho_0 u_0^2}\frac{dP_{CR}}{dp} = 0. \tag{2.22}$$

Using the definition of P_{CR} and multiplying by p, this equation becomes

$$p\frac{dU}{dp}\left[1 - \frac{1}{M_0^2} U^{-(\gamma_g+1)}\right] = \frac{4\pi}{3\rho_0 u_0^2} p^4 v(p) f_0(p), \tag{2.23}$$

where f_0 is known once $U(p)$ is known. Eq. 2.23 is therefore an integral-differential nonlinear equation for $U(p)$. The solution of this equation also provides the spectrum of the accelerated particles.

The last missing piece is the connection between R_{sub} and R_{tot}, the two compression factors appearing in Eq. 2.18. The compression factor at the gas shock around $x = 0$ can be written in terms of the Mach number M_1 of the gas immediately upstream through the well known expression

$$R_{sub} = \frac{(\gamma_g + 1)M_1^2}{(\gamma_g - 1)M_1^2 + 2}. \tag{2.24}$$

On the other hand, if the upstream gas evolution is adiabatic, then the Mach number at $x = 0^-$ can be written in terms of the Mach number of the fluid at upstream infinity M_0 as

$$M_1^2 = M_0^2 \left(\frac{u_1}{u_0}\right)^{\gamma_g+1} = M_0^2 \left(\frac{R_{sub}}{R_{tot}}\right)^{\gamma_g+1},$$

so that from the expression for R_{sub} we obtain

$$R_{tot} = M_0^{\frac{2}{\gamma_g+1}} \left[\frac{(\gamma_g + 1)R_{sub}^{\gamma_g} - (\gamma_g - 1)R_{sub}^{\gamma_g+1}}{2}\right]^{\frac{1}{\gamma_g+1}}. \tag{2.25}$$

[3]For the cases of interest, $D(p)$ increases with p faster than u_p does, therefore Δx is a monotonically increasing function of p.

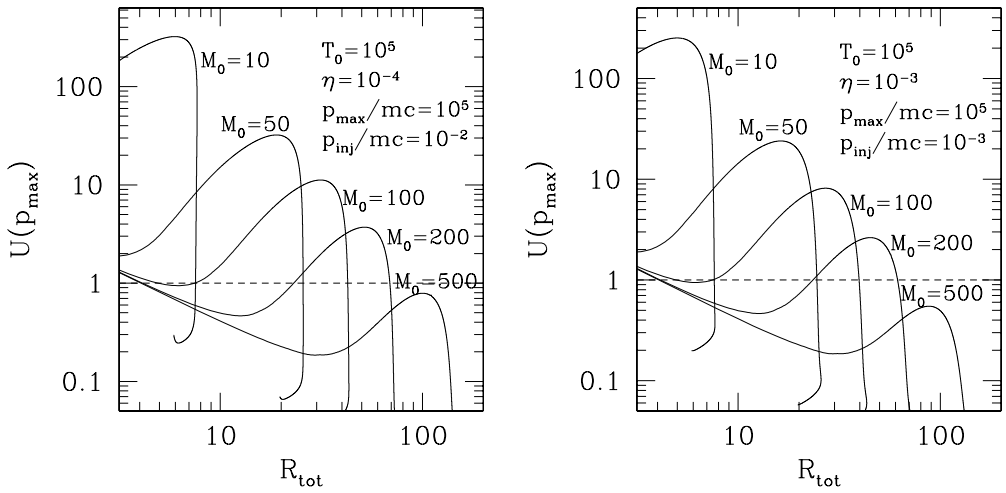

Figure 2.1: *Left panel*: $U(p_{max})$ as a function of the total compression factor for $T_0 = 10^5$ K, $\eta = 10^{-4}$, $p_{max} = 10^5\ mc$ and $p_{inj} = 10^{-2}\ mc$ for the Mach numbers indicated. *Right panel*: same as in left panel but for $\eta = 10^{-3}$ and $p_{inj} = 10^{-3}\ mc$.

In all the equations above, γ_g is the gas adiabatic index.

Now that an expression between R_{sub} and R_{tot} has been found, Eq. 2.23 basically is an equation for R_{sub}, with the boundary condition that $U(p_{max}) = 1$. Finding the value of R_{sub} (and the corresponding value for R_{tot}) such that $U(p_{max}) = 1$ also provides the whole function $U(p)$ and, through Eq. 2.18, the distribution function $f_0(p)$. If the reaction of the accelerated particles is small, the *test particle* solution is recovered.

2.2.1 The appearance of multiple solutions

In the problem described in the previous section there are several independent parameters. While the Mach number of the shock and the maximum momentum of the particles are fixed by the physical conditions in the environment, the injection momentum and the acceleration efficiency are free parameters. The procedure to be followed to determine the solution was defined by Blasi (2002): the basic problem is to find the value of R_{sub} (and therefore of R_{tot}) for which $U(p_{max}) = 1$. In Fig. 2.1 we plot $U(p_{max})$ as a function of R_{tot}, for $T_0 = 10^5 K$, $p_{max} = 10^5 mc$ and $p_{inj} = 10^{-2} mc$ in the left panel and $p_{inj} = 10^{-3} mc$ in the right panel (m here is the mass of protons). The parameter η was taken 10^{-4} in the left panel and 10^{-3} in the right panel. The different curves refer to different choices of the Mach number at upstream infinity. The physical solutions are those corresponding to the intersection points with the horizontal line $U(p_{max}) = 1$, so that multiple solutions occur for those values of the parameters for which there is more than one intersection with $U(p_{max}) = 1$. These solutions are all physically acceptable, as far as the conservation of mass, momentum and energy are concerned.

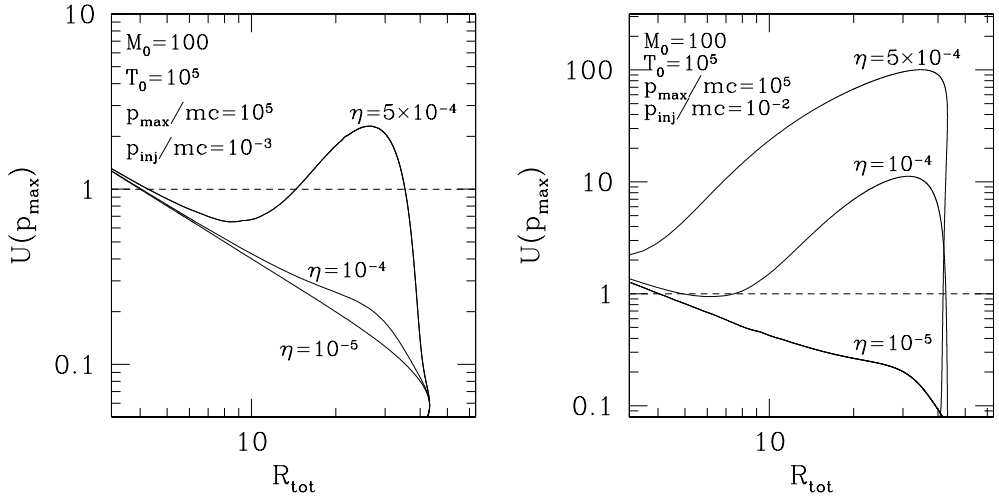

Figure 2.2: *Left panel*: $U(p_{max})$ as a function of the total compression factor for $T_0 = 10^5$ K, $p_{max} = 10^5\ mc$ and $p_{inj} = 10^{-3}\ mc$ at fixed Mach number $M_0 = 100$ for the efficiencies indicated. *Right panel*: same as in left panel but for $p_{inj} = 10^{-2}\ mc$.

It can be seen from both panels in Fig. 2.1 that for low values of the Mach number, only one solution is found. This solution may be significantly far from the quasi-linear solution. Indeed, for $M_0 = 10$ the solution corresponds to $R_{tot} \sim 8$, instead of the usual $R_{tot} \sim 4$ solution expected in the linear regime. Lower values of the Mach number are required to fully recover the linear solution.

When the Mach number is increased, there is a threshold value for which three solutions appear, one of which is the quasi-linear solution. For very large values of the Mach number the solution becomes one again, and it coincides with the quasi-linear solution.

In Fig. 2.2 we show the appearance of the multiple solutions for the case $T_0 = 10^5 K$, $p_{max} = 10^5 mc$ and $p_{inj} = 10^{-3} mc$ with Mach number $M_0 = 100$ ($p_{inj} = 10^{-2} mc$ and $M_0 = 100$) in the left (right) panel. The curves here are obtained by changing the value of η. The same comments we made for Fig. 2.1 apply here as well: low values of η correspond to weakly modified shocks, while for increasingly larger efficiencies multiple solutions appear. The solution becomes one again in the limit of large efficiencies, and it always corresponds to strongly modified shocks.

The problem of multiple solutions is not peculiar of the kinetic approaches to the non-linear theories of particle acceleration at shock waves. The same phenomenon was in fact found initially in two-fluid models (Drury & Voelk 1981), where however no information on the spectrum of the accelerated particles and on the injection efficiency was available.

2.3 A recipe for injection from the thermal pool

The presence of multiple solutions is typical of many non-linear problems and should not be surprising from the mathematical point of view. In terms of physical understanding however, multiple solutions may be disturbing. The typical situation that takes place in nature when multiple solutions appear in the description of other non linear systems is that (at least) one of the solutions is unstable and the system *falls* in a stable solution when perturbed. The stable solutions are the only ones that are physically meaningful. Some attempts to investigate the stability of cosmic ray modified shock waves have been made by Mond & O'C. Drury (1998); Toptygin (1999), but all of them refer to the two-fluid models.

In addition to the stability, another issue that enters the physical description of our problem is the identification of possible processes that determine some type of backreaction on the system. It may be expected that when some types of processes of self-regulation are included, the phenomenon of multiple solutions is reduced. In this section we investigate the type of reaction that takes place when a self-consistent, though simple, recipe for the injection of particles from the thermal pool is adopted. This recipe is similar to that proposed by Kang et al. (2002) in terms of the underlying physical interpretation of the injection, but probably simpler in its implementation.

For non-relativistic shocks, the distribution of particles downstream is quasi-isotropic, so that the flux of particles crossing the shock surface from downstream to upstream can be written as

$$\Phi = -2\pi \int_{p_{min}}^{\infty} dp \int_{-1}^{-u_d/v(p)} d\mu \frac{f_{th}(p)}{4\pi} 4\pi p^2 \left[u_d + v(p)\mu\right], \tag{2.26}$$

where $v(p)$ is the velocity of particles with momentum p and u_d is the shock speed in the frame comoving with the downstream fluid. The term $u_d + v(p)\mu$ is the component along the direction perpendicular to the shock surface of the velocity of particles with momentum p moving in the direction μ. It follows that the flux of particles moving tangent to the shock surface (namely with $\mu = -u_d/v(p)$) is zero. We recall that, having in mind collisionless shocks, the typical thickness of the shock, λ, is the collision length associated with the magnetic interactions that give rise to the formation of the discontinuity. Useless to say that these interactions are all but well known, and at present the best we can do is to attempt a phenomenological approach to take them into account, without having to deal with their detailed physical understanding. It is however worth recalling that many attempts have been made to tackle the problem of injection at a more fundamental level (e.g. Malkov & Voelk 1995; Malkov 1998). Here, we consider the reasonable situation in which $\lambda \propto r_L^{th}$, where $r_L^{th} \propto p_{th}$ is the Larmor radius of the particles in the downstream fluid that carry most of the thermal energy, namely those with momentum 1.5 p_{th} ($p_{th} = (2mk_BT_2)^{1/2}$ here is the momentum of the particles in the thermal peak of the maxwellian distribution in the downstream plasma, having temperature T_2). We stress here the important point that the temperature of the downstream gas

(and therefore p_{th}) is determined by the shock strength, which in the presence of accelerated particles, is affected by the pressure of the non-thermal component. In particular, the higher the efficiency of the shock as a particle accelerator, the weaker its efficiency in terms of heating of the background plasma (see section 2.4.3).

For collisionless shocks, it is not clear whether the downstream plasma can actually be thermalized and the distribution function be a maxwellian. On the other hand, it is generally assumed that this is the case, so that in the following we consider the case in which the bulk of the background plasma is thermal and has a maxwellian spectrum at temperature T given by the generalized Rankine-Hugoniot relations in the presence of accelerated particles (see section 2.4.3). For modified shocks, the points discussed above apply to the so-called subshock, where the injection of particles from the thermal pool is expected to take place. We recall that for strongly modified shocks the subshock is weak, and rather inefficient in the heating of the background plasma.

From Eq. 2.26 we get:

$$\Phi = \frac{1}{4}\int_{p_{min}}^{\infty} dp 4\pi p^2 f_{th}(p) \frac{(v(p)-u_d)^2}{v(p)}, \tag{2.27}$$

where we assumed that the temperature downstream implies non-relativistic motion of the quasi-thermal particles ($p \approx mv(p)$). In Eq. 2.27 we write the minimum momentum in terms of a parameter α, such that $\lambda = \alpha r_L^{th}$. With this formalism, the particles that can cross the shock surface are those that satisfy the condition:

$$p > p_{min} = 1.5\ \alpha\ p_{th}. \tag{2.28}$$

The parameter α defines the thickness of the shock in units of the gyration radius of the bulk of the thermal particles. According to this picture, thermal particles have a pathlength smaller than the shock thickness and cannot cross the shock surface, being advected downstream before the crossing occurs. Only particles with momentum sufficiently larger than the thermal momentum of the downstream particles can actually return upstream and be accelerated.

In the following we will neglect the fluid speed u_d compared with $v(p)$, which is a good approximation if the injected particles are sufficiently more energetic than the thermal particles. This is done only to make the interpretation of the result simpler, but there is no technical difficulty in keeping the dependence of the results on u_d.

We introduce an effective injection momentum $p_{inj} = \xi p_{th}$ defined by the equation:

$$\Phi = \int_{\xi p_{th}}^{\infty} dp 4\pi p^2 f_{th}(p) v(p), \tag{2.29}$$

which in terms of dimensionless quantities, with $f_{th}(p) = e^{-(p/p_{th})^2}$ reads:

$$\int_{1.5\alpha}^{\infty} dx x^3 e^{-x^2} = 4\int_{\xi}^{\infty} dx x^3 e^{-x^2}. \tag{2.30}$$

It is easy to show that $\xi \approx 2$ for $\alpha = 1$ (half a Larmor rotation of the particles with momentum $1.5 p_{th}$ inside the thickness of the shock) and $\xi \approx 3.25$ for $\alpha = 2$ (one

full Larmor rotation of the particles with momentum $1.5p_{th}$ inside the *thickness* of the shock. The fraction of particles at momentum ξ times larger than the thermal one is $\sim 5\%$ for $\xi = 2$ and $\sim 10^{-4}$ for $\xi = 3.25$. The actual values of ξ are expected to be somewhat higher if the effect of advection with the downstream fluid is not neglected. The sharp decrease in the fraction of *leaking* particles that may take part in the acceleration process is due to the exponential behaviour of the maxwellian at large momenta. Although the fraction of particles in the maxwellian that get accelerated only depends on the parameter ξ which in turn is expected to keep the information about the microscopic structure of the shock, the absolute number of and energy carried by these particles depend on the temperature of the downstream gas, which is an output of our calculation. This simple argument serves as an explanation of the physical reason why there is a nonlinear reaction on the system due to injection. If the parameter ξ is assumed to be determined by the microphysics of the shock, and if we adopt our simple recipe to describe such microphysics, then the shock thickness is easily estimated once the temperature of the downstream gas is known, and the latter can be calculated from the modified Rankine-Hugoniot relations. The parameter η in Eq. 2.18 is no longer a free parameter, being related in a unique way to the parameter ξ and to the physical conditions at the subshock. The condition that fixes η is that the total number of particles in the non-thermal spectrum equals the number of particles in the maxwellian at momenta larger than p_{inj}. Due to the very strong dependence of the spectrum on the momentum for both the maxwellian and the power law at low momenta, the condition described above is very close to require the continuity of the distribution function, namely that $f_{th}(p_{inj}) = f_0(p_{inj})$. In the following we adopt this condition for the calculations. This can be shown to imply the following expression for η:

$$\eta = \frac{4}{3\pi^{1/2}}(R_{sub} - 1)\xi^3 e^{-\xi^2}. \tag{2.31}$$

We recall that the compression factor at the subshock, R_{sub}, approaches unity when the shock becomes cosmic ray dominated. This makes evident how the backreaction discussed above works: when the shock becomes increasingly more modified, the efficiency η tends to decrease, limiting the amount of energy that can be channelled in the non-thermal component. Although the recipe provided here is certainly far from representing the complexity of the reality of injection of particles from the thermal pool, it may be considered as a useful attempt to include the main physical aspects of this phenomenon.

2.3.1 Self-consistent injection and multiple solutions

In this section we describe the role played by the injection recipe discussed above for the appearance of multiple solutions. It can be expected that the phenomenon is somewhat reduced because, as discussed in the previous section, the injection provides an efficient backreaction mechanism on the shock as a particle accelerator. Indeed we find that the appearance of multiple solutions is drastically reduced, and that the phenomenon still exists only in regions of the parameter space which are

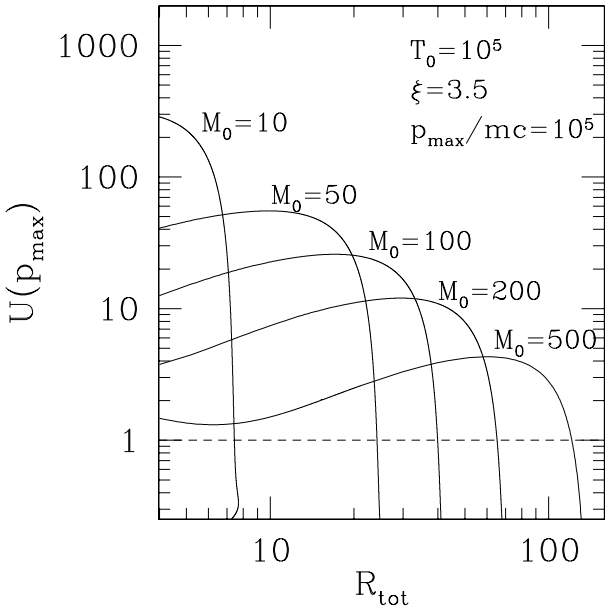

Figure 2.3: $U(p_{max})$ as a function of the total compression factor for $T_0 = 10^5$ K, $p_{max} = 10^5\ mc$ and $\xi = 3.5$ for the Mach numbers indicated.

very narrow and of limited physical interest. In the quantitative calculations we use the value $\xi = 3.5$ for the injection parameter, as suggested by the simple estimate in Section 2.3 and as suggested also in the numerical work of Kang & Jones (1995). The dependence of the effect on the value of ξ is discussed below. In Fig. 2.3 we illustrate the dramatic change in the physical picture by plotting $U(p_{max})$ as a function of R_{tot} for $\xi = 3.5$ and adopting the same values for the parameters as those used in obtaining Fig. 2.1. The efficiency η is now calculated according with the recipe described in the previous section. It can be seen very clearly that when the Mach number of the shock is changed, there is a single solution (compare with Fig. 2.1 where multiple solutions where found for the same values of the parameters, but without thermal leakage).

The appearance of multiple solutions can be investigated in the whole parameter space, in order to define the regions where the phenomenon appears, when it does. In Fig. 2.4 we highlight the regions where there are multiple solutions (dark regions) in a plane $\xi - \log(p_{max})$, for different values of the Mach number of the shock. In most cases the dark regions are very narrow and cover a region of values of ξ which is rather high (small efficiency). In Fig. 2.5 we plot the value of R_{tot} as a function of ξ for $M_0 = 200$, $u_0 = 5 \times 10^8$cm s^{-1} and $p_{max} = 10^3, 10^4,\ 10^5,\ 10^7\ mc$ from left to right. The line is continuous when there are no multiple solutions and dashed when multiple solutions appear. The dashed regions are, as stressed above, rather narrow. For instance, for $p_{max} = 10^4 mc$ there are multiple solutions only for $3.67 \leq \xi \leq 3.7$. Any small perturbation of the system that changes the values of ξ at the percent

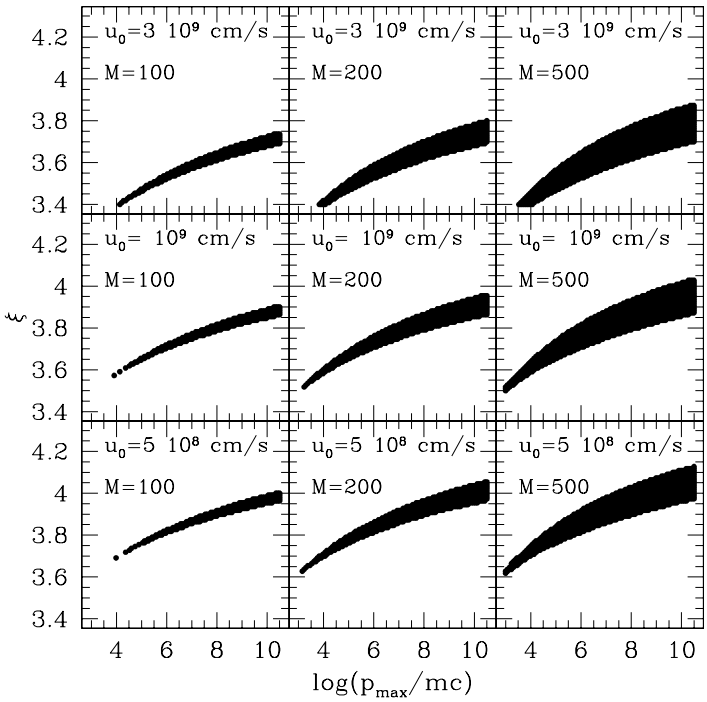

Figure 2.4: Parameter space for multiple solutions. The dark regions illustrate the regions of parameters for which multiple solutions are still present. Figure from Gabici et al. (2005).

level implies that the system shifts to one of the single solutions if it is sitting in the intermediate solution before the perturbation. The sharp transition between the strongly modified solution and the quasi-linear solution when ξ is increased suggests that the intermediate solution may be unstable, though a formal demonstration cannot be provided here. In order to make sure that this is the case, a careful analysis of the stability is required. On the other hand, a previous study, carried out in the context of the two-fluid models, showed that when multiple solutions are present, the solution with intermediate efficiency is in fact unstable to corrugations of the shock surface (Mond & O'C. Drury 1998).

2.4 Particle spectra, velocity profiles, escaping particles, and suppression of shock heating

2.4.1 Particle spectra and velocity profiles

All approaches to particle acceleration at modified shocks predict the formation of a precursor in the upstream region, resulting in a gradient of the velocity profile of the fluid. Since qualitatively the spectrum of the accelerated particles is still determined

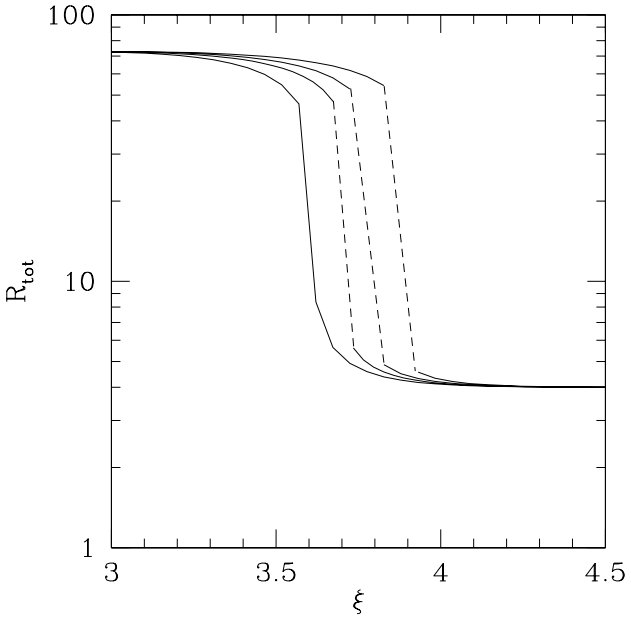

Figure 2.5: Dependence of R_{tot} as a function of ξ for $M_0 = 200$, $u_0 = 5 \times 10^8$cm s^{-1} and $p_{max} = 10^3, 10^4,\ 10^5,\ 10^7\ mc$ from left to right. The sharpness of the transition suggests that the small perturbations of the parameters make the solution fall on one of the two sides.

by an effective compression factor felt by the particles of given momentum, and the velocity in the precursor increases with the distance from the shock, it is easy to infer that the spectrum of the accelerated particles is not expected to be a power law and more precisely that it should be concave (steeper at low energies and flatter at high energies). Here we discuss the detailed shape of the spectrum at the shock as obtained through the kinetic approach described above. In Fig. 2.6 (left panel) we plot the spectra as a function of the momentum of particles (dashed lines). The curves are obtained for $p_{max} = 10^5 m_p c$, $u_0 = 5 \times 10^8$cm s^{-1}, $\xi = 3.5$ and for the values of the Mach number at upstream infinity as indicated in the figure ($M_0 = 10$, 100, 1000). Solid lines show the same results for an alternative and more sophisticated kinetic model presented by Amato & Blasi (2005) (to make a long story short: this latter model does not adopt the approximation given by Eq. 2.21 and thus is more accurate than the model presented in the previous sections). The agreement between the two sets of curves is excellent for relatively low Mach numbers ($M_0 \sim 10$) and remains good even up to much larger Mach numbers, and in fact for all values we have tried. The largest discrepancies between the two methods are at the level of $\sim 20\%$. Thus, the approximate method used here can be safely adopted.

The velocity profile of the fluid in the precursor is plotted in Fig. 2.6 (right panel) with dashed lines. Again, solid lines refer to the model by Amato & Blasi (2005).

On the x-axis we plot the distance x from the shock in the upstream region in

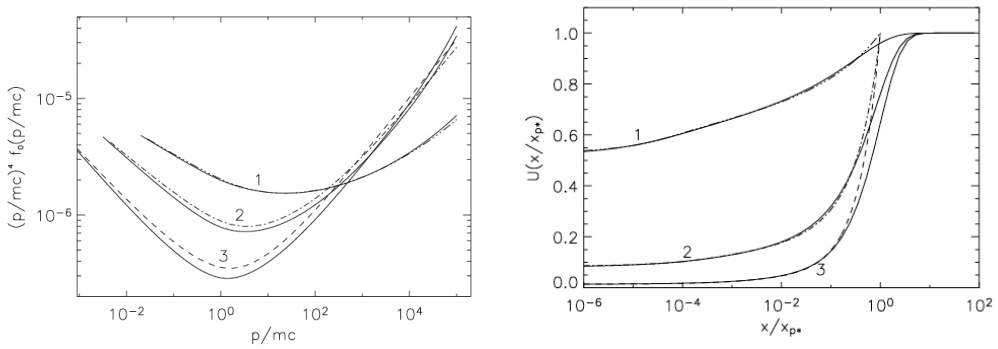

Figure 2.6: *Left Panel:* Spectra of accelerated particles for $p_{max} = 10^5 m_p c$, $u_0 = 5 \times 10^8$cm s^{-1}, $\xi = 3.5$ and for $M_0 = 10, 100, 1000$ (dashed lines 1, 2, and 3, respectively). As a comparison, the solid lines are obtained with the calculation of Amato & Blasi (2005). *Right Panel:* Velocity profiles in the precursor for the cases in the left panel.

units of $x_{p_{max}}$, which is defined as

$$|x_{p_{max}}| = \frac{D(p_{max})}{u_0 U_p(p_{max})}.$$

Some comments are required on the calculation of $U(x)$. As discussed in the previous section, our model does not keep any information about the spatial dependence of the quantities in the precursor, although such information is somehow contained in the relation between a momentum p and the mean diffusion length of particles with such momentum, $|x(p)| \approx D(p)/u_p(p)$. The dashed lines in Fig. 2.6 (right panel) are obtained in the following way: for a given location x upstream, the equation $x = D(p)/u_p(p)$ is inverted and a corresponding value p of the minimum momentum of particles that may have diffused to the point x is obtained. At this point the velocity $U(x)$ (in units of u_0) is by definition $U_p(p)$ for the value of p corresponding to x. By definition the fluid velocity in this simplified model is bound to be unity at $x/x_{p_{max}} = 1$ because no particles are supposed to be able to reach farther regions. In reality, there is a spread in the distances that can be diffusively reached at given momentum and the transition to $U(x) = 1$ is smoother (this is shown by the solid lines). This difference in the velocity profile affects mainly the results for the spectrum at $p \sim p_{max}$, but since these particles carry an appreciable amount of energy in the case of modified shocks, the whole spectral shape is somewhat affected (at the level of at most $\sim 20\%$ in the strongly modified cases).

It is interesting to note that the concavity in the particle spectra become more and more pronounced for larger Mach numbers. The modification in the particle spectrum with respect to the E^{-2} (or p^{-4}) behavior expected in the linear case will affect also the expected spectrum of the gamma ray emission resulting from proton-proton interactions between the accelerated particles and the ambient gas. This aspect will be treated in the next Chapter.

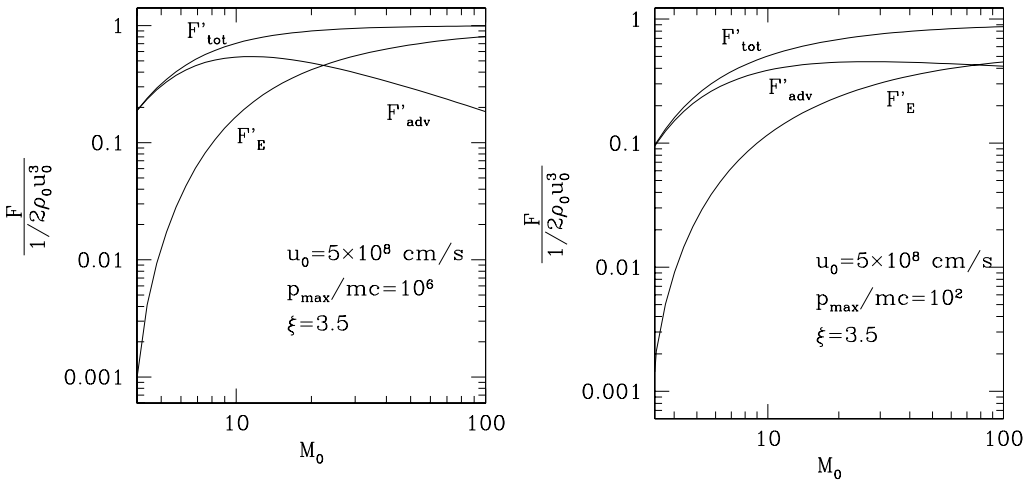

Figure 2.7: Escaping flux (F'_E), advected flux (F'_{adv}) and the sum of the two (F'_{tot}) normalized to the incoming flux $(1/2)\rho_0 u_0^3$, as functions of the Mach number at upstream infinity M_0. Left panel: $u_0 = 5 \times 10^8$ cm s^{-1}, $p_{max} = 10^6\ mc$ and $\xi = 3.5$. Right Panel: $u_0 = 5 \times 10^8$ cm s^{-1}, $p_{max} = 10^2\ mc$ and $\xi = 3.5$.

2.4.2 Escaping flux of accelerated particles

It is rather remarkable that the kinetic model described here does not require explicitly the use of the equation for energy flux conservation. However, once the solution of the kinetic problem has been found, the equation for conservation of the energy flux provides very useful information, as we show below. The equation can be written in the following form:

$$\frac{1}{2}\rho_2 u_2^3 + \frac{\gamma_g}{\gamma_g - 1} P_{g,2} u_2 + \frac{\gamma_c}{\gamma_c - 1} P_{c,2} u_2 = \frac{1}{2}\rho_0 u_0^3 + \frac{\gamma_g}{\gamma_g - 1} P_{g,0} u_0 - F_E, \qquad (2.32)$$

where F_E is the flux of particles escaping at the maximum momentum from the upstream section of the fluid (Berezhko & Ellison 1999). Notice that this term is usually neglected in the linear approach to particle acceleration at shock waves because the spectra are steep enough that, in most cases, we can neglect the flux of particles leaving the system at the maximum momentum. The fact that particles leave the system make the upstream fluid behave as a radiative fluid, and makes it more compressible. This is a crucial consequence of particle acceleration at modified shocks, and is shown here to be a natural consequence of energy conservation.

In Eq. 2.32 we can divide all terms by $(1/2)\rho_0 u_0^3$ and calculate the normalized escaping flux:

$$F'_E = 1 - \frac{1}{R_{tot}^2} + \frac{2}{M_0^2(\gamma_g - 1)} - \frac{2}{R_{tot}} \frac{\gamma_g}{\gamma_g - 1} \frac{P_{g,2}}{\rho_0 u_0^2} - \frac{2}{R_{tot}} \frac{\gamma_c}{\gamma_c - 1} \frac{P_{c,2}}{\rho_0 u_0^2}. \qquad (2.33)$$

From momentum conservation at the subshock we also have:

$$\frac{P_{c,2}}{\rho_0 u_0^2} = \frac{R_{sub}}{R_{tot}} - \frac{1}{R_{tot}} + \frac{1}{\gamma_g M_0^2}\left(\frac{R_{sub}}{R_{tot}}\right)^{-\gamma_g}, \tag{2.34}$$

so that the escaping flux only depends upon the *environment* parameters (for instance the Mach number at upstream infinity) and the compression parameter R_{sub} which is part of the solution. Note also that the adiabatic index for cosmic rays, γ_c, is here calculated self-consistently as:

$$\gamma_c = 1 + \frac{P_c}{E_c} = 1 + \frac{\frac{1}{3}\int_{p_{inj}}^{p_{max}} dp 4\pi p^3 v(p) f_0(p)}{\int_{p_{inj}}^{p_{max}} dp 4\pi p^2 f_0(p)\epsilon(p)}, \tag{2.35}$$

where E_c is the energy density in the form of accelerated particles and $\epsilon(p)$ is the kinetic energy of a particle with momentum p. It can be easily seen that $\gamma_c \to 4/3$ when the energy budget is dominated by the particles with $p \sim p_{max}$ (namely for strongly modified shocks) and $\gamma_c \to 5/3$ for weakly modified shocks. In Eq. 2.33 the term $F'_{adv} = \frac{2}{R_{tot}}\frac{\gamma_c}{\gamma_c - 1}\frac{P_{c,2}}{\rho_0 u_0^2}$ is clearly the fraction of flux which is advected downstream with the fluid.

In Fig. 2.7 we plot the escaping flux (F'_E), the advected flux (F'_{adv}) and the sum of the two (F'_{tot}) normalized to the incoming flux $(1/2)\rho_0 u_0^3$, as functions of the Mach number at upstream infinity M_0. Here we used $u_0 = 5 \times 10^8$ cm s^{-1}, and $\xi = 3.5$, while the maximum momentum has been chosen as $p_{max} = 10^6\ mc$ in the left panel and $p_{max} = 10^2\ mc$ in the right panel. Several comments are in order:

1) At low Mach numbers the escaping flux is inessential, as one would expect for a weakly modified shock. We recall that the escaping flux is due to the particles with momentum p_{max} leaving the system from upstream infinity. For a weakly modified shock at low Mach number the spectrum is steeper than E^{-2}, so that the energy carried by the highest energy particles is a small fraction of the total.

2) At large Mach numbers the shock becomes increasingly more cosmic ray dominated, and for the cases at hand the total efficiency gets very close to unity, meaning that the shock behaves as an extremely efficient accelerator. At Mach numbers around 4 on the other hand the total efficiency is around 20% for $p_{max} = 10^6\ mc$ and $\sim 10\%$ for $p_{max} = 10^2\ mc$, dropping fast below Mach number 4. Clearly the efficiency would be higher in this region for lower values of the parameter ξ.

3) Despite the fact that the total efficiency of the shock as a particle accelerator is close to unity at large Mach numbers, the fraction of the incoming energy which is actually advected toward downstream infinity is only $\sim 20\%$ at $M_0 \approx 100$ for $p_{max} = 10^6\ mc$. Most of the enegy flux in this case is in fact in the form of energy escaping from upstream infinity at the highest momentum p_{max}. For $p_{max} = 10^2\ mc$ the normalized advected flux roughly saturates at $\sim 40\%$

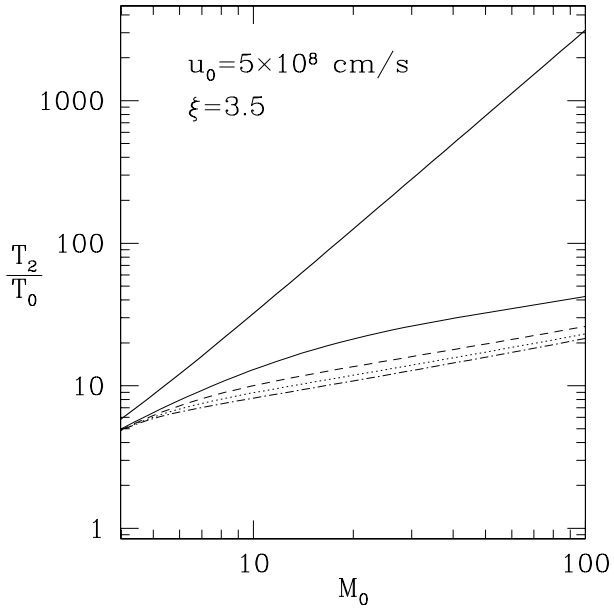

Figure 2.8: Temperature jump T_2/T_0 for $p_{max}/mc = 10^3$ (thin solid line), $p_{max}/mc = 10^5$ (dashed line), $p_{max}/mc = 10^7$ (dotted line) and $p_{max}/mc = 5 \times 10^{10}$ (dash-dotted line). The thick solid line shows the jump for ordinary shocks.

and is comparable with the escape flux at the same Mach number. For a distant observer these escaping particles would have a spectrum close to a delta function around p_{max}.

2.4.3 Shock heating in the presence of efficient particle acceleration

Energy conservation has the natural consequence that a smaller fraction of the kinetic energy of the fluid is converted into thermal energy of the downstream plasma in cosmic ray modified shocks, compared with the case of ordinary shocks. The reduction of the heating at nonlinear shock waves is fully confirmed by our calculation in the context of the injection recipe introduced in section 2.3. In Fig. 2.8 we plot the temperature jump between downstream infinity (at temperature T_2) and upstream infinity (at temperature T_0). The thick solid line is the jump as predicted by the standard Rankine-Hugoniot relations without cosmic rays. The other lines represent the temperature jump at cosmic ray modified shocks with $p_{max}/mc = 10^3$ (thin solid line), $p_{max}/mc = 10^5$ (dashed line), $p_{max}/mc = 10^7$ (dotted line) and $p_{max}/mc = 5 \times 10^{10}$ (dash-dotted line).

Such a drastic reduction of the downstream temperature is expected to reflect directly in the thermal emission of the downstream gas in those environments in which collisions are relevant. Note that for strongly modified shocks the compression factor between upstream infinity and downstream are much larger than for ordinary shocks, so that the downstream turns out to be denser but colder than in the linear

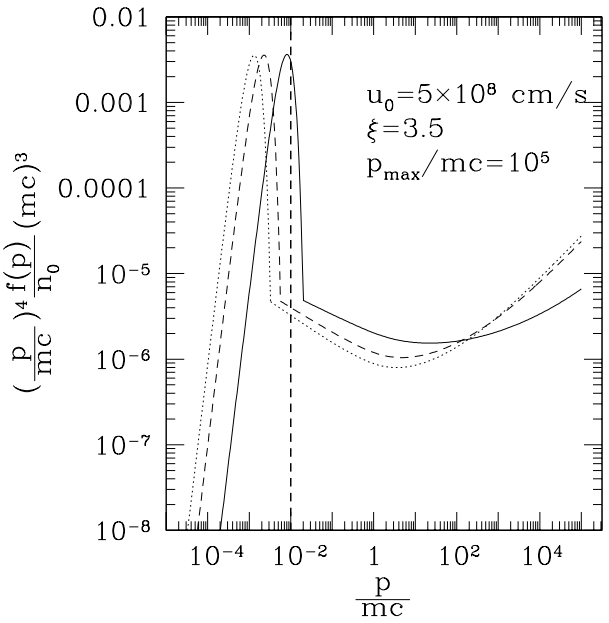

Figure 2.9: Particle Spectra (thermal plus non-thermal) for $M_0 = 10$ (solid line), $M_0 = 50$ (dashed line) and $M_0 = 100$ (dotted line). The vertical dashed line represents the position of the thermal peak for ordinary shocks (it is almost independent of the Mach number for large Mach numbers).

case. The missing energy ends up in the form of accelerated particles.

The effect of suppression of the heating in cosmic ray modified shocks also appears in the spectra of the particles (thermal plus non-thermal) in the shock vicinity. In Fig. 2.9 we show these spectra (including the maxwellian thermal bump) for $u_0 = 5 \times 10^8$ cm s^{-1}, $\xi = 3.5$ and $p_{max}/mc = 10^5$. The vertical dashed line shows the position of the thermal peak as expected in the absence of accelerated particles. In fact this position should depend on the Mach number, but the dependence is very weak for large Mach numbers. The positions of the thermal peaks clearly show the effect of cooler downstream gases for modified shocks. At the same time, the effect is accompanied by increasingly more modified spectra of accelerated particles, with most of the energy pushed toward the highest momenta.

2.5 Particle escape in a time dependent model: the case of supernova remnant shocks

In the previous sections we described the acceleration of particles at a planar and infinite (in both time and space) shock moving at a constant velocity. The maximum energy attainable by particles has been treated as a free parameter of the model. Moreover, the cosmic ray transport equation has been solved by assuming such maximum energy to be independent on time. On the other hand, if one considers the

case of particle acceleration in supernova remnants, one main difference needs to be pointed out. This is the fact that supernova remnant shocks are obviously finite in size and time, are (roughly) spherical, and are decelerated by the surrounding matter. This implies, as explained in Sec. 2.1, that the maximum energy of particles at the shock is determined by a geometric condition (i.e. particle's Larmor radius greater than shock radius) and is expected to decrease with time, roughly as $E_{max}(t) \propto t^{-1}$. If this happens, particles with energy above E_{max} which have been accelerated at earlier times, leave the remnant. Thus, at each time, the spectrum of runaway particles is monocromatic, i.e. close to a delta function in energy $\delta(E - E_{max}(t))$. It follows that, in order to obtain the total spectrum released in the interstellar medium by a supernova remnant during its whole lifetime, one has to integrate over time such delta function. A rigorous treatment of that can be found in Ptuskin & Zirakashvili (2005), and below we give only a simplified and qualitative derivation.

Let us consider an expanding supernova remnant shock. The kinetic energy flux across the shock is given by:

$$L_{kin} = \frac{1}{2}\varrho_{ISM} v_s^3 \left(4\pi R_s^2\right) \propto t^{-1} \ , \tag{2.36}$$

where v_s and R_s are the shock velocity and radius, and ϱ_{ISM} is the density of the interstellar medium. The scaling with time has been obtained by assuming that the remnant is in the Sedov-Taylor phase, i.e. $R_s \propto t^{2/5}$ and $u_s \propto t^{-3/5}$. A fraction of this energy is converted into cosmic rays. We assume here that a constant fraction of L_{kin} leaves the remnant in form of runaway cosmic rays. Thus, the energy in form of cosmic rays released in the interstellar medium over a time interval dt is proportional to $d\Phi_{esc} \propto t^{-1}dt$. We recall here that the particle energy of cosmic rays which are released in the interstellar medium decreases with time, and we parametrize this as $E_{max} \propto t^{-\delta}$ (see above). Under this circumstances, a time interval dt corresponds to an energy interval dE as:

$$dt \propto E^{-\frac{1}{\delta}-1} dE \tag{2.37}$$

and thus we can rewrite $d\Phi_{esc}$ as:

$$d\Phi_{esc} \propto t^{-1}dt \propto \left(E^{\frac{1}{\delta}}\right)\left(E^{-\frac{1}{\delta}-1}dE\right) = E^{-1}dE \ . \tag{2.38}$$

Remarkably, this expression does not depend on δ. Since $d\Phi_{esc}$ is an energy, the differential energy spectrum of runaway cosmic rays is given by:

$$N_{esc}(E) \propto \frac{1}{E}\frac{d\Phi_{esc}}{dE} \propto E^{-2} \ . \tag{2.39}$$

Though probably oversimplified, this argument should illustrate why supernova remnants are believed to release in the interstellar medium cosmic rays with a power law spectrum with index close to 2. It is quite remarkable that the shape of the spectrum of escaping particles is not depending on the details of the spectral shape of the cosmic rays at the shock (i.e. on its concavity due to non-linear effects).

The results presented in this chapter have been first published in:

- P. Blasi, S. Gabici & G. Vannoni, MNRAS **361**, 907 (2005)
- E. Amato, P. Blasi, & S. Gabici, MNRAS **385**, 1946 (2008)

Chapter 3

Multi-TeV emission from supernova remnants (and nearby molecular clouds): a conclusive test for cosmic ray origin?

3.1 Multi-TeV emission from supernova remnants and nearby molecular clouds

As said in the Introduction, SNRs are currently considered as the best-bet candidate sources to accelerate galactic CRs up to at least the energy of the CR knee, at $\sim 4 \times 10^{15}$eV $= 4$ PeV. If this is indeed the case, SNRs are expected to emit both gamma rays and neutrinos due to hadronic interactions between the accelerated CRs and the interstellar medium swept up by the shock wave. The detection of neutrinos would of course constitute an unambiguous proof of acceleration of protons in these objects. However, predictions of the neutrino fluxes from the most prominent SNRs in TeV gamma rays tell us that their detection remains challenging also for km^3-scale detectors (e.g. Kappes et al. 2007; Costantini & Vissani 2005).

On the other hand, the detection of SNRs in TeV gamma rays, though expected (and indeed detected from several objects) in this scenario, does not constitute *per se* a proof for the acceleration of protons. This is because competing processes, such as inverse Compton scattering, can also explain the observed emission (for a review see e.g. Aharonian et al. 2008b). However, as stressed in the Introduction, a decisive and unambiguous indication of acceleration of PeV protons in SNRs can be provided by observations of γ-rays at energies up to 100 TeV and beyond. Because of the Klein-Nishina effect the efficiency of inverse Compton scattering in this energy band is dramatically reduced. Therefore unlike other energy intervals, the interpretation of gamma-ray observations at these energies is free of confusion and reduces to the

only possible mechanism - decay of secondary π^0-meson. Although the potential of the current ground-based instruments for detection of such energetic gamma-rays is limited, it is expected that the next generation arrays of imaging Cherenkov telescopes, exploring a broad energy region extending up to the multi–TeV energy range will become powerful tools for this kind of studies.

It should be noted that the number of SNRs currently bright in > 10 TeV gamma rays is expected to be rather limited. Multi–PeV protons can be accelerated only during a relatively short period of the SNR evolution, namely, at the end of the free–expansion phase/beginning of the Sedov phase, when the shock velocity is high enough to allow sufficiently high acceleration rate. When the SNR enters the Sedov phase, the shock gradually slows down and correspondingly the maximum energy of the particles that can be confined within the SNR decreases. This determines the escape of the most energetic particles from the SNR (Ptuskin & Zirakashvili 2005). Thus, unless our theoretical understanding of particle acceleration at SNR is completely wrong, we should expect an energy spectrum of CR inside the SNR approaching PeV energies only at the beginning of the Sedov phase, typically for a time $\lesssim 1000$ years. When the remnant enters the Sedov phase, the high energy cutoffs in the spectra of both protons and gamma rays gradually moves to lower energies, while the highest energy particles leave the remnant (Ptuskin & Zirakashvili 2005). This can naturally explain why the gamma-ray spectrum of the best studied SNR RX J1713.7–3946 above 10 TeV becomes rather steep with photon index ≈ 3 (Aharonian et al. 2006a).

Here we suggest to search for multi–TeV gamma-rays generated by the CRs that escape the SNR. A molecular cloud located close to the SNR can provide an effective target for production of γ-rays (Aharonian & Atoyan 1996; Gabici & Aharonian 2007b; Gabici et al. 2009). The highest energy particles ($\sim$ few PeV) escape the shell first. Moreover, generally they diffuse in the interstellar medium faster than low energy particles. Therefore they arrive first to the cloud, producing there gamma rays and neutrinos with very hard energy spectra. Note that an association of SNRs with clouds is naturally expected, especially in star forming regions (Montmerle 1979). The duration of the gamma-ray emission in this case is determined by the time of propagation of CRs from the SNR to the cloud, which in turn depends on the value of the CR diffusion coefficient in the vicinity of the SNR. It is a very well known fact that the CR diffusion coefficient at specific locations in the Galaxy is very poorly constrained from observations (but see Chapters 4 and 5 for perspectives in this direction), and theoretical predictions are still far from giving solid and reliable estimates for this quantity. However, it is often believed that the CR diffusion coefficient in the vicinity of CR sources might be suppressed with respect to the average galactic one (i.e. the one determined from CR spallation measurements) due to CR streaming instability (e.g. Wentzel 1974; Cesarsky 1980). This CR-induced instability would increase the magnetic turbulence and in turn suppress the diffusion of CRs themselves (see Ptuskin et al. 2008, for an attempt to quantify this effect). Therefore the gamma-ray emission of the cloud may last much longer than the emission of the SNR itself. This makes the detection of delayed gamma-ray

and neutrino signals from clouds more probable. The detection of these multi–TeV gamma-rays from nearby clouds would thus indicate that the nearby SNR in the past was acting as an effective CR PeVatron. In the following section, a model is developed to investigate this possibility.

3.1.1 The model

Consider a supernova of total energy $10^{51}E_{51}$ erg exploding in a medium of density n cm^{-3}. The initial shock velocity is $10^9 u_9$ cm/s and remains roughly constant until the mass of the swept up material equals the mass of the ejecta. This happens at a time $t_{Sedov} \approx 200[E_{51}/(n\,u_9^5)]^{1/3}$yr, when the shock radius is $\approx 2.1[E_{51}/(n\,u_9^2)]^{1/3}$pc. Then the SNR enters the Sedov phase and the shock radius and velocity scales with time as $R_{sh} \propto t^{2/5}$ and $u_{sh} \propto t^{-3/5}$.

The spectrum of particles accelerated at the SNR shock is determined by the transport equation (e.g., Drury 1983):

$$\frac{\partial f}{\partial t} - \nabla D \nabla f + \mathbf{u}\nabla f - \frac{\nabla \mathbf{u}}{3} p \frac{\partial f}{\partial p} = 0. \tag{3.1}$$

where $D = D(p)$ is the momentum dependent diffusion coefficient and $\mathbf{u}$ the flow velocity. For a strong shock with compression factor $r_s = 4$, the test particle theory predicts an universal shape for the CR spectrum at the shock $f_0(p) \propto p^{-4}$ (e.g Drury 1983). If the shock is an efficient accelerator (as SNR shocks are believed to be), the CR pressure modifies the flow structure, making the shock more compressible and the spectrum of the accelerated particles harder, $f_0(p) \propto p^{-\alpha}$ with $3.5 \lesssim \alpha \leq 4$ (e.g. Malkov & O'C Drury 2001, and Chapter 2). Detailed calculations compared with multiwavelength observations of SNRs suggest the values $r_s \approx 7$ and $\alpha \approx 3.7$ (e.g. Ellison et al. 2007; Berezhko & Völk 2006), which we adopt in the following.

The maximum momentum of the accelerated particles is determined by a confinement condition, namely that the diffusion length l_d of the particles cannot exceed the characteristic size of the system R_{sh}:

$$l_d = \frac{D(p_{max})}{u_{sh}} \lesssim R_{sh}. \tag{3.2}$$

The maximum possible energies are achieved when the acceleration proceeds in the Bohm diffusion limit, $D \propto p/B_{sh}$, with B_{sh} the magnetic field strength at the shock. In this case the maximum momentum decreases with time as $p_{max}(t) \propto B_{sh} t^{-1/5}$. In fact, the drop of p_{max} is even faster, given that the magnetic field is also expected to decrease with time. This implies that at any time, particles with momentum above $p_{max}(t)$ quickly escape the remnant, generating a cutoff in the spectrum. The spectrum of the runaway particles can be approximated as a δ–function (see Ptuskin & Zirakashvili 2005):

$$q_{esc}(p,t) = -\delta(p - p_{max}) \times \int_0^\infty d^3R \left(\frac{\partial p_{max}}{\partial t} + \frac{\nabla \mathbf{u}}{3} p_{max} \right) f(p_{max}, R) \tag{3.3}$$

where the integration has to be performed where the integrand is negative. Thus, to calculate the flux of the runaway particles one has to know: *(i)* the CR particle distribution function at p_{max} at any location in the SNR, *(ii)* the flow velocity both inside the shock and outside it, where the CR precursor forms and *(iii)* how the maximum momentum varies during the SNR evolution. Ptuskin and Zirakashvili (2005) showed that it is straigthforward to derive *(i)* and *(ii)* using an approximate (but still reasonably accurate) linear velocity profile inside the SNR :

$$u = \left(1 - \frac{1}{r_s}\right) \frac{u_{sh}(t)}{R_{sh}(t)} R \tag{3.4}$$

and assuming that the CR pressure at the shock P_{sh}^{CR} is a fraction ξ_{CR} of the incoming ram pressure ϱu_{sh}^2 and that $f_0(p_{max}) \propto P_{sh}^{CR}$.

The determination of p_{max} and its evolution with time requires the knowledge of the diffusion coefficient (see Eq. 3.2), which is in turn determined by the level of magnetic turbulence generated by the accelerated particles themselves. This makes the problem nonlinear and very difficult to be solved. The value of p_{max} depends on a few crucial but poorly known aspects of the problem, including the nature of CR–driven instability operating in the shock precursor and the level of wave damping (Bell 1978, 2004). Because of these uncertainties, we adopt here a phenomenological approach, namely we parametrize the maximum momentum as $p_{max}(t) \propto t^{-\delta}$. We further assume $p_{max} \sim 5$ PeV and ~ 1 GeV at the early ($t = 200$ yr) and late ($t = 5 \times 10^4$ yr) epochs of the Sedov phase respectively. This requires $\delta \approx 2.48$. Remarkably, if the maximum momentum is a power law function of time, the spectrum of the escaping particles integrated over the whole Sedov phase is also a power law of the form $\propto p^{-4}$ (see Ptuskin & Zirakashvili 2005, and Section 2.5), which is close (sligthly harder) to what needed to fit the CR data below the knee (Berezinskii et al. 1990).

Following Ptuskin & Zirakashvili (2005), the approximate spectrum of the CRs inside the SNR $f_{in}(R, p, t)$ can be obtained from Eq. 3.1 by dropping the diffusion term, while the spectrum of the runaway CRs at a given distance R from the SNR and at a given time t can be obtained by solving the diffusion equation:

$$\frac{\partial f_{out}}{\partial t}(R, p, t) = D_{ISM}(p) \nabla^2 f_{out}(R, p, t) + q_{esc}(p, t) \delta(R). \tag{3.5}$$

The diffusion coefficient $D_{ISM}(p)$ describes the propagation of CRs in the galactic disk. The available CR data require a power–law energy dependence, $D_{ISM}(E) \propto E^{-s}$, with $D_{ISM} \approx 10^{28} \mathrm{cm}^2/\mathrm{s}$ at $E \approx 10$ GeV and $s \approx 0.3 \div 0.7$ (Berezinskii et al. 1990). The constraints on the diffusion coefficient are obtained from the comparison between diffusion models and CR data and have to be considered as average galactic values. However, the conditions might be rather different in regions close to CR sources, in particular due to the presence of strong gradients in the CR distribution, which may enhance the generation of plasma waves and thus suppress the diffusion coefficient (Wentzel 1974; Cesarsky 1980; Ptuskin et al. 2008). The change in s within the allowed range or the choice of a different normalization for D_{ISM} does

not alter qualitatively the results, the main effect being that the characteristic time scales of the problem change proportional to $1/D_{ISM}$.

Remarkably, if $p_{max}(t)$ scales as a power law of time, Eq. 3.5 can be solved analytically and the distribution function of escaping cosmic rays at any given distance R from the SNR and at any given time t reads, for energies $E \geq c \times p_{max}(t)$:

$$f_{out}(t, R, E) = \frac{\eta E_{SN}}{\pi^{3/2} \ln(E_{MAX}/E_{MIN})} \frac{e^{-(\frac{R}{R_d})^2}}{R_d^3} E^{-2} \tag{3.6}$$

where E_{SN} is the total supernova explosion energy, η is the fraction of such energy converted into CRs and E_{MAX} and E_{MIN} are the maximum and minimum energies of CRs accelerated during the Sedov phase. The diffusion distance for a CR of energy E is:

$$R_d(E) = \sqrt{4D(E)(t - \chi(E))} \tag{3.7}$$

where

$$\chi(E) = t_{Sedov} \left(\frac{E}{E_{MAX}} \right)^{-1/\delta} \tag{3.8}$$

represents the time after the supernova explosion at which CRs with energy E are released in the interstellar medium. The solution derived by Ptuskin and Zirakashvili (2005) for the total CR spectrum injected by a SNR in the interstellar medium during the whole Sedov phase can be easily derived by integrating Eq. 3.6 over space. Finally, it has to be noticed that the total CR spectrum at a given time and at a given distance from the SNR is the sum of two contributions: *i)* a time dependent contribution from CRs coming from the SNR, whose spectrum is described by Eq. 3.6 and *ii)* a steady contribution from the galactic CR background.

Following the procedure described above, it is possible to evaluate, for any given time, the CR spectrum in proximity of a molecular cloud located at a given distance from the SNR. If the diffusion coefficient inside the cloud is not significantly smaller than the Galactic one, CR freely penetrate the cloud and the CR spectrum inside the cloud is not affected by propagation effects. Conversely, if the diffusion coefficient is significantly (more than one order of magnitude) reduced, low energy CRs are excluded from the cloud and a low energy cutoff appears in the CR spectrum, at an energy that depends on the value of the diffusion coefficient (see Gabici et al. 2007, and Chapter 6 for details). Here, we assume free penetration of CRs and we refer the reader to Gabici et al. (2007) (and references therein) for a detailed discussion on CR exclusions from molecular clouds. We do not consider here any contribution from CR electrons coming from the SNR, since they do not escape the remnant due to diffusive confinement (for low energy electrons) and severe synchrotron losses in the strong magnetic field (for high energy electrons).

3.1.2 Results

The top panel of Fig. 3.1 shows the energy spectrum of gamma-ray emission from a SNR produced by interactions of accelerated protons with ambient medium, calculated for typical parameters characterizing SNRs: $E_{51} = n = u_9 = 1$. The bottom

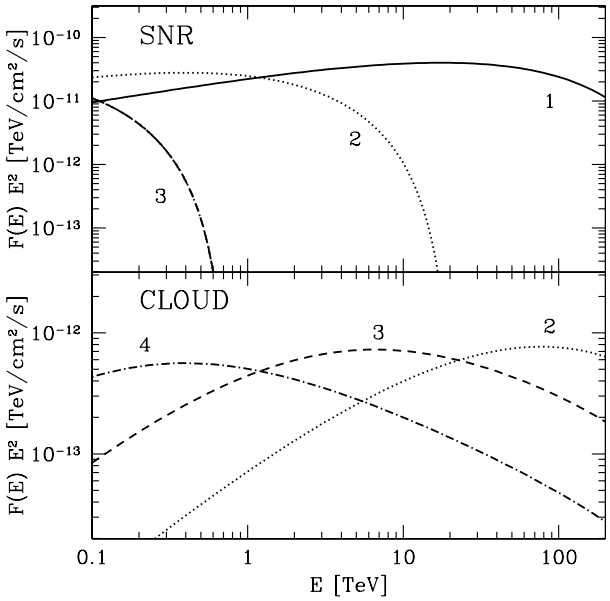

Figure 3.1: Gamma ray spectra from the SNR (TOP) and from a cloud of $10^4 M_\odot$ located 100 pc away from the SNR (BOTTOM). The distance is 1 kpc. Curves refer to different times after the explosion: 400 (curve 1), 2000 (2), 8000 (3), $3.2\,10^4$ (4) yr.

panel shows the emission from a cloud of mass $M_{cl} = 10^4 M_\odot$ located at a distance $d_{cl} = 100$ pc away from the SNR. Gamma ray spectra have been calculated following Kelner et al. (2006). The distance of the SNR is assumed $D = 1$ kpc and different curves refer to different times after the supernova explosion. The efficiency of CR acceleration at the SNR shock is regulated by the parameter ξ_{CR} (the ratio between the CR pressure at the shock to the shock ram pressure), which is assumed to be equal to 0.3 and constant during the SNR evolution. This assumption is reasonable for strong shocks, for which the acceleration efficiency saturates to very high values (see Chapter 2), and it becomes less reliable in the late stages of the Sedov phase, when the SNR shock becomes progressively weaker. Finally, we assume a value of the diffusion coefficient equal to $D_{ISM} = 3 \times 10^{29} (E/1\ PeV)^{0.5} \mathrm{cm}^2/\mathrm{s}$, which is significantly suppressed with respect to the extrapolation at PeV energies of the average galactic one.

Early in the Sedov phase (curve 1, 400 yr after the explosion), the gamma-ray spectrum from the SNR is hard and extends up to $\gtrsim 100$ TeV, revealing the acceleration of PeV particles. The hardness of the spectrum reflects the fact that, due to nonlinear effects in particle acceleration, the underlying CR spectrum becomes harder than $p^2 f_0(p) \propto p^{-2}$. Conversely, the gamma-ray flux from the cloud is extremely weak, because for the epoch of 400 yr after the explosion CRs do not have sufficient time to reach the cloud. The emission of $\gtrsim 100$ TeV photons from

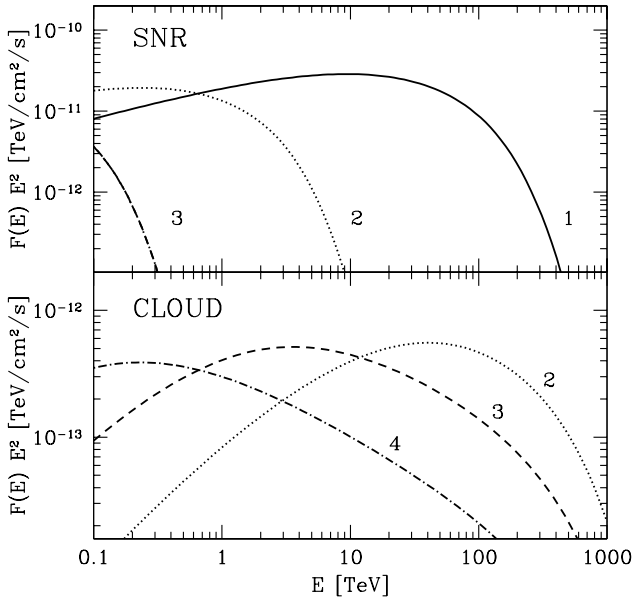

Figure 3.2: Muonic neutrino spectra from the SNR (TOP) and from the cloud (BOTTOM) for the same set of parameters of Fig. 3.1. Neutrino oscillations are not taken into account.

the SNR lasts a few hundreds years, and after that the cutoff in the gamma-ray spectrum moves to lower energies (curves 2, 3 and 4 correspond to the epochs of 2×10^3, 8×10^3 and 3.2×10^4 yr after the explosion). As time passes, CRs finally reach the cloud and produce there gamma rays when interacting with the dense cloud environment. This makes the cloud an effective multi–TeV gamma-ray emitter, with a flux at the sensitivity level of next generation Cherenkov telescopes operating in that energy range. As lower and lower energy particles reach the cloud, the peak of the gamma-ray emission accordingly shifts towards the lower, TeV and GeV, energies at flux levels which can be probed by ground based instruments and *Fermi*.

The shape of the gamma-ray spectrum is naturally explained as follows: at a time t, only particles with energy above E_*, given by $d_{cl} \approx \sqrt{6 D_{ISM}(E_*) t}$, reach the cloud. Thus the CR spectrum inside the cloud has a sharp low energy cutoff at E_*. The corresponding gamma-ray spectrum exhibits a prominent peak at the energy $\approx 0.1 E_*$.

The multi-TeV hadronic gamma-ray emission from the cloud is significantly weaker than the one from the SNR, but its detection might be easier because of its longer duration ($\lesssim 10^4$ yr versus few hundreds years). Moreover, the leptonic contribution to the cloud emission is likely to be negligible. Electrons accelerated at the SNR cannot reach the cloud because they remain confined in the SNR due to severe synchrotron losses. Secondary electrons can be produced in the cloud, but they cool mainly via synchrotron emission in the cloud magnetic field $\sim 10 \div 100 \mu G$ (Crutcher 1999). This makes the production of $\gtrsim$ TeV gamma rays due to inverse

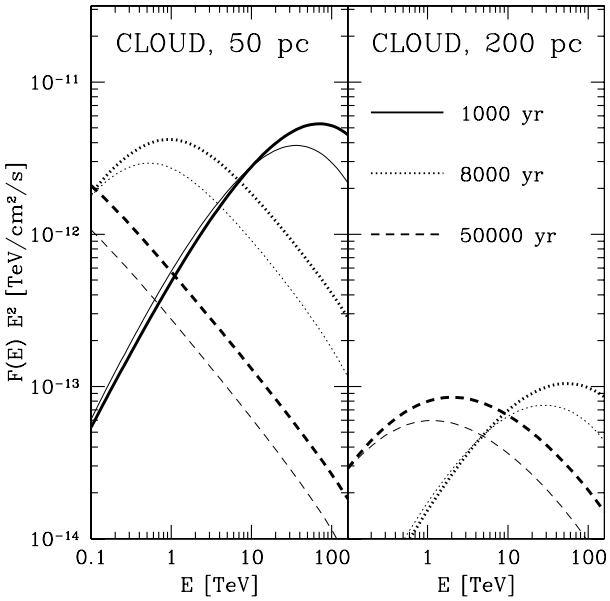

Figure 3.3: Gamma ray (thick lines) and neutrino (thin lines) spectra from a cloud located at 50 (left) and 200 pc (right) from the SNR. Different curves refer to different times after the explosion.

Compton scattering and non–thermal Bremsstrahlung negligible.

Fig. 3.2 shows the muonic neutrino fluxes from the SNR (top panel) and the cloud (bottom panel) for the same parameters adopted in Fig. 3.1. The flux at Earth is a factor of ≈ 2 smaller than what showed due to neutrino oscillations. For a young SNR (curve 1), the spectrum extends up to ~ 100 TeV, where km^3–scale neutrino telescopes achieve their best performance. The flux level is $\gtrsim 10^{-11}$TeVcm^{-2}s^{-1}, which makes such sources detectable in several years, and this is in agreement with earlier predictions (Costantini & Vissani 2005). Unfortunately, the high energy cutoff in the neutrino spectrum moves fast towards low energies (curves 2 and 3), making the detection more problematic for older SNRs. Note that the gamma ray and neutrino fluxes from the SNR itself and from the cloud scale as n/D^2 and M_{cl}/D^2 respectively. Thus, the presence of a very massive molecular cloud with mass $M_{cl} \sim 10^5 M_\odot$ would considerably increase the chances of detection of multi-TeV gamma rays and neutrinos from such systems.

The impact of the distance between the SNR and the cloud on the flux of gamma ray and neutrino emission is illustrated in Fig. 3.3, where gamma ray (thick lines) and neutrino (thin lines) spectra are shown for a cloud at a distance of 50 and 200 pc from the SNR. Note that the neutrino flux of the cloud may become marginally detectable only if the cloud is very close to the SNR. On the other hand, clouds can be detectable in gamma rays even if their distance from the SNR is as large as ~ 200 pc (right panel). Remarkably, the TeV emission from the cloud lasts $\gtrsim 10^4$

yr, significantly longer than the emission from the SNR.

To conclude, the acceleration of CRs up to the knee in SNRs can be unambiguously revealed by means of observations of multi-TeV gamma rays and neutrinos coming from the SNR and nearby molecular clouds. The emission from the clouds is weaker than the one from the SNR, but may last much longer, depending on the actual value of the diffusion coefficient, and this might significantly enhance the probability of detection. Both gamma rays and neutrinos are emitted with fluxes detectable by currently operating and forthcoming instruments. Since the gamma-ray spectra from clouds are extremely hard, gamma-ray telescopes operating at very high energies ($\gtrsim$ 10 TeV), like the Cherenkov Telescope Array, would be the best instruments for this kind of study. For neutrinos, detections are possible but remain challenging, and for this reason in the next section we examine in detail the conditions for detectability of neutrino sources with km^3-scale telescopes such as *Icecube* or *KM3NeT*

3.2 Capabilities of neutrino telescopes

As a rule of thumb, km^3–scale neutrino telescopes can detect a persistent and point–like source at a flux level of $\approx 10^{-11}\nu$ cm^{-2} s^{-1} after a few years of continuous observations. This flux is the total flux integrated above $\approx$ 1 TeV and roughly corresponds to the observed flux of the Crab nebula in gamma rays, and is also comparable to the most optimistic predictions made in the previous section. An accurate determination of the detection rate from a Crab-like source of neutrinos can be obtained by considering the telescope's effective area and the spectrum of the neutrinos received by the source. The rate obtained in this way has to be compared with the detection rate of atmospheric neutrinos, which constitute the dominant background. All these aspects will determine which is the optimal energy range for the detection of astrophysical neutrinos.

As an illustrative example, we consider here a hypothetical point–like and steady source of neutrinos with differential flux:

$$J(E) = J_0 \left(\frac{E}{\mathrm{TeV}}\right)^{-\alpha} e^{(-E/E_{\mathrm{cut}})} \tag{3.9}$$

with J_0 normalised such that the integrated flux above 1 TeV is 10^{-11} cm^{-2} s^{-1}. α and E_{cut} are free parameters. For the effective area we used the one provided in the Conceptual Design Report for the KM3NeT infrastructure [1] and in Kappes et al. (2007). In the calculations, we used a convenient fit to the effective area which reads:

$$A_{\mathrm{eff}}(E) = 10^{4.7}\ E^{3.4}\ \left(\frac{0.24}{0.24+E}\right)\ \left(\frac{0.31}{0.31+E}\right)\ \left(\frac{37}{37+E}\right)\ \mathrm{cm}^2 \tag{3.10}$$

where E is the neutrino energy in TeV. The product between the effective area and the neutrino flux within one angular resolution element results in the expected

[1] downloadable at http://www.km3net.org/CDR/CDR-KM3NeT.pdf

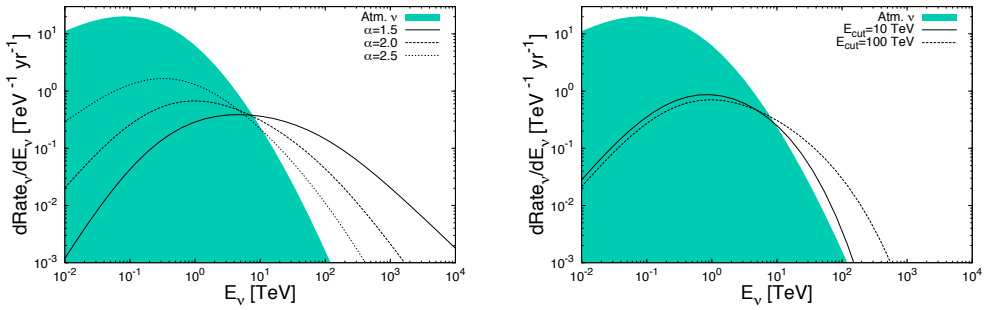

Figure 3.4: Differential detection rates for neutrino sources with flux $F(> 1\ TeV) = 10^{-11}\nu$ cm^{-2} s^{-1}. The dashed region represents atmospheric neutrinos. **Left panel:** Solid, dashed and dotted lines represent the count rates for neutrino sources with power law spectrum with slope 1.5, 2 and 2.5 respectively and high energy cutoff at $E \gg 1$PeV. **Right panel:** Count rates for neutrino sources with $\propto E^{-2}$ spectra and exponential cutoff at $E_{\rm cut} = 10$ and 100 TeV (solid and dashed line respectively). Figures from Gabici et al. (2008).

differential detection rate by KM3NeT, and it is shown in Fig. 3.4. Rates are defined as the number of neutrinos detected after one year of exposure.

In the left panel of Fig. 3.4 we demonstrate the effect of changing the spectral slope of the neutrino source. The solid, dashed and dotted curves refer respectively to $\alpha = 1.5$, 2 and 2.5, that cover the most plausible spectra for neutrino sources. The position of the exponential cutoff is $E_{\rm cut} \gg 1$ PeV. In the right panel we fix α =2 and we change the energy at which the spectrum cuts off. Solid and dashed lines refer to $E_{\rm cut} = 10$ and 100 TeV respectively. In both the plots the shaded region represents the level of the atmospheric neutrino background, assumed to follow the spectrum predicted in Volkova (1980). The resulting atmospheric background rate is shown to be consistent with Barr et al. (1989); Gaisser & Stanev (1995); Honda et al. (1995). The adopted atmospheric background assumed a zenith angle of $\sim 70°$. The energy resolution of the detector is assumed to be constant across the entire energy range. It is accounted for by convolving the contents of each energy bin with a Gaussian distributed in logarithmic energy space. The Gaussian has an RMS in the difference between the natural logarithm of the reconstructed and true neutrino energies of 0.3. The angular resolution of the detector is given by a parameterisation of the RMS difference between the reconstructed neutrino direction and the true neutrino direction from the same simulations used to produce the effective area curve (see Conceptual Design Report), and above 1 TeV drops below 0.2°. In these generic plots it is assumed the source is point-like, and both the signal and background neutrino fluxes are integrated across a cone of optimal opening angle 1.58 times the angular resolution (Alexandreas et al. 1993).

It is evident from Fig. 3.4 that the prospects for km^3 size neutrino telescopes to

detect such fluxes are optimal in the 10-1000 TeV energy range, where the signal flux is well above that due to atmospheric background events and the effective area grows sufficiently quickly with energy for detection to be possible. This result comes with the caveat that the cutoff energy of the flux, $E_{\rm cut}$, sits at sufficiently high energies (>100 TeV). Thus, the best targets for neutrino telescopes are sources exhibiting a hard spectrum which extends up to at least hundreds of TeV, which are the characteristics of the spectra predicted in the previous section for molecular clouds illuminated by CRs from a nearby SNR. However, fluxes of the order of 1 Crab unit or more are required in order to have a meaningful detection.

The results presented in this chapter have been first published in:

- S. Gabici, & F.A. Aharonian, ApJ Lett., **665**, L131 (2007)
- S. Gabici, A.M. Taylor, R.J. White, S. Casanova, & F.A. Aharonian, Astropart. Phys., **30**, 180 (2008)

Chapter 4

How to use molecular clouds to constrain the propagation of cosmic rays in the Galaxy

In the previous Chapter we showed how the detection of molecular clouds in gamma rays can serve to identify excesses of the CR intensity at specific locations in the Galaxy. These excesses would reveal the presence of an accelerator of CRs in the vicinity of the cloud. With this respect, the CR diffusion coefficient is a crucial quantity in determining most of the characteristics of the gamma ray emission from the cloud. For example, the expected duration of the gamma ray emission from a cloud is proportional to the diffusion time of CRs, which scales like the inverse of the diffusion coefficient. Thus, suppressing (enhancing) the diffusion of CRs would increase (decrease) the duration of the gamma ray emission from a given cloud, and this in turn would increase (decrease) the number of such clouds that one might expect to see with a given telescope. Moreover, it is a very well known fact that also the spectrum of the expected gamma ray emission strongly depends on the diffusion coefficient or, more precisely, on the way in which the diffusion coefficient depends on energy. For these reasons, observations of molecular clouds illuminated by CRs coming from nearby accelerators can be used as a powerful tool to constrain the value of the diffusion coefficient at specific locations in the Galaxy. This would be of great importance, since our knowledge of the diffusion coefficient (both from a theoretical and observational point of view) is very poor, and basically limited to its average value in the galactic disk (see Introduction).

However, in order to obtain meaningful constraints on the diffusion coefficient, a realistic model for the CR acceleration itself is needed. This model would give us the spectrum of the CR injected in the interstellar medium by the accelerator, and the rate at which particles are released. In the previous Chapter, we considered the case of SNRs, which are generally believed to be the sources of CRs. The present understanding of these objects is, we feel, good enough to allow a satisfactorily realistic and accurate modeling of their main physical properties. Here, we develop in more details the model presented in the previous Chapter. We consider again

the case of a molecular cloud located in the vicinity of a SNR, and we extend the predictions for the radiation from the cloud to encompass the whole electromagnetic spectrum, from radio waves to multi-TeV photons. Once developed, the model will be applied in the next Chapter to two specific SNRs (the SNRs RX J1713.7-3946 and W28) and in one case an attempt will be made to constrain the CR diffusion coefficient.

In order to extend our predictions to lower photon energies (from GeV down to the radio band), we will need to make a significant addiction to our model. This is because CR protons propagating inside a molecular cloud produce not only gamma rays, but also secondary electrons and positrons during inelastic interactions in the dense intercloud medium. These electrons in turn produce synchrotron and Bremsstrahlung photons over a broad energy range. Thus, in the following we calculate the spectrum of the injected secondary electrons $Q_e(t, E)$ by using the parameterization given by Kelner et al. (2006) and we then follow the time evolution of the electron distribution function $f_e(t, E)$ by solving the equation:

$$\frac{\partial f_e(t,E)}{\partial t} = \frac{\partial}{\partial E}\left[\left(\frac{dE}{dt}\right)_e f_e(t,E)\right] + Q_e(t,E) - \frac{f_e(t,E)}{\tau^e_{esc}} \tag{4.1}$$

where $(dE/dt)_e = E/\tau^e_{loss}$ is the energy loss rate for electrons, τ^e_{loss} the energy loss time, and τ^e_{esc} the diffusive escape time from the cloud. All these time scales will be discussed and estimated in the following. Once both the proton and electron CR spectra have been derived, the non-thermal radiation from the molecular cloud can be calculated.

4.1 Cosmic ray spectrum at the cloud location

We consider here a molecular cloud located at a given distance d_{cl} from a SNR and we calculate the CR spectrum at the cloud location. The spectrum is the sum of two disctinct components: *i)* the CRs coming from the nearby SNR, described by Eq. 3.6, and *ii)* the galactic CR background, which results from the superposition of all the CR sources in the Galaxy. While the latter contribution is constant in time, the first one changes, since the flux of CRs escaping from the SNR evolves in time as described in Sec. 3.1.1.

Fig. 4.1 shows the spectrum of CRs at the location of the molecular cloud. The Galactic CR background is plotted as a thin dot–dashed line labeled as *CR sea*, while the spectrum of the CRs coming from the SNR is plotted as a thin line for different times after the supernova explosion: 2000 yr (solid), 8000 yr (short – dashed), and 32000 yr (long–dashed). Thick lines represent the sum of the two contributions. The distance between the SNR and the molecular cloud is 50 pc (left panel) and 100 pc (right panel). We assume a total supernova explosion energy of 10^{51} ergs and a high CR acceleration efficiency at the SNR shock equal to $\eta = 30\%$. The normalization of the CR spectrum at the cloud scales linearly with these two quantities [1]. The

[1]This is true only as a first approxiamation for the parameter η, since the estimated flux of particles escaping the SNR comes from a nonlinear theory of shock acceleration

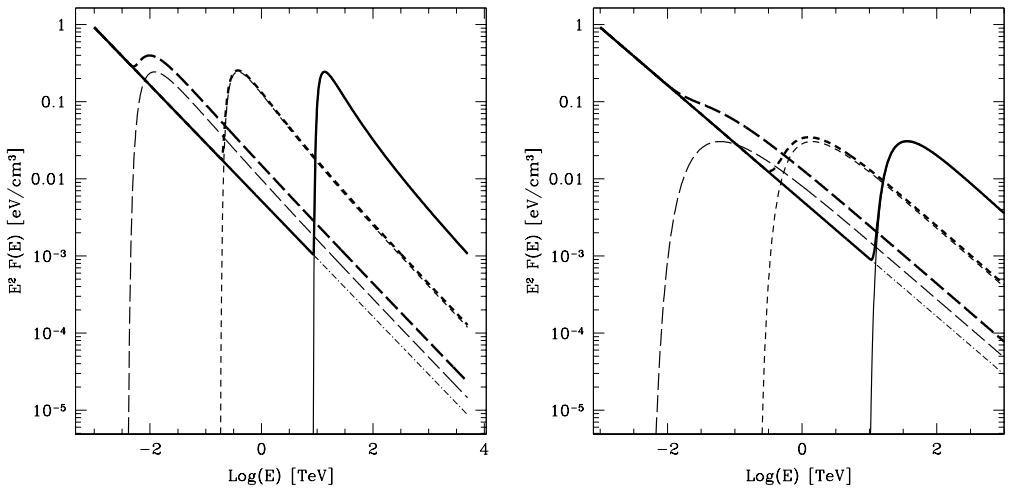

Figure 4.1: Spectrum of CRs at the location of the molecular cloud. The cloud is located at 50 pc (left) and 100 pc (right panel) from a SNR. The thin dot–dashed line shows the Galactic CR spectrum, while the thin solid, short–dashed, and long-dashed lines represent the spectrum of CRs coming from the SNR for 2000, 8000, and 32000 years after the supernova explosion, respectively. The thick lines show the total CR spectrum at the cloud location.

diffuse Galactic cosmic ray spectrum is assumed to be identical to the one observed near the Sun (see e.g. Dermer 1986):

$$J_{CR}(E) = 2.2 \left(\frac{E}{GeV} \right)^{-2.75} \mathrm{cm}^{-2}\mathrm{s}^{-1}\mathrm{GeV}^{-1}\mathrm{sr}^{-1} \tag{4.2}$$

while the diffusion coefficient, needed to evaluate Eq. 3.6, is taken equal to:

$$D(E) = 10^{28} \left(\frac{E}{10\ GeV} \right)^{0.5} \mathrm{cm}^2/\mathrm{s}\ , \tag{4.3}$$

compatible with CR propagation models (e.g. Berezinskii et al. 1990).

The evolution with time of the CR spectrum at the position of the molecular cloud can be understood as follows. According to the model described in Sec. 3.1.1, CRs with different energies leave the SNR at different times. The highest energy ($\sim$ PeV) CRs leave the SNR first, while CRs with lower and lower energy are released at later times. Moreover, higher energy CRs diffuse faster, thus the spectrum of CRs at the cloud exhibit a sharp low energy cutoff at an energy E_{low}, which moves to lower and lower energies as time passes. The position of the cutoff represents the energy of the least energetic particles that had enough time to reach the cloud.

From Fig. 4.1 it is clear that the influence of the presence of a nearby SNR close to the cloud is reflected in the CR spectrum at the cloud position, but this influence depends on many parameters, such as the distance between the SNR and the cloud,

the time since the supernova explosion, and the CR particle energy. The CRs coming from the SNR dominate the total CR spectrum at high energy, while at lower ($\sim$ GeV) energies the galactic CR background is always the dominant component, unless the molecular cloud is located at distances significantly smaller than ≈ 50 pc from the SNR. However, such small distances are comparable to the size of the SNR itself and thus in this case an interaction between the SNR shock and the molecular cloud is expected (see e.g. Aharonian et al. 1994b). The investigation of this scenario goes beyond the scope of this work and thus we limit ourselves to the case in which the distance between the SNR and the cloud is significantly larger than the size of both objects.

Aharonian and Atoyan (1996) also evaluated the CR spectrum in the vicinity of a CR accelerator by using an approach similar to the one developed here. They made no specific assumption about the nature of the accelerators and solved the CR transport equation by assuming that a power law spectrum of CRs is injected in the interstellar medium. They considered both the case of a continuous injection of particles during the whole lifetime of the accelerator and the case of an impulsive source that releases all the CRs at the same time. The approach we adopt here is different, because it is specific for a given class of sources, namely SNRs. In this specific case, particles having different energies are released at different times in the interstellar medium.

4.2 Relevant time scales for cosmic ray propagation inside a molecular cloud

Molecular clouds are characterized by a wide range of masses, going from $\approx 10\ M_{\odot}$ to $10^5 M_{\odot}$ or even more and have typical sizes ranging from few to few tens of parsecs. The typical density of a cloud is of about few hundred atoms per cubic centimeter, but much higher densities can be found in less massive and smaller (parsec or sub-parsec scale) molecular cloud cores, dark clouds or Bok globules (see Stahler & Palla 2005, for a review). The typical magnetic field of the intercloud medium is $\approx 10\ \mu$G (Shu et al. 1987), and it scales roughly as the square root of the gas density, thus reaching the mG level in the densest regions with density $10^5 \div 10^6$ cm^{-3} (Crutcher 1999).

The propagation of high energy CRs inside molecular clouds has been studied in Gabici et al. (2007) (see also Chapter 6), where an extensive discussion can be found. Here we summarize the most relevant aspects. Once the CRs from the SNR reach the molecular cloud, they diffusively penetrate with typical time scale:

$$\tau_{diff} \sim \frac{R_{cl}^2}{6\ D(E,B)} \tag{4.4}$$

where R_{cl} is the cloud radius and D is the diffusion coefficient which we assume here to depend on energy and on magnetic field as:

$$D(E) = \chi\ 10^{28} \left(\frac{E}{10\ GeV}\right)^{0.5} \left(\frac{B}{3\ \mu G}\right)^{-0.5}\ \mathrm{cm}^2/\mathrm{s}\ . \tag{4.5}$$

Here χ is a factor that takes into account deviations from the average Galactic diffusion coefficient described by Eq. 4.3 (see Gabici et al. 2007) and 3 μG is the average magnetic field in the Galactic disk. At very high energies, when the Larmor radius of the particle becomes comparable with or even larger than the size of the cloud, particles propagate almost rectilinearly, and the propagation time reduces to the crossing time $\tau_{cross} = R_{cl}/c$. In the following we assume the characteristic propagation time for a CR in a molecular cloud to be:

$$\tau_{prop} \approx \tau_{diff} + \tau_{cross}, \tag{4.6}$$

which is a rough approximation which still describes with sufficient accuracy the two different regimes of propagation.

CRs can freely penetrate the molecular cloud if the diffusion time is shorter than the energy loss time which, for CR protons with energy above $\sim$ 1 GeV, is dominated by inelastic proton–proton interactions in the dense gas and reads (see e.g. Berezinskii et al. 1990):

$$\tau_{pp} = \frac{1}{n_{gas} c \kappa \sigma_{pp}} = 6 \times 10^5 \left(\frac{n_{gas}}{100 \text{ cm}^{-3}} \right)^{-1} \text{yr}, \tag{4.7}$$

where n_{gas} is the gas density, c is the speed of light and σ_{pp} and κ are the cross section and inelasticity of the process, respectively. For nonrelativistic protons (energies below 1 GeV) ionization losses become relevant, with time scale (e.g. Berezinskii et al. 1990):

$$\tau^p_{ion} \sim 2.8 \times 10^7 \left(\frac{n_{gas}}{100 \text{ cm}^{-3}} \right)^{-1} \left(\frac{E_k}{m_p c^2} \right)^{\frac{3}{2}} \left[11.8 + \ln \left(\frac{E_k}{m_p c^2} \right) \right]^{-1} \text{ yr}. \tag{4.8}$$

Here E_k is the proton kinetic energy and m_p is the proton mass. The total energy loss time for CR protons due to both processes is given by:

$$\tau^p_{loss} = \left(\frac{1}{\tau_{pp}} + \frac{1}{\tau^p_{ion}} \right)^{-1}. \tag{4.9}$$

Secondary electron-positron pairs are produced inside the cloud during inelastic collisions between CR protons in the dense gas. The typical diffusion time for such electrons is given by Eq. 4.4, while the relevant channels for electron energy losses are ionization losses, Bremsstrahlung emission, and synchrotron emission with characteristic time scales (e.g. Ginzburg & Syrovatskii 1964):

$$\tau^e_{ion} = 1.9 \times 10^4 \left(\frac{n_{gas}}{100 \text{ cm}^{-3}} \right)^{-1} \frac{\gamma}{3 \ \ln(\gamma) + 18.8} \text{ yr} \tag{4.10}$$

$$\tau_{Brems} = 3.3 \times 10^5 \left(\frac{n_{gas}}{100 \text{ cm}^{-3}} \right)^{-1} \text{ yr} \tag{4.11}$$

$$\tau_{syn} = 1.3 \times 10^5 \left(\frac{E}{\text{TeV}} \right)^{-1} \left(\frac{B}{10 \ \mu\text{G}} \right)^{-2} \text{ yr} \tag{4.12}$$

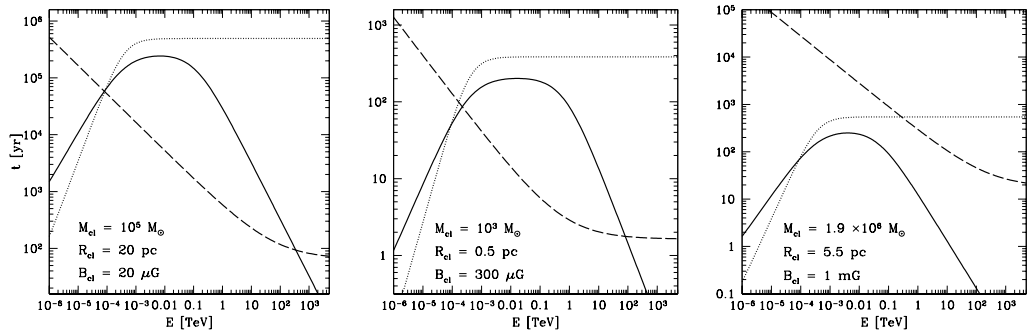

Figure 4.2: **LEFT PANEL:** time scales for CR propagation inside a molecular cloud with mass $M_{cl} = 10^5 M_\odot$, radius $R_{cl} = 20$ pc, and magnetic field 20 μG. Assuming a flat density profile gives a density of ~ 120 cm^{-3}. The dashed line represents the CR propagation time scale over a distance R_{cl}. The dotted line represents the energy loss time for CR protons (ionization losses are relevant below 1 GeV, inelastic proton-proton interaction at higher energies) while the solid line refers to the energy loss time for CR electrons, including ionization losses, Bremsstrahlung losses and synchrotron losses, which dominates at low, intermediate and high energies respectively. **MIDDLE PANEL:** same as left panel, but for a cloud with mass $M_{cl} = 10^3 M_\odot$, radius $R_{cl} = 0.5$ pc, and magnetic field 300 μG. The corresponding density is $\sim 1.6 \times 10^5$cm^{-3}. **RIGHT PANEL:** same as the left panel, but for the specific case of the SgrB2 cloud with mass $1.9 \times 10^6 M_\odot$, radius 5.5 pc and magnetic field 1 mG. This implies an average density of 1.1×10^5 cm^{-3} (see text for an explanation of the choice of parameters adopted).

respectively. Here, γ is the electron Lorenz factor and E the total electron energy. The ionization losses are computed for ultra-relativistic electrons. The total energy loss time for CR electrons due to the three processes listed above is given by:

$$\tau^e_{loss} = \left(\frac{1}{\tau^e_{ion}} + \frac{1}{\tau_{Brems}} + \frac{1}{\tau_{syn}} \right)^{-1} . \tag{4.13}$$

In writing the equation above, we neglected the possible role of inverse Compton losses off soft background photons. Such losses are expected to be relevant when the energy density in the radiation field ω_{rad} is greater than the magnetic field energy density. In the following we will consider a cloud with radius $R_{cl} =$ 20 pc and magnetic field $B = 20\mu$G, and in this case the condition reads: $\omega_{rad} > 10\ (B/20\ \mu G)^2$ eV/cm^3. Such condition can be realized inside molecular clouds only close to star forming regions. In particular, if a star forming region or a stellar OB association with total photon output equal to $4 \times 10^{33} L/L_\odot$ erg/s is located within a molecular cloud, inverse Compton losses will dominate over synchrotron losses around the star forming region up to a distance of $R \approx 8 \times 10^{-3} (L/L_\odot)^{1/2} (B/20\ \mu G)^{-1}$ pc, which becomes comparable with or larger than the molecular cloud radius R_{cl} when $L \geq 6 \times 10^6 (B/20\ \mu G)^2 (R_{cl}/20\ \mathrm{pc})^2 L_\odot$. Since this is a quite high luminosity, only a small fraction of molecular clouds are expected to host such luminous OB

associations (Williams & McKee 1997). We can thus safely neglect the role of inverse Compton losses in most of the situations. Inverse Compton losses can certainly play a role if one considers small regions within the cloud which surrounds star forming regions. Such regions constitute a small fraction of the cloud volume and thus are not expected to affect significantly the non thermal emission from the whole cloud.

In Fig. 4.2 (left panel) the characteristic time scales listed above have been plotted as a function of particle energy for a giant molecular cloud with total mass $M_{cl} = 10^5 M_\odot$ and radius $R_{cl} = 20$ pc. Assuming a flat density profile the density is $n_{gas} \sim 120$ cm^{-3}. The magnetic field is assumed to be $B_{cl} = 20$ μG. The dotted line refers to proton energy losses, which are dominated by ionization losses at energies below ~ 1 GeV and by inelastic proton–proton interactions at higher energies. The solid line represents the electron energy loss time. The three different power law behaviors reflect the dominance of ionization, Bremsstrahlung and synchrotron losses at low, intermediate and high energies, respectively. Finally, the dashed line represents the propagation time over a distance equal to the cloud radius. The propagation time has been evaluated by using the diffusion coefficient from Eq. 4.5 with $\chi = 1$ (no suppression with respect to the average Galactic value).

For proton energies above the threshold for pion production ($E_{th} \sim 280$ MeV), the propagation time is always shorter than the energy loss time. This means that CR protons which produce gamma rays and secondary electrons can freely penetrate the cloud and their flux is not attenuated due to energy losses. The propagation time for CR electrons is also shorter than the energy loss time for particle energies between $E \sim 100$ MeV and a few hundreds of TeV. This implies that, within this energy range, the secondary electrons produced inside the cloud quickly escape, and have little effect on the non-thermal emission from the cloud. On the other hand, extremely energetic electrons with energies above a few hundreds TeVs radiate all their energy in form of synchrotron photons before leaving the cloud. In a typical magnetic field of a few tens of microGauss, these electrons emit synchrotron photons with energy:

$$E_{syn} \approx 1 \left(\frac{B_{cl}}{10\ \mu\mathrm{G}} \right) \left(\frac{E}{100\ \mathrm{TeV}} \right)^2\ \mathrm{keV}\ . \tag{4.14}$$

Thus, the most relevant contribution from secondary electrons to the cloud non thermal emission falls in the hard X-ray band.

The middle panel of Fig. 4.2 shows the time scales for a compact cloud with radius $R_{cl} = 0.5$ pc and mass $M_{cl} = 10^3 M_\odot$, which implies, in case of a flat density profile, a density of $\sim 1.6 \times 10^5$ cm^{-3}. A strong magnetic field of 300 μG is assumed, as suggested by observations of very dense clouds (Crutcher 1999). These parameters are typical for molecular cloud cores or for dark clouds (Stahler & Palla 2005). The left and middle panels in Fig. 4.2 looks very similar, except for a scaling factor. This implies that the same conclusions can be drawn as for the case of a giant molecular cloud, and thus a similar behavior is expected from giant molecular clouds and compact clouds, the only difference being that all the time scales are much shorter in the latter case, due to the high gas density and to the reduced size of the system.

The properties of giant molecular clouds located in the galactic centre region

can differ significantly from the average figures reported above. As an example, we plot in the right panel of Fig. 4.2 the typical time scales for the SgrB2 cloud. This is a very massive cloud located at 100 pc (projected distance) from the galactic centre. The cloud virial mass is $M_{SgrB2} = 1.9 \times 10^6 M_\odot$ (Protheroe et al. 2008) and a magnetic field at the milliGauss level has been measured in the outer envelope of the cloud complex (Crutcher 1999). The mass distribution can be fitted with a radial gaussian density profile with $\sigma = 2.75$ pc (Protheroe et al. 2008, and references therein). To compute the curves plotted in Fig. 4.2 (right panel), we assumed a cloud radius of $R_{SgrB2} = 2\sigma = 5.5$ pc, which encloses $\approx 95\%$ of the total cloud mass. This gives an average density of $n_{gas} = 1.1 \times 10^5 \mathrm{cm}^{-3}$ (roughly a factor of 2 below the central density). It is evident from the right panel of Fig. 4.2 that the SgrB2 cloud is remarkably different from a typical giant molecular cloud. In particular, the very high values of the magnetic field and of the gas density make the energy loss time of CR protons significantly shorter than the propagation time for energies below a few hundred GeVs. Moreover, for CR electrons the energy loss time is always shorter than the propagation time. This means that CR protons with energies up to few hundred GeVs cannot penetrate the molecular cloud, as they do in the cases considered in the left and middle panel of Fig. 4.2. Primary CR electrons cannot penetrate the cloud, while secondary CR electrons produced inside the cloud in hadronic interactions cannot leave the cloud and radiate all their energy close to their production site. These characteristics make SgrB2 a very peculiar objects whose modelling needs a specific treatment. A detailed study of the CR penetration in the SgrB2 cloud has been performed by Protheroe et al. (2008), who also computed the synchrotron radio emission from secondary electrons. The effects of CRs exclusion from giant molecular clouds on their gamma ray emission have been discussed in detail by Gabici et al. (2007) and in Chapter 6. In the following we will not focus onto any specific object but rather investigate the case of the typical molecular clouds as the ones considered in the left and middle panels of Fig. 4.2.

To conclude the discussion on characteristic time scales, it is interesting to note that under certain conditions all the energy loss times, for both protons and electrons, scales in the same way with gas density, namely as n_{gas}^{-1}. This is evident from Eqns. 4.7 and 4.8, that describe inelastic proton-proton scattering and ionization losses for protons respectively, and from Eqns. 4.10 and 4.11 that describe ionization and Bremsstrahlung losses for electrons respectively. Moreover, also for synchrotron losses (Eq. 4.12) it is possible to derive the same scaling with gas density by recalling that observations suggest that the magnetic field in molecular clouds scales as the square root of gas density (Crutcher 1999). This has the important consequence that, in typical molecular clouds, particles with a given energy (protons or electrons) lose their energy always through the same channel, independently on the gas density. As said above, this conclusion may not hold for peculiar objects such as SgrB2.

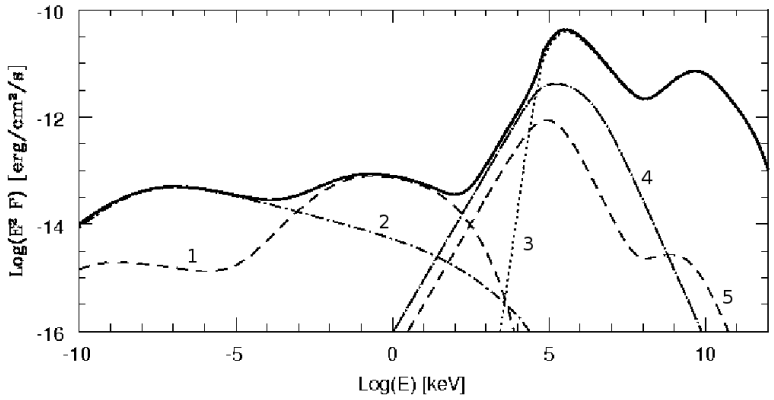

Figure 4.3: Broad band spectrum for a molecular cloud of mass $10^5 M_\odot$, radius 20 pc, density $\sim$ 120 cm^{-3}, magnetic field 20μG. The molecular cloud is at 100 pc from a SNR that exploded 2000 yr ago. The distance of the cloud is 1 kpc. The dotted line shows the emission from π^0–decay (curve 3), the dot-dashed lines represent the synchrotron (curve 2) and Bremsstrahlung (curve 4) emission from background CR electrons that penetrate the molecular cloud and the dashed lines the synchrotron (curve 1) and Bremsstrahlung (curve 5) emission from secondary electrons.

4.3 Non-thermal radiation from a molecular cloud

Molecular clouds are now estabilished gamma ray sources (Aharonian et al. 2006b, 2008a). Their gamma ray emission is believed to be the result of the decay of neutral pions produced during the inelastic collisions of CRs with the dense gas which constitutes the cloud (Bloemen et al. 1984; Blitz et al. 1985; Aharonian 1991; Gabici et al. 2007). During the same interactions, also electrons and positrons are produced via the decay of charged pions. These electrons and positrons produce a broad spectrum of radiation from radio waves to gamma rays due to synchrotron emission and non thermal Bremsstrahlung.

In this section we compute the expected non-thermal emission from a molecular cloud located in the proximity of a SNR. The emission is the result of CR interactions with the dense gas and magnetic field in the cloud and is made up of two contributions: a steady state contribution from the interactions of background CRs that penetrate the cloud and a time dependent contribution from the interactions of CRs coming from the nearby SNR.

We consider a giant molecular cloud of mass $M_{cl} = 10^5 M_\odot$, radius $R_{cl} = 20$ pc and we assume an uniform density of $n_{gas} \sim 120$ cm^{-3}. The magnetic field is $B_{cl} = 20$ μG. The relevant time scales for CR propagation and energy losses in such an environment have been plotted in the left panel of Fig. 4.2. In order to show all the different contributions to the total non-thermal emission, in Fig. 4.3 we plot the broad band spectrum from the cloud at a time $t = 2000$ years after the

supernova explosion. The SNR is located 100 pc away from the molecular cloud and the distance to the observer is 1 kpc. The dotted line (curve 3) represents the emission from neutral pion decay (from both background CRs and CRs from the SNR), the dot–dashed lines represent the synchrotron (curve 2) and Bremsstrahlung (curve 4) emission from background CR electrons that penetrate the molecular cloud and the dashed lines represent the synchrotron (curve 1) and Bremsstrahlung (curve 5) emission from secondary electrons produced during inelastic CR interactions in the dense gas. For the spectrum of background CR electrons we use a fit to the measured spectrum at Earth (see Kobayashi et al. 2004 for a recent compilation of data). Electrons can freely penetrate the cloud except for the highest ($\gtrsim$ 300 TeV) and lowest ($\lesssim$ 100 MeV) part of the energy spectrum, where the energy loss time scale is significantly shorter than the propagation time (see Fig. 4.2). For this energies the CR electron flux inside the cloud is suppressed and we estimated the suppression by assuming that CR electrons can penetrate undisturbed the cloud only up to a given depth, which is estimated as $\approx c\tau^e_{loss}$ and $\approx \sqrt{D\tau^e_{loss}}$ for the high and low energy end of the spectrum respectively. This approximation is satisfactory for the purposes of this paper, given that the suppression becomes crucial only for particles which emit negligible non-thermal emission.

The decay of neutral pions dominates the total emission for energies above $\approx$ 100 MeV. The two peaks in the emission reflects the shape of the underlying CR spectrum, which, as illustrated in Fig. 4.1, is the sum of the steep background CR spectrum, which produces the π^0–bump at a photon energy of $m_{\pi^0}/2 \sim 70$ MeV (in the photon flux F), and an hard CR component coming from the SNR that produces the bump at higher energies. The flux level at 1 TeV is approximatively 5×10^{-12}erg/cm^2/s, detectable by currently operating Imaging Atmospheric Cherenkov Telescopes, even taking into account the quite extended ($\approx 2^\circ$) nature of the source. It is remarkable that such a cloud would be detectable even if it were located at the distance of the Galactic centre, as can be easily estimated by taking into account that the sensitivity of a Cherenkov telescope like H.E.S.S. after 50 hours of exposure, is $\approx 10^{-13}(\theta_s/0.1^\circ)$TeV/cm^2/s, where θ_s is the source extension. This means that very massive clouds can be used to reveal the presence of enhancements of the CR density in different locations throughout the whole Galaxy. Similar conclusions can be drawn for the expected emission in the GeV range, which is currently probed by the AGILE and FERMI satellites. In particular, FERMI, with a point source sensitivity of $\lesssim 10^{-9}$GeV/cm^2/s at energies above 1 GeV (www-glast.slac.stanford.edu), will be able to detect such giant molecular clouds as extended sources if they are located within $1\div 2$ kpc from the Earth, or as point sources if they are at larger distances. Such a use of molecular cloud as CR *barometers* has been discussed in several papers for both GeV (Bloemen et al. 1984; Blitz et al. 1985; Issa & Wolfendale 1981; Casanova et al. 2010a) and TeV gamma rays (Aharonian 1991; Gabici 2010). Here we demonstrated that SNRs can provide enhancements in the CR density that can generate gamma ray fluxes well within the capabilities of currently operating instruments.

The spectral shape in the gamma ray energy range deserves further discussion. For the situation considered in Fig. 4.3, the GeV gamma rays are the result of

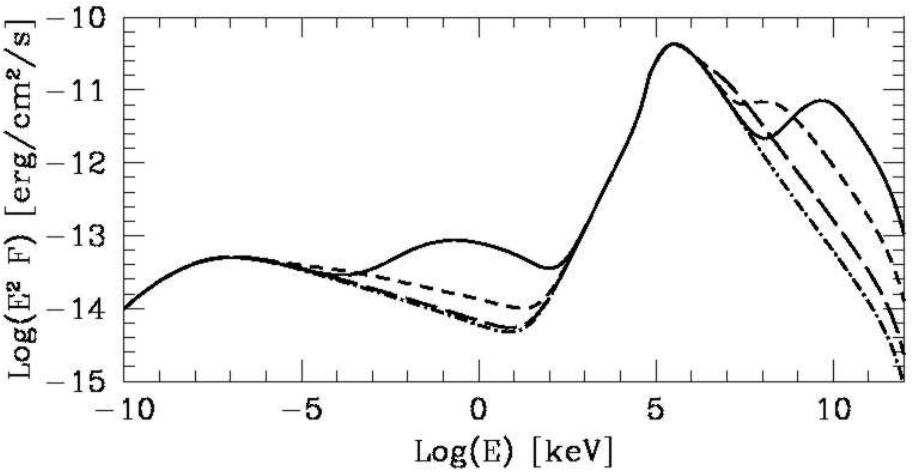

Figure 4.4: Time dependence of the broad band spectrum for the same giant molecular cloud considered in Fig. 4.3. The solid, short–dashed, and long–dashed lines refers to the emission at a time 2000, 8000, and 32000 years after the explosion. The dot–dashed line represent the spectrum of a molecular cloud with no SNR in its proximity.

the decay of neutral pions produced by background CRs that penetrate the cloud. Thus, the gamma ray spectrum above GeV energies simply mimics the underlying CR spectrum, which is a steep power law of the form $\approx E^{-2.75}$. On the other hand, the neutral pion decay spectrum at TeV energies is, in this case, dominated by the contribution from CRs coming from the nearby SNR. After 2000 years from the supernova explosion, only CRs with energies above several tens of TeV had enough time to leave the SNR and reach the cloud and thus the CR spectrum at the cloud exhibits an abrupt low energy cutoff at that energy, that we call here E_{CR}^{cut} (see Fig. 4.1). As a consequence, the gamma ray spectrum is expected to be peaked at an energy $\sim E_{CR}^{cut}/10$ of several TeV. The slope of the gamma ray spectrum below the peak is determined by the physics of the interaction only, and not by the shape of the underlying CR spectrum, and is roughly of the form $E^2 dN/dE \propto E^2$ (e.g. Kelner et al. 2006). Thus, a loose association between a SNR and a massive molecular cloud as the one studied here, is expected to be characterized, at least at some stage of the SNR evolution, by a very peculiar spectrum which is steep at low (GeV) energies and hard at high (TeV) energies.

The possibility of detecting sources with such a distinct spectrum is also relevant for the issue of identifying GeV and TeV unidentified sources. One of the criteria suggested to support an association between a GeV and TeV source is, beside the positional coincidence, the spectral compatibility. In a recent paper, Funk et al. (2008), investigated the spectral compatibility of EGRET and H.E.S.S. unidentified sources located in the inner Galactic region. For sources showing positional coincidence,

they found generally a good spectral compatibility, but due to the small number of sources, it was not possible to claim an association between the two populations of sources at a statistically significant level. For sources detected by only one of the two instruments, Funk et al. (2008) investigated the consequences of extrapolating the measured spectrum at higher or lower energies. They considered only single power laws extending over the whole (GeV–TeV) energy range and discussed the implications of adding a high or low energy cutoff. The scenario presented here adds the new interesting possibility of a single source showing a dramatically different behavior at GeV and TeV energies, namely a spectrum which shows a significant hardening at higher energies.

The evolution with time of the emission from the cloud is shown in Fig. 4.4, where the solid, short–dashed, and long–dashed lines show the spectrum at a time equal to 2000, 8000, and 32000 years after the supernova explosion respectively. For comparison, the emission from a molecular cloud, with no SNR located in its proximity, is plotted as a dot–dashed line. In this case, only background CRs that penetrate the molecular cloud contribute to the emission.

It is evident from Fig. 4.4 that the radio ($\lambda \gtrsim 0.1$ mm) and the soft gamma ray (≈ 1 MeV $\div 1$ GeV) emission from the cloud is constant in time. This reflects the fact that such emission is produced by background CRs that enter the cloud. The emission in the other energy bands is variable in time, being produced by the CRs coming from the SNR. The flux of this latter component changes with time as indicated in Fig. 4.1. The two most prominent features in the variable emission are two peaks, in X– and gamma–rays respectively.

The peak observable at $\sim$ TeV gamma ray energies is the result of the decay of neutral pions produced when CRs of different energies coming from the SNR reach the cloud at different times. The peak moves at lower and lower energies with time, reflecting the fact that CRs with lower and lower energies progressively reach the cloud as time flows. At early times, the emission can extend up to tens of TeVs (solid line), or even more (see Chapter 3), revealing the presence of very energetic CRs and thus indirectly the fact that the nearby SNR is accelerating particles up to 100 TeV - 1 PeV (see Gabici & Aharonian 2007b, and Chapter 3 for a discussion of this issue). Moreover, the gamma ray emission in the TeV range is enhanced with respect to the one expected from an isolated molecular cloud (dashed–dotted line in Fig. 4.4) for a period of several 10^4 yr. This is much longer than the period during which SNRs are effectively accelerating the multi-TeV CRs responsible for the TeV emission, which lasts few thousands years. This is because the duration of the gamma ray emission from the cloud is determined by the time of propagation of CRs from the SNR to the cloud and not by the much shorter CR confinement time in the SNR. Therefore, the gamma ray emission from the cloud lasts much longer than the emission from the SNR, making the detection of clouds more probable.

The peak in the X-ray spectrum is due to synchrotron emission from secondary electrons produced in CR interactions in the cloud. The peak is moving to lower energies with time but, unlike the gamma ray peak, it is also becoming less and less pronounced. This fact can be understood with the help of Fig. 4.2 (left panel).

After 2000 yr from the supernova explosion (solid line in Fig. 4.4), $\approx$ 100 TeV CRs from the SNR reach the cloud and produce there secondary electrons with energy in the $\approx$ 10 TeV range. For these electrons, the synchrotron cooling time is roughly one order of magnitude longer than the escape time from the cloud. Thus, they release a non negligible ($\approx$ 10%) fraction of their energy in form of X-ray synchrotron photons before leaving the cloud. As time passes, lower energies CRs reach the cloud and secondary electrons with lower energies are produced. For these electrons the cooling time becomes progressively longer than the escape time and this explain the suppression of the synchrotron emission. The X-ray synchrotron emission is weaker than the TeV emission for any time and for times $>$ 2000 yr the ratio between TeV and keV emission can reach extreme values of a few tens or more. These values are observed from some of the unidentified TeV sources, and more in general unidentified TeV sources are characterized by the absence of any clear counterpart at other wavelengths. Due to this peculiar spectral properties, such sources have been labeled as *dark*, since they seems to emit gamma rays only. However, in the scenario presented in this paper, spectra showing a high TeV/kev flux ratio can be produced very naturally if a cloud is illuminated by CRs coming from a nearby SNR. This suggestion is also supported by the fact that most of the unidentified TeV sources are spatially extended, as molecular clouds are expected to be.

In the hard X-ray/soft gamma ray region of the spectrum (from tens of keVs to hundreds of MeVs), partially covered by the INTEGRAL satellite, extremely hard spectra ($dN/dE \propto E^{-1}$) may result due to the Bremsstrahlung emission from primary and secondary CR electrons.

Finally, the radio emission from the cloud is the result of the synchrotron emission of background CR electrons that penetrate the cloud. The contribution from secondary electrons is subdominant, due to the fact that the $\sim$ GeV secondary electrons that might emit synchrotron radio waves escape from the cloud before losing energy (see Fig. 4.2). Moreover, in the GeV energy range, ionization and Bremsstrahlung losses dominate, and this would further reduce the expected synchrotron emission. Recently, Protheroe et al. (2008) estimated the expected synchrotron radio emission from secondary electrons produced by CR interactions in the Sgr B2 giant molecular cloud. They did not consider the contribution from background CR electrons and neglected the effects of diffusive transport of secondary electrons (namely, they assumed no penetration of electrons from outside the cloud and instantaneous cooling of secondary electrons produced inside the cloud). These assumptions are valid for the very strong magnetic field of the order of one milliGauss measured for SgrB2. Such field is much stronger than the one assumed here. Thus, due to these somewhat extreme assumptions, possibly justified in the particular case of Sgr B2 cloud, a direct comparison between their findings and the results presented here is not straightforward. Protheroe et al. (2008) also noticed that the radio emission from a cloud at frequencies above $\sim$ 1 GHz can be dominated by free–free thermal emission. Being focused on the non-thermal emission from clouds, we did not attempt here to model their thermal emision. However, our findings can still be tested and

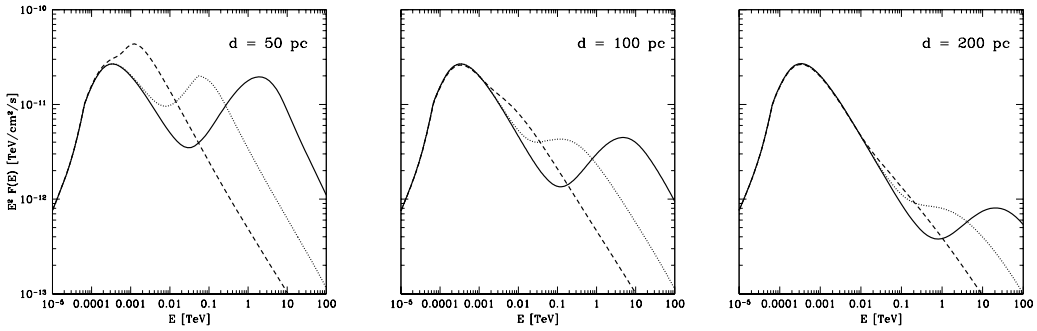

Figure 4.5: Total gamma ray emission from a molecular cloud of mass $10^5 M_\odot$ located at a distance of 1 kpc. The distance between the molecular cloud and the SNR is 50, 100 and 200 pc for left, centre and right panel, respectively. The solid, dotted, and dashed lines refers to the emission at a time 2000, 8000, and 32000 years after the explosion.

constrained by observations in the GHz range. This can be done by requiring the predicted synchrotron emission not to overproduce the observed free–free thermal emission. A similar approach has been adopted by Jones et al. (2008).

4.3.1 The spectral shape at GeV-TeV energies

As noticed in the previous section, concave gamma ray spectra may be produced in a molecular cloud located in proximity of a SNR, as the result of the decay of neutral pions produced in CR interactions. Such concavity reflects the shape of the underlying CR spectrum, which consist of the superposition of two components: the galactic CR background, characterized by a steep spectrum, and the CRs coming from the nearby SNR, which exhibit a hard spectrum. With this respect, the distance between the SNR and the molecular cloud d_{cl} plays a crucial role. This is because, the larger the distance between the SNR and the cloud, the lower the level of the CR flux coming from the SNR. Moreover, also the time evolution of the emission from a cloud changes with d_{cl} since the time it takes a particle with given energy to cover such a distance scales as $t \sim d_{cl}^2/D$, where D is the diffusion coefficient.

In Fig. 4.5 the total gamma ray spectrum from a molecular cloud is shown as a function of the distance between the SNR and the cloud. The cloud mass is $10^5 M_\odot$ and the distance from the SNR is 50, 100 and 200 pc for the left, central and right panel, respectively. Similarly to Fig. 4.4, the solid, dotted, and dashed lines refer to the emission for 2000, 8000, and 32000 years after the supernova explosion. It is evident from Fig. 4.5 that a great variety of gamma ray spectra can be produced. In almost the entirety of the cases considered, the gamma ray emission is characterized by the presence of two pronounced peaks. The low energy peak, located in the GeV domain is steady in time and it is the result of the decay of neutral pions produced in hadronic interactions of background CRs in the dense intercloud gas. The high energy peak is the result of hadronic interactions of CRs coming from the nearby

SNR, and thus it is moving in time to lower and lower energies (see previous section for a discussion). Both the relative intensity and position of the two peaks depend on the distance between the SNR and the cloud. Interestingly, the GeV emission from the cloud is affected by the presence of the nearby SNR only at late times after the explosion and only if the distance from the SNR is comparable or smaller than $\approx$ 50 pc (see Fig. 4.5, left panel). In all the other cases the GeV emission is always the result of the interactions of background CRs and thus, at least in this case, observations of molecular clouds in the GeV gamma ray domain cannot be used to infer the presence of a CR accelerator located at a distance greater that $\approx$ 50 pc from the cloud.

Similar concave or "V–shaped" spectra have been recently obtained by Rodriguez Marrero et al. (2008) in a different context in which two molecular clouds are assumed to be located in the proximity of a CR accelerator. If the two clouds happen to be located at different distances from the CR accelerator but within an angular separation smaller than the FERMI angular resolution, then they would appear as a single GeV source, and the superposition of their emission might result in concave spectra. However, Rodriguez Marrero et al. (2008) did not include in their calculations the contribution to the emission coming from the ubiquitous galactic CR background, which in most cases dominates over the contribution of CRs from the nearby SNR, at least for what concerns the GeV emission from the cloud (see e.g. Fig. 4.5). Moreover, they also considered very short distances between the cloud and the CR accelerator (down to 5 pc), but in this case an accurate modeling of the CR accelerator itself is needed, especially for what concerns its own gamma ray emission that might add up to the total emission. In addition to that, distances as short as $\sim 5 \div 10$ pc are, under many circumstances, smaller than both the source size and the radius of the molecular cloud itself, and this changes significantly the problem since the interactions between the accelerator and the molecular cloud are likely to play an important role.

The prediction of V-shaped spectra that we make in this paper is more general than the one by Rodriguez Marrero et al. (2008), since it represents an intrinsic feature of a single molecular cloud which is located close to a CR source. The V-shaped gamma ray spectrum reflects the shape of the underlying CR spectrum which is the superposition of the steep spectrum of the background CRs and the hard spectrum of CRs coming from the nearby SNR.

4.3.2 The role of the magnetic field

The value of the magnetic field in the cloud is an important parameter since it regulates the synchrotron energy losses of high energy electrons, and the diffusive escape time of relativistic particles from the cloud. Observations suggest that the value of the magnetic field in a molecular cloud scales with the square root of the gas density, reaching very high values (1 mG or more) in the very dense sub-parsec scale cloud cores (Crutcher 1999). However, dense cores constitute a very small fraction of the total volume of molecular clouds. Since here we are interested in calculating the emission from the whole cloud, the relevant parameter is the volume averaged value

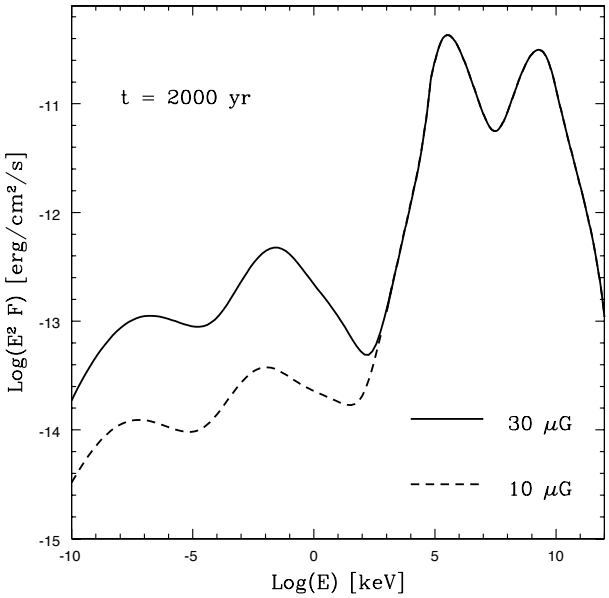

Figure 4.6: Broad band emission from a molecular cloud of mass $10^5 M_\odot$, radius 20 pc, density ~ 120 cm^{-3}. The distance between the cloud and the SNR is 50 pc. Time is 2000 years after the supernova explosion. The magnetic field is 30 μG (solid lines) and 10 μG (dashed lines).

of the cloud magnetic field. It seems reasonable to assume that the total magnetic energy in the cloud $W_B = (B^2/8\pi) \times V$, where V is the cloud volume, does not exceed the total gravitational energy of the cloud $W_G = 3GM^2/5R_{cl}$. This leads to a maximum value of the average magnetic field of: $B \leq 30\ (M/10^5 M_\odot)(R_{cl}/20\mathrm{pc})^{-2} \mu$G. This is in general agreement with observations, from which a value of $\approx 10\ \mu$G can be inferred for typical cloud densities of ≈ 100 cm^{-3}. However, since the dispersion around this mean value is considerable (see e.g. Crutcher 1999), it is worth to investigate how the non thermal emission from a molecular cloud depends on the actual value of the magnetic field.

Fig. 4.6 shows the broad band spectrum from a molecular cloud of mass $10^5 M_\odot$, radius 20 pc, density ~ 120 cm^{-3}. The distance between the cloud and the SNR is 50 pc and the curves refer to a time equal to 2000 years from the supernova explosion. The solid line refers to a value of the magnetic field of 30 μG, while the dashed line represents the emission for a smaller value of the field equal to 10 μG. The cloud emission from radio frequencies up to the hard X-ray band strongly depends on the value of the magnetic field, while the gamma ray emission is unaffected, being the result of hadronic interactions of CR protons. The strong dependence of the radio and X-ray emission on the magnetic fields is evident, and this demonstrate that this effect has to be taken into account in multi wavelength studies of molecular clouds.

4.4 Brief discussion on the validity of the diffusion approximation

In the previous chapters we assumed that cosmic rays escaping form SNRs propagate in a diffusive way. However, since we are considering relatively short time scales and distances, it is worth checking the validity of this assumption. This can be done by remembering that in the diffusion limit, a particle of given energy E and characterized by a diffusion coefficient $D(E)$, propagates over a time t a distance:

$$l_d \sim \sqrt{6\ D\ t}. \tag{4.15}$$

A requirement for this limit to be valid is that the effective velocity $v_d = l_d/t$ must not exceed the speed of light c. This leads to the relation:

$$l_d < c \times t \tag{4.16}$$

which can also be rewritten as a bound on time:

$$t > \frac{6\ D(E)}{c^2}\ . \tag{4.17}$$

The shortest propagation time we adopted in this Chapter is $t = 2000$ yr, which leads to the condition $l_d < 600$ pc. The condition on the propagation time is energy dependent. The most critical energies are the highest ($\sim$ PeV), for which the propagation might be almost rectilinear instead than diffusive over short distances. If we assume a diffusion coefficient for PeV particles of $D \sim 3 \times 10^{30}\mathrm{cm}^2/\mathrm{s}$ we obtain $t \gtrsim 700$ yr.

The condition $l_d/t < c$ can be rewritten as a function of the particle mean free path λ by reminding that the diffusion coefficient can be written as $D = \frac{1}{3}\lambda c$, leading to: $\lambda < ct/2$, which is another way to say that the propagation is non-rectilinear. If we consider the solid line in Fig. 4.5 we see that the peak of the gamma ray emission is at photon energy of ~ 30 TeV, which corresponds to proton energies of ~ 300 TeV. For these energies the mean free path is $\lambda \sim 60$ pc. This means that, if we assume that cosmic rays undergo a random motion with mean free path λ, they can cover the distance to the cloud (200 pc) after ~ 10 scatterings. Since this is the most extreme case considered in this Chapter, the diffusion approximation seems quite well justified.

The results presented in this chapter have been first published in:

- S. Gabici, F.A. Aharonian, & S. Casanova, MNRAS **396**, 1629 (2009)

Chapter 5

Two test-cases: the supernova remnants RX J1713.7-3946 and W28

5.1 Modeling the gamma-ray emission produced by runaway cosmic rays in the environment of RX J1713.7-3946

In order to fully exploit the present and future experimental facilities and to test the standard scenario for injection of CRs in the interstellar medium by SNRs and their subsequent propagation, we present here model predictions of the spectral and morphological features of the hadronic gamma-ray emission surrounding the candidate CR source RX J1713.7-3946, by constructing a model as quantitative as possible. In particular, we will convey all information concerning the environment, the source age, the acceleration rate and history, which all play a role in the physical process of CR injection and propagation. Building upon the modeling of the broadband emission from MCs close to CR accelerators developed in Gabici et al. (2009) and upon the analysis of the CR background discussed in Casanova et al. (2010a), we compute the expected gamma-ray emissivity from hadronic interactions of runaway CRs for the region of galactic coordinates $340^\circ < l < 350^\circ$ and $-5^\circ < b < 5^\circ$, assuming that a historical SNR event occurred in 393 C.E., at the location of the SNR RX J1713.7-3946 (Wang et al. 1997).

RX J1713-3946 is thought of as one of the best examples of a shell-type SNR, for which the multi-wavelength data suggests hadronic CR particle acceleration migth be active up to at least 100 TeVs (Aharonian et al. 2004, 2006a). The acceleration site within RX J1713.7-3946 is spatially coincident with the sites of non-thermal X-ray emission and brightening and decay of the X-ray hot spots on year time-scales have been detected (Uchiyama et al. 2007). The observed rapid variability of the X-ray emission provides strong evidence for the amplification of the magnetic field around the SNR shell, which is is key condition for the acceleration of protons up

to the knee. The multi-wavelength analysis of the emission from RX J1713.7-3946 supports therefore the hypothesis that CRs up to the knee are accelerated in SNRs. However, no compelling evidence for the acceleration of protons and nuclei up to PeV energies has been found until now. Also, the most energetic CRs cannot be confined for long time within the SNR and, even if RX J1713-3946 might have accelerated particles up to about PeV energies once, such highly energetic protons have already left the source. In fact, these very energetic particles, which are released first by SNRs and diffuse faster than lower energy CRs, reach first the clouds surrounding the injection sites and produce there gamma-ray photons. This enhanced gamma ray emission, once detected, can reveal the presence of the cosmic ray accelerator. This is why studies of the gamma-ray emission from the environment surrounding RX J1713-3946, such as the one presented here, are important.

The SNR RX J1713.7-3946 is located at 1 kpc distance from the Sun and has galactic coordinates (l,b) = (347.3,-0.5). CRs are assumed to be accelerated via diffusive shock acceleration at the SNR shock and then injected in the interstellar medium. The spectrum of the injected CRs integrated over the whole SNR lifetime is assumed to be a power law in energy with index -2. To model the injection of particles in the interstellar medium we follow the procedure described in Chapter 4 and in Gabici et al. (2009), which closely follows the work by Ptuskin & Zirakashvili (2005). The SNR accelerates the most energetic particles at the transition from the free expansion phase to the Sedov phase. Following Gabici et al. (2009) we assume that the most energetic cosmic rays leave the SNR at the beginning of the Sedov phase. The particles are released at different times, depending on their energy: the most energetic first, and the ones with lower and lower energy are gradually released as time flows. The maximum injection energy for accelerated particles is assumed to be 500 TeV and this particles are released at the beginning of the Sedov phase, at about 100 yr after the explosion. To be consistent with the gamma ray observations of RX J1713.7-3946, which show a cutoff in the gamma ray spectrum in the multi-TeV region, we assume that CRs of energy 150 TeV are being released now (about 1600 yr after the supernova explosion). When runaway protons diffuse into the interstellar medium, their energy density varies with energy, distance from the injection source, SNR age, and with the diffusion properties of the interstellar medium as explained in Chapter 4. We further assume that the fraction of the supernova explosion energy, $E_{SN} = 10^{51}$ ergs, which goes into the CRs is $\eta = 30\,\%$. For the CR diffusion coefficient we adopt the following expression:

$$D(E_p) = D_0 \left[\frac{E_p}{10\mathrm{GeV}}\right]^{0.5} \mathrm{cm}^2\mathrm{s}^{-1}\,. \tag{5.1}$$

We take D_0 to be 10^{26}, 10^{27} or 10^{28} cm^2/s. The diffusion of CRs into molecular clouds depends upon the highly uncertain diffusion coefficient. It is thought that CRs can penetrate clouds if the diffusion coefficient inside the cloud is the same as the average diffusion coefficient in the Galaxy, derived from spallation measurements. CRs are effectively excluded if the diffusion coefficient is significantly suppressed compared to the average galactic one. However, it has been shown that even in

this case CRs at TeV energies can diffuse into even the densest parts of molecular clouds, whilst GeV energy CRs might have trouble penetrating the densest parts of molecular clouds (e.g. Gabici et al. 2007; Protheroe et al. 2008). Once calculated the CR distribution around the SNR, we computed the expected gamma ray emission by using the parametrization of proton-proton interactions given by Kelner et al. (2006). In order to do so, the distributions of atomic and molecular hydrogen in the Galaxy is needed. Here, we use the data from the Leiden/Argentine/Bonn (LAB) Galactic HI Survey (Kalberla et al. 2005) and from the NANTEN Survey (e.g. Fukui et al. 2008), for atomic and molecular hydrogen, respectively. We neglect here the contribution from inverse Compton scattering to the total diffuse gamma ray emission. This is justified by the fact that electrons are believed to remain confined within the SNR due to strong synchrotron losses (see Chapter 4).

Results are shown in Fig. 5.1, where the predicted hadronic gamma-ray emission at 1 TeV arising from the sum of background CRs and runaway CRs is plotted for three different choices of the diffusion coefficient D_0. The spatial distribution of the emission depends upon the CR diffusion coefficient, D_0. The three panels refers to values of diffusion coefficient of $D_0 = 10^{26}$, 10^{27}, and 10^{28}cm^2/s for the top, middle, and bottom panel, respectively. The faster the CRs diffuse into the interstellar medium, the further the enhanced emission extends beyond the linear extent of RX J1713.7-3946. Of course, this goes at the expenses of the CR intensity, which decreases for fast diffusions. This is evident from the bottom panel, which shows that for very fast diffusion ($D_0 = 10^{28}$ cm^2/s) the runaway protons are too diluted around the SNR and they do not produce any appreciable emission above the gamma ray background.

One would expect the excess (over the gamma ray background) in the diffuse gamma-ray emission around the SNR to be spatially correlated with the atomic and molecular gas distribution. This is, generally speaking, true. However, one has to take into account that both the acceleration history of the source and the diffusion timescale are processes dependent upon the particle energy. In other words, when considering the gamma-ray emission at a given energy from the region surrounding a SNR, one should expect a correlation between excess of hadronic gamma rays and the gas distribution if and only if the parent CRs have already been released by the SNR and had time enough to diffuse into the interstellar medium. On the other hand, the enviroment of a CR source, which is dense in atomic and molecular hydrogen, might nonetheless appear faint at some energies in gamma rays simply because the parent CRs have not escaped the injection source or have not had time enough to propagate throughout the region nearby the source.

Figure 5.2 shows the ratio of the hadronic gamma-ray emission due to total CR spectrum to that of the background CRs for the entire region under consideration. In our modeling only CRs with energies above about 100 TeV have left the acceleration site and the morphology of the emission depends upon the energy at which one observes the hadronic gamma-ray emission. The different spatial distribution of the emission is due to the different diffusion coefficients assumed in the three different panels.

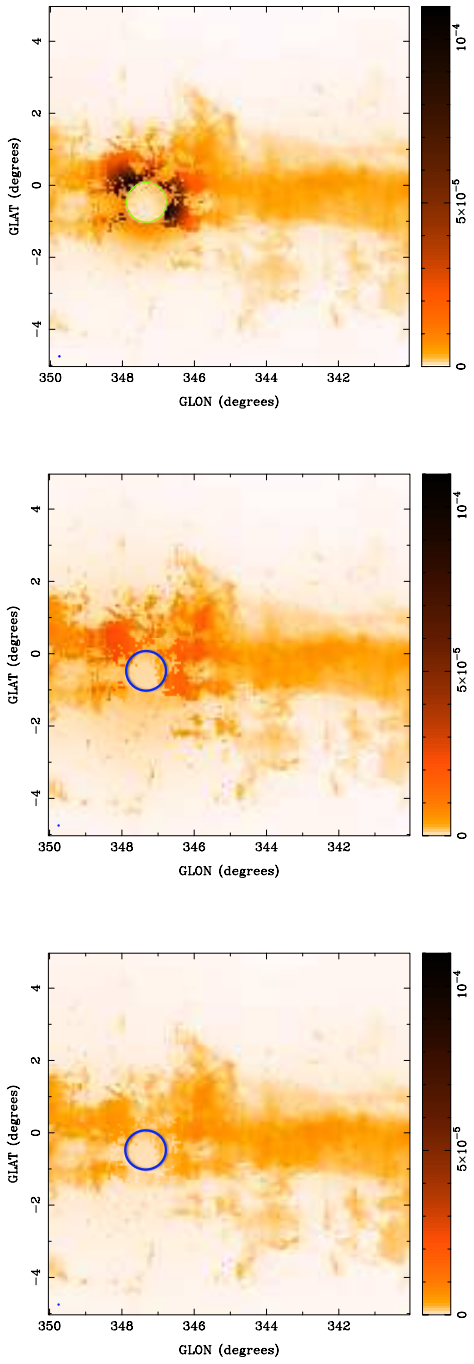

Figure 5.1: The predicted hadronic γ-ray energy fluxes at 1 TeV, expressed in GeV cm^{-2} sr^{-1} s^{-1}, arising from background CRs and from CRs escaping the SNR shells if the CR diffusion coefficient, D_0, is equal to 10^{26} cm^2/s (upper panel), 10^{27} cm^2/s (middle panel) and 10^{28} cm^2/s (bottom panel). We assume that the SNR has started releasing the particles of energy 500 TeV 100 years after the explosion. Also indicated in the left bottom corner the angular resolution of the NANTEN survey.

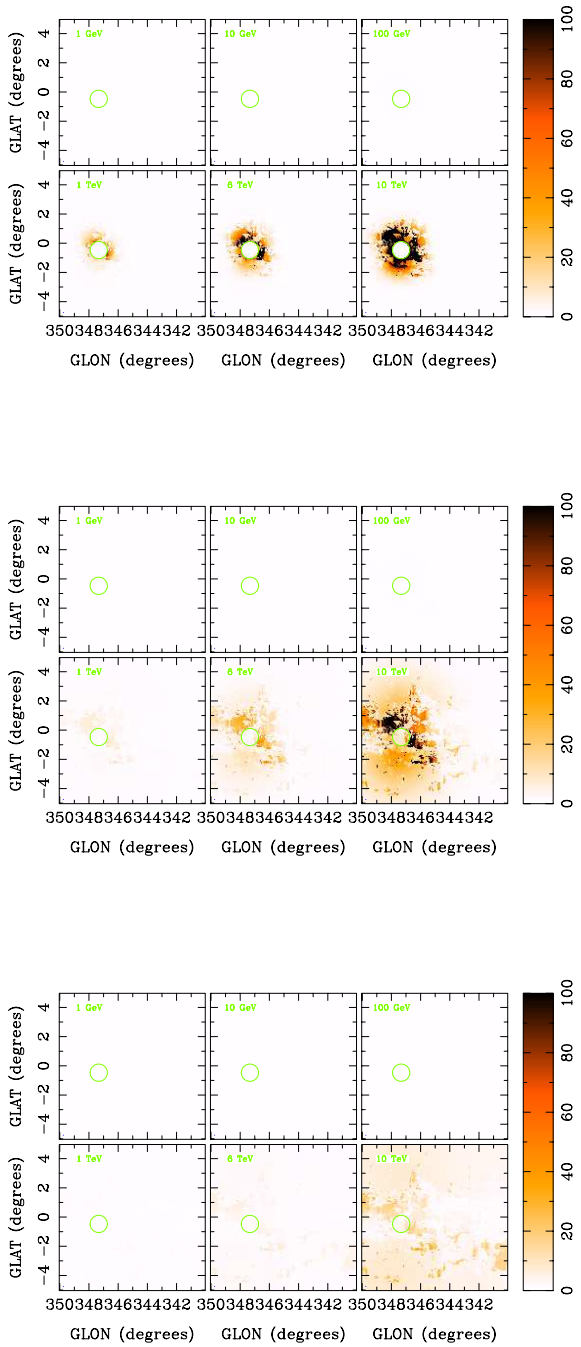

Figure 5.2: Ratio of the emission due to the sum of background CRs and runaway CRs and background CRs only. The position of the SNR is indicated with a circle. The diffusion coefficient is 10^{26} cm^2/s, 10^{27} cm^2/s, and 10^{28} cm^2/s (top to bottom panel). The ratio is shown for different photon energies from 1 GeV to 10 TeV.

As discussed at length in Casanova et al. (2010a), the distance to the molecular and atomic gas is highly uncertain, and this might affect the results presented here. The principle uncertainty in the determination of the distance, which especially at distances close to the Sun, is as large as 2 kpc, comes from errors in the accuracy of the estimates of radial velocity of gas clouds. Uncertainties in the distance estimates affect also the determination of the conversion factor X (Arimoto et al. 1996), by which the emissivity of the CO line is converted to ambient matter density, and the determination of the number density of H_2 molecules from the measured CO intensity. This has to be taken into account when interpreting the results presented above.

To summarize, the emission from the regions surrounding SNR shells can provide crucial informations about the history of the SNR acting as a CR source and can also put important constraints on the highly unknown diffusion coefficient. Also, depending on the time and energy at which one observes the remnants and the surrounding medium, one will observe different spectra and morphologies. This has important implications for the current and future generations of gamma-ray observatories. The high sensitivity and high resolution, which will be reached by future detectors, such as the Cherenkov Telescope Array and HAWC (http://hawc.umd.edu/) makes the detection of the predicted emission possible.

5.2 Constraining the diffusion coefficient in the surroundings of the supernova remnant W28

W28 is an old SNR in its radiative phase of evolution, located in a region rich of dense molecular gas with average density $\gtrsim 5$ cm^{-3}. At an estimated distance of ~ 2 kpc the SNR shock radius is ~ 12 pc and its velocity ~ 80 km/s (e.g. Rho & Borkowski 2002). By using the dynamical model by Cioffi et al. (1988) and assuming that the mass of the supernova ejecta is $\sim 1.4\ M_\odot$, it is possible to infer the supernova explosion energy ($E_{SN} \sim 0.4 \times 10^{51}$erg), initial velocity ($\sim 5500$ km/s), and age ($t_{age} \sim 4.4 \times 10^4$yr).

Gamma ray emission has been detected from the region surrounding W28 both at TeV (Aharonian et al. 2008a) and GeV energies (Abdo et al. 2010a; Giuliani et al. 2010), by *HESS*, *FERMI*, and *AGILE*, respectively. The TeV emission correlates quite well with the position of three massive molecular clouds, one of which is interacting with the north-eastern part of the shell (and corresponds to the TeV source HESS J1801-233), and the other two being located to the south of the SNR (TeV sources HESS J1800-240 A and B) . The masses of these clouds can be estimated from CO measurements and result in ≈ 5, 6, and $4 \times 10^4 M_\odot$, respectively, and their projected distances from the centre of the SNR are ≈ 12, 20, and 20 pc, respectively (Aharonian et al. 2008a). The GeV emission roughly mimics the TeV one, except for the fact that no significant emission is detected at the position of HESS J1800-240 A.

Here, we investigate the possibility that the gamma ray emission from the W28 region could be the result of hadronic interactions of CRs that have been accelerated

in the past at the SNR shock and then escaped in the surrounding medium [1]. To do so, we follow the approach described in Chapter 4 and in Gabici et al. (2009, 2010), which we briefly summarize below.

For each particle energy E we solve the diffusion equation for CRs escaping the SNR. For simplicity we treat the SNR as a point like source of CRs and we consider an isotropic and homogeneous diffusion coefficient: $D \propto E^{\delta}$. A value of $\delta = 0.5$ is found to provide a good fit to data (see below), though reasonably good fits can be obtained also for values in the range $\delta = 0.3 - 0.7$. The solution of the diffusion equation gives the spatial distribution of CRs around the source f_{CR}, which is roughly constant up to a distance equal to the diffusion radius $R_d = \sqrt{4\ D\ t_{diff}}$, and given by $f_{CR} \propto \eta E_{SN}/R_d^3$, where η is the fraction of the supernova explosion energy converted into CRs, and t_{diff} is the time elapsed since CRs with energy E escaped the SNR. For distances much larger than R_d the CR spatial distribution falls like $f_{CR} \propto \exp(-(R/R_d)^2)$, ad expected for diffusion. Following the approach described in Chapter 4, we assume that CRs with energy 5 PeV (1 GeV) escape the SNR at the beginning (end) of the Sedov phase, at a time ~ 250 yr ($\sim 1.2 \times 10^4$ yr) after the explosion, and that the time integrated CR spectrum injected in the interstellar medium is $\propto E^{-2}$. In this scenario, particles with lower and lower energies are released gradually in the interstellar medium (Ptuskin & Zirakashvili 2005), and we parametrize the escape time as: $t_{esc} \propto E^{-\alpha}$ which, during the Sedov phase, can also be written as $R_s \propto E^{-2\alpha/5}$, where R_s is the shock radius at time t_{esc} and $\alpha \sim 4$. From this it follows that the assumption of point like CR source is good for high energy CRs only ($\sim$ TeV or above), when R_s is small, but it becomes a rough approximation at significantly lower energies. This is because low energy particles are believed to be released later in time, when the SNR shock radius is large (i.e. non negligible when compared to R_d).

We now provide a simplified argument to show how we can attempt to constrain the diffusion coefficient by using the TeV gamma ray observations of the MCs in the W28 region. The time elapsed since CRs with a given energy escaped the SNR can be written as: $t_{diff} = t_{age} - t_{esc}$. However, for CRs with energies above 1 TeV (the ones responsible for the emission detected by HESS) we may assume $t_{esc} << t_{age}$ (i.e. high energy CRs are released when the SNR is much younger than it is now) and thus $t_{diff} \sim t_{age}$. Thus, the diffusion radius reduces to $R_d \sim \sqrt{4\ D\ t_{age}}$. We recall that within the diffusion radius the spatial distribution of CRs, f_{CR}, is roughly constant, and proportional to $\eta E_{SN}/R_d^3$. On the other hand, the observed gamma ray flux from each one of the MCs is: $F_\gamma \propto f_{CR} M_{cl}/d^2$, where M_{cl} is the mass of the MC and d is the distance of the system. Note that in this expression F_γ is calculated at a photon energy E_γ, while f_{CR} is calculated at a CR energy $E_{CR} \sim 10 \times E_\gamma$, to account for the inelasticity of proton-proton interactions. By using the definitions of f_{CR} and R_d we can finally write the approximate equation, valid within a distance

[1] This scenario has been described in a number of recent papers (Fujita et al. 2009; Ohira et al. 2010; Li & Chen 2010).

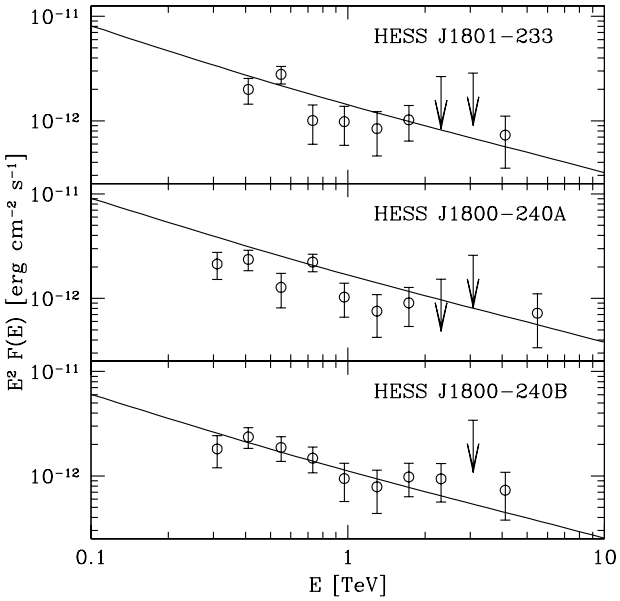

Figure 5.3: Simultaneous fit to the three TeV sources detected by HESS in the W28 region. Gamma ray spectra have been calculated by using the parameterizations by Kamae et al. (2006), where a multiplicative factor of 1.5 has been applied to account for the contribution to the emission from nuclei heavier than H both in CRs and in the interstellar medium.

R_d from the SNR:

$$F_\gamma \propto \frac{\eta\ E_{SN}}{(D\ t_{age})^{3/2}} \left(\frac{M_{cl}}{d^2}\right).$$

Estimates can be obtained for all the physical quantities in the equation except for the CR acceleration efficiency η and the local diffusion coefficient D. By fitting the TeV data we can thus attempt to constrain, within the uncertainties given by the errors on the other measured quantities (namely, E_{SN}, t_{age}, M_{cl}, and d) and by the assumptions made (e.g. the CR injection spectrum is assumed to be E^{-2}), a combination of these two parameters (namely $\eta/D^{3/2}$). The fact that the MCs have to be located within a distance R_d from the SNR can be verified a posteriori. Given all the uncertainties above, our results have to be interpreted as a proof of concept of the fact that gamma ray observations of SNR/MC associations can serve as tools to estimate the CR diffusion coefficient. More detection of SNR/MC associations are needed in order to check whether the scenario described here applies to a whole class of objects and not only to a test-case as W28. Future observations from the Cherenkov Telescope Array will most likely solve this issue.

Fig. 5.3 shows a fit to the *HESS* data for the three massive MCs in the W28 region. A simultaneous fit to all the three MCs is obtained by fixing a value for $\eta/D^{3/2}$, which implies that the diffusion coefficient of particle with energy 3 TeV

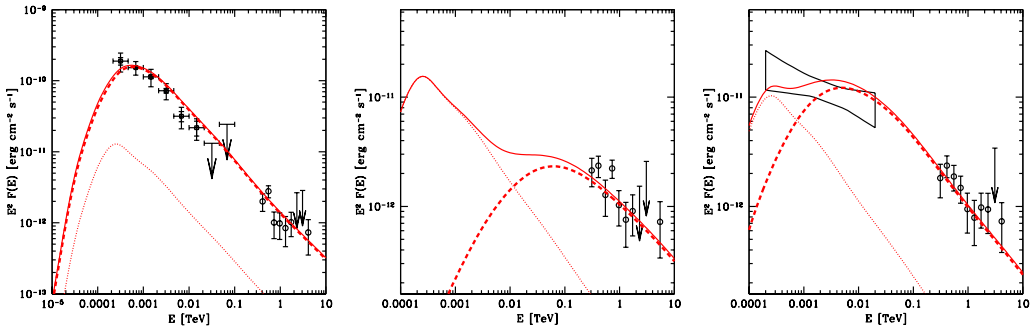

Figure 5.4: Broad band fit to the gamma ray emission detected by *FERMI* and *HESS* from the sources HESS J1801-233, HESS J1800-240 A and B (left to right). Dashed lines represent the contribution to the gamma ray emission from CRs that escaped W28, dotted lines show the contribution from the CR galactic background, and solid lines the total emission. Distances to the SNR centre are 12, 65, and 32 pc (left to right). *FERMI* and *HESS* data points are plotted in black. No GeV emission has been detected from HESS J1800-240 A.

(these are the particles that produce most of the emission observed by *HESS*) is:

$$D(3\ \mathrm{TeV}) \approx 5 \times 10^{27}\ \left(\frac{\eta}{0.1}\right)^{2/3}\ \mathrm{cm}^2/\mathrm{s}\ . \tag{5.2}$$

This value is significantly smaller (more than an order of magnitude) than the one normally adopted to describe the diffusion of $\sim$ TeV CRs in the galactic disk, which is $\approx 10^{29}$ cm^2/s. For example, an acceleration efficiency $\eta = 30\%$ corresponds to a CR diffusion coefficient of $D \sim 10^{28}$ cm^2/s, which in turn gives a diffusion distance for 3 TeV particles of $R_d \approx 80$ pc. This means that the results in Fig. 5.3 are valid if the physical (not projected) distances between the MCs and the SNRs do not significantly exceed R_d. Small values of the diffusion coefficient have been also proposed by Giuliani et al. (2010); Fujita et al. (2009); Li & Chen (2010). Note that, since we are considering gamma rays in a quite narrow (about one order of magnitude) energy band around ≈ 1 TeV, we can actually constraining the diffusion coefficient of CRs with energy $\approx 3 - 30$ TeV, and we cannot say much about the energy dependence of the diffusion coefficient on a broad energy interval.

In principle, observations by *FERMI* and *AGILE* might be used to constrain the diffusion coefficient down to GeV particle energies. However, in this energy band the uncertainties are more severe because of the following reasons: *i)* low energy CRs are believed to be released late in time, when the SNR shock is large, and thus the assumption of point-like source is probably not well justified (see Ohira et al. 2010 for a model that takes into account the finite size of the SNR) ; *ii)* for the same reason, we can no longer assume that $t_{diff} \sim t_{age}$, as we did for high energy CRs. In other words, we need to know the exact time at which CRs with a given energy escape the SNR. Though some promising theoretical studies exist (e.g. Ptuskin & Zirakashvili 2005), our knowledge of the escape time of CRs from SNRs is still quite

limited.

Fig. 5.4 shows a fit to the broad band gamma ray spectrum measured from *FERMI* and *HESS*. The three panels refers to (left to right) the sources HESS J1801-233, HESS J1800-240 A and B, respectively. Dashed lines represent the contribution to the emission from CRs that escaped from W28, dotted lines the contribution from background CRs, and solid lines the total emission. Since *FERMI* data refers to the emission after background subtraction, dashed lines have to be compared with data points. The (often non-trivial) background subtraction issue might add another source of uncertainty in the comparison between data and predictions. An acceleration efficiency $\eta = 30\%$ and a diffusion coefficient $D = 10^{28}$ cm^2/s at 3 TeV have been assumed, while the distance from the SNR centre is assumed to be (left to right) 12, 65, and 32 pc. Keeping in mind all the above mentioned caveats, it is encouraging to see that a qualitative agreement exists between data and predictions also in the GeV band.

Summarizing, we investigated the possibility that the gamma ray emission detected from the MCs in the region of the SNR W28 is produced by CRs that escaped the SNR. This interpretation requires the CR diffusion coefficient in that region to be significantly suppressed with respect to the average galactic one. Such suppression might be the result of an enhancement in the magnetic turbulence due to CR streaming away from the SNR.

The results presented in this chapter have been first published in:

- S. Gabici, S. Casanova, F.A. Aharonian, & G. Rowell, SF2A-2010: Proceedings of the Annual meeting of the French Society of Astronomy and Astrophysics, in press – arXiv:1009.5291
- S. Casanova, D.I. Jones, F.A.Aharonian, Y. Fukui, S. Gabici, A. Kawamura, T. Onishi, G. Rowell, H. Sano, K. Torii, & H. Yamamoto, PASJ, **62**, 1127 (2010)

Chapter 6

Checking the assumptions: are molecular clouds cosmic ray barometers?

In the previous Chapters we computed the expected gamma ray emission from MCs located in the vicinity of a CR accelerator. We always assumed that MCs can be used as CR barometers, namely, that their gamma ray emission is simply proportional to the product between their mass (that can be measured from CO observations) and the CR pressure in the region of the Galaxy where the MC is located. To do so, we had (obviously) to assume that CRs can freely penetrate the MC.

The issue of the penetration or exclusion of cosmic rays from clouds has been investigated in several theoretical papers (Cesarsky & Volk 1978; Skilling & Strong 1976; Dogel' & Sharov 1990), in which quite different conclusions have been drawn, going from the almost-free penetration to the exclusion of cosmic rays up to tens of GeV. Observations in the GeV range of molecular clouds have also been used with this respect (Lebrun & Paul 1978; Bloemen et al. 1984; Blitz et al. 1985), while in the TeV range the first detections of clouds are much more recent (e.g. Aharonian et al. 2006b). Since a theoretical determination of the cosmic ray diffusion coefficient is a very difficult task, and since we are mainly interested here in checking the assumption made in the previous Chapters, we adopt a fully phenomenological approach: the diffusion coefficient is parametrized, and observable quantities (such as the gamma ray flux) capable of constraining it are proposed.

For simplicity, we limit ourselves to consider only the case of *passive* clouds embedded in the diffuse galactic CR flux and located far away from cosmic ray accelerators. This will suffice to investigate the effects of CR penetration into (or exclusion from) MCs on their gamma ray emission (Gabici et al. 2007).

6.1 Charcateristic time scales of the problem

Before solving the equation that describes the transport of cosmic rays inside a magnetized, dense cloud, it is worth giving an estimate of the typical time scales

involved in the problem. Consider a giant MC of radius $R_{cl} \sim 20$ pc, mass $M_{cl} \sim 2 \times 10^5 M_\odot$ and average magnetic field $B_{cl} \sim 10$ μG. The average density (Hydrogen atoms) of such cloud is thus $n_{gas} \sim 300$ cm^{-3}, which gives a dynamical (free–fall) time for the system of the order of:

$$\tau_{dyn} \sim (G\rho)^{-\frac{1}{2}} \sim 5.5 \times 10^6 \left(\frac{n_{gas}}{300\,\mathrm{cm}^{-3}} \right)^{-\frac{1}{2}} \ \mathrm{yr} \tag{6.1}$$

where G is the gravitational constant and ρ the mass density. This free–fall time has probably to be considered as a strict lower limit to the lifetime of the cloud, since additional pressure support from fluid turbulence and magnetic field may inhibit the collapse (e.g. Shu et al. 1987).

The effectiveness of the CR penetration into the cloud depends on the interplay of several physical processes: (i) diffusion in the cloud magnetic field, (ii) advection due to turbulent bulk motion inside the cloud, (iii) energy losses in the dense cloud medium. Moreover, the cosmic ray density can be enhanced if a CR accelerator is embedded in the MC (Aharonian & Atoyan 1996), or if CRs coming from outside the cloud are reaccelerated via Fermi–like processes that may take place in the magnetized cloud turbulence (Dogel' & Sharov 1990). In the following we consider the MC as a passive target for galactic CRs and neglect any effect related to the possible presence of acceleration and/or reacceleration of CRs inside the cloud.

We parametrized the diffusion coefficient for protons of energy E propagating in the cloud magnetic field B in the following way:

$$D(E) = \chi \ D_0 \left(\frac{E/\mathrm{GeV}}{B/3 \ \mu\mathrm{G}} \right)^{\delta} \tag{6.2}$$

where $D_0 = 3 \times 10^{27} \mathrm{cm}^2/\mathrm{s}$ and $\delta = 0.5$ are the typical galactic values (Berezinskii et al. 1990) and the parameter $\chi < 1$ accounts for a possible suppression of the diffusion coefficient inside the turbulent cloud medium. In general, the values of χ and δ will depend on the power spectrum of the magnetic field turbulence. For such a choice of parameters, one can estimate the proton diffusion time, namely, the time it takes a proton to penetrate into the core of the cloud:

$$\tau_{diff} = \frac{R_{cl}^2}{6 \ D(E)} \sim 1.2 \times 10^4 \ \chi^{-1} \left(\frac{R_{tot}}{20 \ \mathrm{pc}} \right)^2 \left(\frac{E}{\mathrm{GeV}} \right)^{-0.5} \left(\frac{B}{10 \ \mu\mathrm{G}} \right)^{0.5} \ \mathrm{yr} \tag{6.3}$$

To study the effective propagation of CRs into MCs, it is instructive to compare the diffusion time with the energy loss time. In the dense cloud environment, CR protons suffer energy losses due to ionization and nuclear p–p interactions. Above the energy threshold for pion production $E_{th} \approx 300$ MeV nuclear interactions dominate. Since both the cross section $\sigma_{pp} \sim 40$ mb and inelasticity $\kappa \sim 0.45$ of this process are not changing significantly over a broad range of proton energies from ~ 1 GeV to hundreds of TeVs, the proton lifetime is almost energy independent:

$$\tau_{pp} = \frac{1}{n_{gas} \ c \ \kappa \ \sigma_{pp}} \sim 2 \times 10^5 \left(\frac{n_{gas}}{300 \ \mathrm{cm}^{-3}} \right)^{-1} \ \mathrm{yr} \tag{6.4}$$

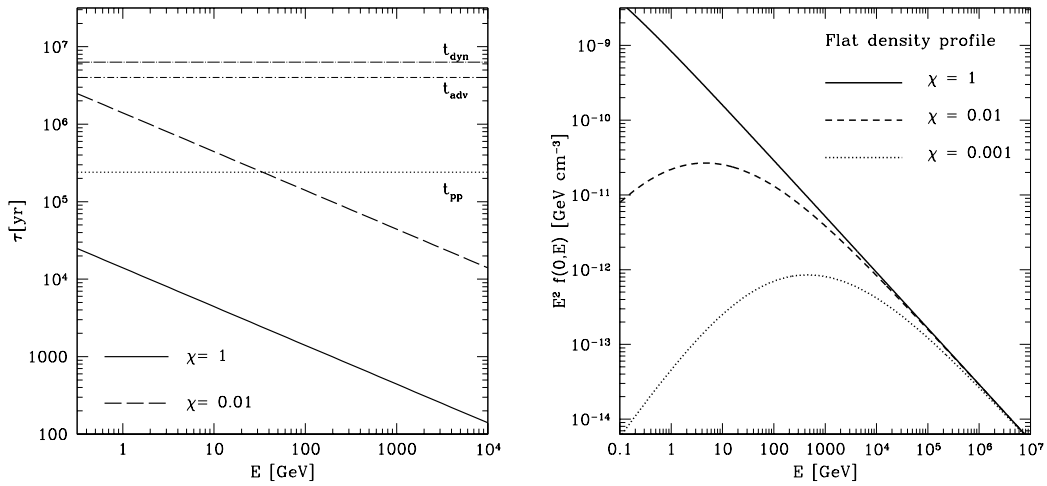

Figure 6.1: **LEFT PANEL**: typical time scales for cosmic rays in a giant molecular cloud with average number density ~ 300 cm^{-3}, radius 20 pc and average magnetic field 10 μG. Solid and dashed lines represent the diffusion time, horizontal lines represent the dynamical, advective and energy loss times (top to bottom). **RIGHT PANEL**: cosmic ray spectrum in the cloud center for different values of the parameter χ, describing the suppression of the diffusion coefficient with respect to the measured galactic value (see text for details).

CRs can also be transported (advected) by the fluid turbulence which is known to be present in MCs. Several molecular lines are observed in the direction of clouds, and their width Δv reflects the velocity of internal turbulent motions. The line width is known to correlate with the MC size according to the relation: $\Delta v \propto R_{cl}^{0.5}$ (Shu et al. 1987), which for the cloud sizes considered here provides a velocity of a few km/s. The time scale for this advective transport can be roughly estimated as:

$$\tau_{adv} \sim \frac{R_{cl}}{\Delta v} \sim 4 \times 10^6 \left(\frac{R_{cl}}{20 \text{ pc}}\right) \left(\frac{\Delta v}{5 \text{ km/s}}\right) \text{ yr} \tag{6.5}$$

The energy dependence of all the time scales considered above is shown in Figure 6.1 (left panel), where the solid and dashed thick lines represent the diffusion time (for $\chi = 1$ and $\chi = 0.01$, respectively), while the horizontal lines refers to the dynamical, advective and energy loss time scales (from top to bottom). Several comments are in order. First of all, the dynamical lifetime of the cloud is the longest time scale for all the relevant energies. This means that it is possible to search for a steady state solution of the problem. Second, the advection time is comparable with the dynamical time, but it is always significantly longer than both the diffusion and the energy loss time scales. Thus, we can safely ignore the advection term in the CR transport equation. As a consequence, the degree of penetration of CRs inside the cloud can be roughly estimated by comparing the diffusion and energy loss times. To this purpose, in Figure 6.1 (left panel) two different values of the parameter χ

are considered. If $\chi = 1$ the diffusion time is shorter than the energy loss time at all the considered energies. Thus, if the diffusion coefficient inside the cloud is not suppressed with respect to the galactic value, cosmic rays can easily penetrate into the cloud. On the other hand, if diffusion inside the cloud is significantly suppressed ($\chi = 0.01$), the energy loss time becomes shorter than the diffusion time at energies below $E_* \sim 10 - 100$ GeV. This means that only CRs with energy above E_* can penetrate into the cloud before losing their energy. This is a very important fact, since as we will demonstrate in the following sections, the exclusion of low energy CRs may play a crucial role in shaping the gamma ray spectrum of MCs.

Finally, it is worth stressing that the value of E_* increases if one considers a realistic density profile for the cloud instead of average quantities. Despite the fact that density profiles cannot be easily extracted from available observations, it is well known that molecular clouds contain cores of size ~ 1 pc or less, in which density can reach very high values, up to $n_{gas} \sim 10^5$ cm^{-3}. In this case, a proton which is approaching the center of the cloud meets a denser and denser environment. The value of the magnetic field is also increasing towards the cloud center, reaching in the densest regions values of hundreds of μG or even more (Crutcher 1999). These facts make the energy loss time shorter and the diffusion time longer, leading to a more efficient exclusion of cosmic rays from clouds cores.

6.2 Solution of the transport equation

The equation describing the CR transport in a cloud embedded in the galactic CR background is the steady state diffusion–losses equation, which in spherical symmetry reads:

$$\frac{1}{R^2}\frac{\partial}{\partial R}\left[D(R,E)R^2\frac{\partial f}{\partial R}\right] + \frac{\partial}{\partial E}\left[\dot{E}(R)f\right] = 0 \tag{6.6}$$

where $f(R,E)$ is the space and energy dependent particle distribution function, $D(R,E)$ is the diffusion coefficient parametrized as described in the previous section and $\dot{E}(R,E) = dE/dt$ represents energy losses.

We parametrize the density profile as follows:

$$n_H(R) = \frac{n_0}{1 + \left(\frac{R}{R_c}\right)^{\alpha}} \tag{6.7}$$

where n_0 is the central density and R_c the core radius, assumed to be 1/2 parsec. This is of course a simplified assumption, since MCs can exhibit very irregular density profiles. However, we will show in the following that the mechanism of CR exclusion from clouds may work for very different density profiles, from flat ($\alpha = 0$) to very peaked ones ($\alpha \gg 0$). This suggests that the same effect may be present also in more realistic (and complicated) density profiles.

In calculating the energy loss term we consider only inelastic proton–proton collisions, since this is the dominant process above the threshold for the production

of pions ($E_{th} \sim 280$ MeV). The loss term in Eq. (6.6) depends on the density profile through Eq. (6.4), and thus it is space dependent.

For the magnetic field profile we use the results from Crutcher (1999), in which Zeeman measurements of magnetic field strength in MC cores are reported. A correlation between magnetic field strength and gas density is observed and can be roughly fitted by:

$$B \sim 100 \left(\frac{n_H}{10^4 \text{ cm}^{-3}}\right)^{1/2} \mu\text{G} \tag{6.8}$$

Though this correlation has been found for MC cores with density exceeding $n_H \sim 10^3$ cm^{-3}, it provides reasonable values also for low density regions (tens of μG for typical average cloud densities of a few 100 cm^{-3}). Thus, we assume that Eq. (6.8) is valid in the entire density interval. It is worth noticing that in our model the diffusion coefficient is space–dependent, since it depends on the magnetic field as given by Eq. (6.2).

We solved Eq. 6.6 numerically, using an implicit scheme and assuming, as boundary condition, that the CR spectrum outside the cloud must match the galactic cosmic ray spectrum (as done in e.g. Dogel' & Sharov 1990). The galactic spectrum is in turn assumed to be equal to the locally observed CR flux:

$$J_{CR}^{gal}(E) = 2.2 \left(\frac{E}{\text{GeV}}\right)^{-2.75} \text{cm}^{-2}\text{s}^{-1}\text{sr}^{-1}\text{GeV}^{-1} \tag{6.9}$$

The effective exclusion of CRs from the cloud cores is demonstrated in Fig. 6.1 (right panel), where the CR spectrum in the cloud center is plotted for different values of the parameter χ (here δ is set equal to the galactic value 0.5). In obtaining the result, a cloud with mass $2 \times 10^5 M_\odot$, radius 20 pc and a flat density profile (this corresponds to a spatially constant magnetic field of ~ 15 μG) has been considered. If the diffusion coefficient inside the cloud is not suppressed with respect to the galactic value ($\chi = 1$), then the CR spectrum in the cloud center is basically indistinguishable from the galactic CR spectrum, i.e. CR freely penetrate the MC. On the other hand, if diffusion is significantly suppressed ($\chi << 1$), CRs with energy above ~ 10 GeV ($\chi = 0.01$) or ~ 100 GeV ($\chi = 0.001$) cannot penetrate the cloud. As we will show in the following, this fact has important implications for the estimate of the spectrum and intensity of the gamma ray emission expected from MCs.

CR protons propagating inside a MC also produce secondary electrons during inelastic interactions in the intercloud medium. These electrons contribute to the overall gamma ray emission of the cloud via Bremsstrahlung. Once the steady state proton spectrum has been obtained, we calculated the injection spectrum $Q_e(E_e)$ of the secondary electrons by using the analytical fits provided by Kelner et al. (2006). The steady state spectrum of secondary electrons can be obtained using again Eq. (6.6) appropriately modified as follows: *i)* the injection term $Q_e(E_e)$ must be added on the left side; *ii)* the loss term $\dot{E}_e(R, E)$ is now dominated by Coulomb, Bremsstrahlung and synchrotron losses (e.g. Ginzburg & Syrovatskii 1964) and it is both space and energy dependent; *iii)* as boundary condition we assumed that

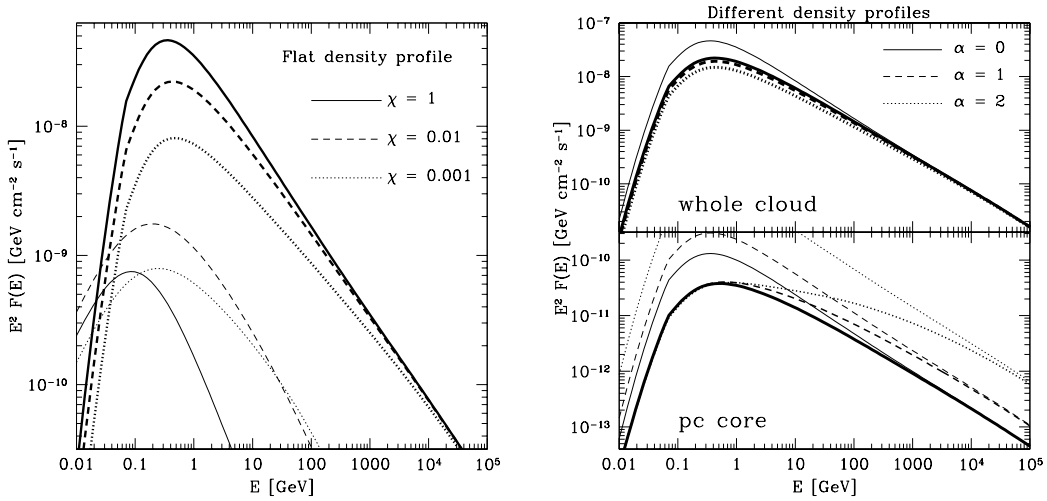

Figure 6.2: **LEFT PANEL**: gamma ray emission from a cloud with $M = 2 \times 10^5 M_\odot$, $R_{cl} = 20$ pc and a flat density profile. The cloud distance is 1 kpc. Thick lines: π^0–decay gamma rays, thin lines: Bremsstrahlung gamma rays. **RIGHT PANEL**: Thick lines: gamma ray emission (only π^0–decay component) from clouds with different density profiles and $\chi = 0.01$. Thin lines show the gamma ray emission one would observe if cosmic rays could freely penetrate the cloud.

the particle distribution function for secondary electron vanishes outside the cloud, where the gas density is low, implying inefficient production of secondaries.

6.3 Gamma ray spectra

Fig. 6.2 (left panel) shows the gamma ray spectra for a cloud of mass $M = 2\times10^5 M_\odot$ and radius $R_{cl} = 20$ pc. A flat density profile is assumed for a cloud at a distance of 1 kpc. The thick lines represent the contribution to the total gamma ray emission from π^0–decay (calculated following Kelner et al. 2006), while the thin lines represents the Bremsstrahlung contribution. Calculations have been performed adopting a diffusion coefficient with $\delta = 0.5$, but assuming three different values for $\chi = 1, 0.01, 0.001$ (curves top to bottom respectively). The Bremsstrahlung contributions become significant only below photon energies of ~ 100 MeV.

The solid line represents the situation in which CRs can freely penetrate the cloud, namely $\chi = 1$ (no suppression of the diffusion coefficient). This gives the maximum possible gamma ray luminosity for a passive cloud immersed in the galactic CR sea. If the diffusion coefficient is suppressed (dashed and dotted lines, corresponding to $\chi = 0.01, 0.001$) the total gamma ray luminosity is reduced, especially at low energies (~ 1 GeV), while at high energies the canonical spectrum for a passive cloud filled by CRs is recovered. This reflects the fact that high energy CRs can freely penetrate inside clouds. At ~ 1 GeV, the suppression of the gamma ray flux is roughly a factor of ~ 2 for $\chi = 0.01$ and a factor of ~ 5 for $\chi = 0.001$. Moreover,

also the shape of the spectrum in modified, appearing flatter for lower values of χ (stronger suppression of diffusion). This fact might have very important implications for *Fermi* observations of MCs. In particular, the observation of gamma ray spectra harder than the ones expected from an isolated (passive) cloud pervaded by galactic CRs can be interpreted in two different ways: *i)* the galactic CR spectrum at the location of the cloud is different than the one measured locally; *ii)* propagation effects inhibit the penetration of low energy CRs in the cloud, making the resulting gamma ray spectrum harder.

MCs are also potential targets for Cherenkov telescopes arrays, operating at photon energies greater than 100 GeV. The apparent angular size of a cloud with radius $R_{cl} \sim 20$ pc located at a distance d is $\vartheta_{cl} \sim 2R_{cl}/d \sim 2.2^{\circ}(d/\mathrm{kpc})^{-1}$. This is significantly smaller than the telescope field of view (e.g. $\sim 5^{o}$ for *HESS*) and much larger than its angular resolution ($\sim 0.1^{\circ}$), thus Cherenkov telescopes can in principle effectively map the gamma ray emission from nearby MCs. Notably, a core with radius of half parsec will subtend an angle comparable with the telescope angular resolution, if the MC is at 1 kpc. For this choice of the parameters, the gamma ray flux (only π^0–decay contribution) for a cloud of mass $2 \times 10^5 M_{\odot}$ is shown in Fig. 6.2 (right panel). The diffusion coefficient is the galactic one suppressed by a factor of 100 and the parameter α describing the slope of the density profile is varied. In the top panel the emission from the whole cloud is shown. Thick lines represent the spectrum for different values of α: 0 (solid), 1 (dashed) and 2 (dotted). The thin line represents the spectrum one would observe if CRs could freely penetrate the cloud. It can be seen that the emission from the whole cloud is not depending strongly on the density profile. The situation is much different if one considers the radiation from the inner parsec region (Fig. 6.2, bottom panel), which in this particular case corresponds to the radiation received within one angular resolution of the Cherenkov telescope. In this case the resulting gamma ray spectrum strongly depends on the assumption made on the density profile, especially at very high energies above ~ 10 GeV. This is because, for peaked density profiles ($\alpha > 0$) the exclusion of CRs from cloud cores is much more effective with respect to the case of a flat profile ($\alpha = 0$), due to the enhanced energy losses and reduced diffusion there. This makes the gamma ray spectrum harder. On the other hand, since the cores are very dense, the suppression of the CR density is compensated by the higher efficiency of production of gamma rays. This explains why a higher level of the gamma ray emission from the densest cores is predicted.

Thus, we arrive at the important conclusion that *the shape of the gamma ray spectrum from molecular cloud cores is determined not only by the diffusion properties of cosmic rays but also by the actual shape of the cloud density profile.*

This statement is confirmed in Fig. 6.3, where the slope of the gamma ray spectrum at photon energies of 100 GeV (top panels) and 1 TeV (bottom panels) is plotted for different combinations of model parameters. In the left panel we fix $\delta = 0.5$ but we change the slope of the density profile α, while in the right panel, α is kept fixed and the energy dependence of the diffusion coefficioen δ is varied. In both plots $\chi = 0.01$. Triangles refer to the spectrum from the whole cloud and circles

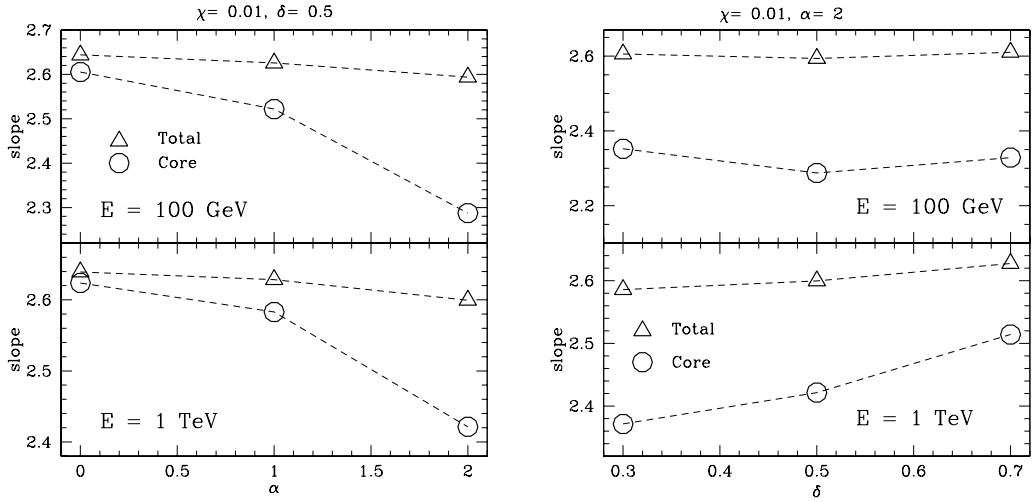

Figure 6.3: Slope of the gamma ray spectrum for different sets of parameters. Triangles refer to the spectrum of the whole cloud, circles refer to the spectrum observed by looking at the cloud core only.

refer to observations of the core region only. Again, we emphasize that, although the total gamma ray spectrum from the whole cloud is not strongly affected by the choice of the model parameters, the cloud cores may show a great variety of energy spectra. As a consequence, gamma ray observations in the TeV energy domain can be very useful to constrain parameters. In principle, if the cloud density profile could be extracted from independent observations (e.g. CO line emission) the shape of the gamma ray spectrum would tell us important information about the diffusion coefficient. Of course, the determination of the density profile is a extremely difficult task, since clouds show very complex structures.

6.4 Conclusions

In this chapter we considered a giant MC embedded in the diffuse galactic CR flux. Assuming that the CR propagation inside the cloud proceeds in the diffusive regime, we studied the exclusion/penetration of CRs into MCs. Results can be summarized as follows:

- if the diffusion coefficient inside the cloud is equal to the measured galactic one, CRs can freely penetrate the cloud and the resulting high energy gamma ray emission has a spectral shape that closely resembles the one of the galactic CRs. In this case MCs can be effectively used as CR barometers.

- The gamma ray emission above 100 MeV is dominated by π^0–decay, and Bremsstrahlung emission from secondary electrons is relevant only at smaller energies.

- If the diffusion coefficient is significantly suppressed (i.e. a factor of 100 or more) with respect to the galactic one, CRs can be effectively excluded from clouds. In particular, for a suppression of the diffusion coefficient of a factor of ~ 100, the exclusion becomes relevant at energies of tens-hundreds of GeV, for a MC with mass $2 \times 10^5 M_{\odot}$.
- The exclusion of CRs from clouds results in a suppression of the gamma ray flux, especially at $\sim$ GeV energies. This can have important consequences for *Fermi* observations.
- Cherenkov telescopes such as *HESS* or *VERITAS* have the capability to map the gamma ray emission from nearby MCs and to resolve the pc-scale cores. In particular, the shape of the gamma ray spectra from cloud cores may strongly depend on both the diffusion properties of CRs and the shape of the cloud density profile. The effect of the density profile in shaping the gamma ray spectrum of MCs is a remarkable result of this work.

The results presented in this chapter have been first published in:

- S. Gabici, F.A. Aharonian, P. Blasi, Astrophys. Space Sci. **309**, 365 (2007)

Chapter 7

Conclusions and future perspectives

Are supernova remnants the sources of galactic cosmic rays?

It is intriguing to see how, one century after their discovery, the origin of cosmic rays is still an open issue. Despite the fact that there is now a general consensus in indicating supernova remnants as the most likely sources of cosmic rays, it is important to stress that there is no conclusive proof of that. It is also worth mentioning that, besides the mainstream research on cosmic ray acceleration at supernova remnant shocks, alternative ideas have been pushed forward throughout the years. These include variations of the supernova remnant hypothesis like the superbubble model (Bykov & Fleishman 1992; Parizot et al. 2004) or the single-source model (Erlykin & Wolfendale 1997), or more extreme scenarios like the cannonball model (Dar & de Rújula 2008). Though less popular than the supernova remnant model, these scenarios would definitely deserve much more attention than they get.

The main problem in identifying the sources of cosmic rays is connected to the fact that cosmic rays are deflected in the turbulent magnetic field of the Galaxy. This fact implies that we cannot infer the position of the source from the arrival direction of cosmic rays, as it is done with photons in traditional astronomy. For this reason, the most promising way to identify cosmic ray sources is through the detection of neutral secondaries produced in cosmic ray interactions within (or near) the source. Such secondary particles, being neutral, are not deflected by magnetic fields and might allow us to identify the production sites of cosmic rays. Neutrinos and gamma rays, both produced in hadronic interactions between cosmic rays and thermal protons can be used for this purpose. Neutrinos, unlike gamma rays, are produced uniquely in hadronic interactions and thus their detection would constitute an unambiguous evidence for the presence of cosmic rays in a given astrophysical object. Though desirable, such a detection appears to be quite challenging also with large detectors such as ICECUBE or the future facility KM3NeT. With this respect, searching for gamma ray signatures of cosmic ray acceleration (and disentangling the hadronic component from the leptonic one) seems to be a promising path to

follow, given the much better sensitivity of gamma ray telescopes.

The popularity of the supernova remnant hypothesis for the origin of galactic cosmic rays resides in the fact that those objects can easily provide the total energy required to explain the observed cosmic ray density in the galaxy. Moreover, diffusive acceleration can operate at supernova remnant shocks, providing an effective mechanism for particle acceleration. The belief that supernova remnants are indeed the sources of cosmic rays has been recently reinforced by their detection in TeV gamma rays. Such emission was expected within the framework of the supernova remnant hypothesis, and its detection long awaited. However, as stressed many times in the previous chapters, the interpretation of the gamma ray emission is not unique and its origin could well be leptonic (i.e. inverse Compton scattering off soft background photons). In order to solve this ambiguity, extensive modeling of the multi-wavelength emission from supernova remnants have been carried out by many research teams but, as summarized in the Introduction, results do not yet converge unambiguously towards either the hadronic or the leptonic scenario. The solution of the degeneracy between hadronic and leptonic interpretation of the observed emission is one of the most important unsolved issues in gamma ray astronomy.

Finally, in order to reach a full comprehension of the origin of cosmic rays, we need to study not only the mechanism through which they are accelerated at their sources, but also the way in which they propagate from the sources to us. The propagation mode is believed to be diffusive and plays a crucial role both in shaping the particle spectrum that we observe at the Earth and in making the cosmic ray flux isotropic in the sky.

How to solve the hadron-versus-lepton degeneracy – past, current, and future research

The ambiguity between hadronic or leptonic origin of the gamma ray photons detected from supernova remnants might be solved in the near future by means of observations in the multi-TeV range (up to $\approx$ hundreds of TeVs). This domain of the electromagnetic spectrum is currently almost unexplored by current instruments. Future facilities such as the Cherenkov Telescope Array are expected to become operative in the next years (from $\sim$ 2015 on) and, besides other things, will extend the observed range of Cherenkov telescopes upwards in energy. In this energy range inverse Compton scattering becomes inefficient due to Klein-Nishina effect and thus the interpretation of the observed gamma ray emission becomes free of ambiguity and reduces to the case of decay of neutral pions produced during hadronic interactions between cosmic rays and ambient gas. Moreover, such photons are produced by $\approx$ PeV cosmic rays, and thus their detection from supernova remnants would prove that cosmic rays are accelerated there up to the energy of the knee. It is truly remarkable to see how photons in this specific energy range can provide, as neutrinos do, evidence for hadronic interactions.

The feasibility of this approach has been extensively investigated and promising results have been obtained (see Chapter 3). The detection of young supernova remnants with a gamma ray spectrum extending up to hundreds of TeVs without

exhibiting any significant attenuation/cutoff would imply that those remnants are currently accelerating PeV cosmic rays, and thus prove that supernova remnants as a class of objects are capable of explaining the observed spectrum of cosmic rays up to the knee. The drawback of this is that the emission in the multi-TeV domain is expected to last for a quite short time (i.e. the time during which the shock speed is fast enough to allow particle acceleration up to the energy of the knee) that can be estimated to be in the range 100-1000 years. After this time, $\sim$ PeV cosmic rays escape the remnant and the multi-TeV emission switches off.

Remarkably, this fact opens another possibility, namely, to search for multi-TeV gamma rays from massive molecular clouds located in proximity of not-so-young supernova remnants. They are expected to emit such radiation because they can be illuminated by the $\sim$ PeV cosmic rays that have been accelerated in the remnant in the past, and then escaped in the surrounding medium. This scenario has two advantages: first, molecular clouds are very massive and can thus provide a thick target for proton-proton interactions; second, the duration of the emission is not determined anymore by the supernova remnant dynamical time, but by the time it takes particles to diffuse from the remnant to the cloud. Since the diffusion coefficient close to cosmic ray sources might be suppressed due to streaming instability of escaping cosmic rays, we might hope this diffusion time to be significantly longer than 100-1000 years. Both these facts (stronger emission that lasts longer) enhance the probability of detection (see Chapter 3). Of course the detection of neutrinos, challenging but not impossible, remains a viable alternative to prove cosmic ray acceleration in supernova remnants (see Chapter 3).

The fact that the characteristics of the gamma ray emission from the molecular cloud depend on the diffusion time of runaway cosmic rays suggests that one might use molecular clouds to constrain the diffusion of cosmic rays in the Galaxy (see Chapter 4). This fact is of crucial importance, since the diffusion coefficient is very difficult to be estimated (both observationally and theoretically). In order to do so, a detailed modeling of the multi-wavelength emission from a cosmic-ray-illuminated cloud needs to be calculated. Such calculations show that the total emission from a cloud is prominently dominated by its gamma ray flux (GeV-TeV range), and quite weak in the other wavelength. Sources with such a spectrum have been detected with Cherenkov telescopes and are normally referred to as *dark* sources by TeV astronomers. They are often not identified with known astrophysical objects. Some of these sources might be molecular clouds. Studying in the gamma ray domain molecular clouds associated with supernova remnants might constitute in the near future an effective way to estimate the (to date virtually unknown) particle diffusion coefficient at specific locations in the Galaxy and thus test our knowledge of plasma phenomena like the cosmic ray streaming instability operating in the interstellar medium, or the diffusive acceleration operating at supernova remnant shocks (see Chapter 4).

To date, only very few examples of associations between clouds and supernova remnants can be listed in TeV gamma ray catalogues, the only firm example being the supernova remnant W28. This object can thus be taken as a case-study

to test all the ideas proposed in Chapters 2, 3, and 4 on the escape of particles from supernova remnants, their propagation in the surrounding medium, and the resulting radiative signatures. Results from this study provide a preliminary evidence of the fact that the diffusion coefficient might be significantly suppressed in the neighborhood of W28, possibly due to streaming instability of escaping cosmic rays (see Chapter 5). Future observations with the Cherenkov Telescope Array will undoubtedly increase the statistic of detected objects and allow an extensive study in this direction. Remarkably, even in the absence of massive molecular clouds (as the one present in the vicinity of W28), one can still expect to detect a faint halo of gamma rays around supernova remnants due to the interactions of runaway cosmic rays with the ambient medium. This emission, at least in the case of the powerful and best studied remnant RX J1713.7-3946, might be detected by the Cherenkov Telescope Array, revealing the presence of escaping cosmic rays (see Chapter 5). An important fact to be stressed here is that multi-TeV electrons can be also accelerated at supernova remnant shocks, but they are not expected to contribute at all to the gamma ray emission emission from the surrounding medium, since they remain trapped within the remnant due to severe synchrotron losses. This makes the detection of this gamma ray glows around supernova remnants a very strong indication for cosmic ray acceleration in such objects.

The effectiveness of diffusive penetration of cosmic rays inside molecular clouds might be an issue, especially at low ($\approx$ GeV or less) energies, while at TeV energies the approach presented above should be quite robust and reliable. However, peculiar cases like the giant molecular clouds in the galactic centre region might constitute an exception to this (see Chapter 6).

To summarize, we have outlined a program aimed to search for conclusive evidences for cosmic ray acceleration in supernova remnants. The results summarized in this thesis encourage belief that observations carried out by gamma ray Cherenkov telescopes of next generation might finally unambiguously prove (or disprove) the supernova remnant hypothesis for the origin of galactic cosmic rays. There is a possibility that Icecube will detect neutrinos from supernova remnants first, and thus prove cosmic ray acceleration there. However, even in this most optimistic case, a complete understanding of the origin of cosmic rays (including mechanism of acceleration and production spectrum, particle propagation from the sources to us, and so on ...) will necessarily require the gamma ray observations envisaged above.

More theoretical/phenomenological work has to be carried out in the immediate future in order to finalize the tools needed to interpret future data. The most urgent needs include the estimate of the number of PeVatrons (and nearby cosmic-ray-illuminated clouds) that are expected to be detected by the Cherenkov Telescope Array. This number is likely to be quite meager, given that the total number of supernova remnants that are accelerating PeV cosmic rays is ≈ 10 in the whole Galaxy. However, even the detection of a few of these objects would be a major result since it would prove that they are indeed cosmic ray PeVatrons (Cristofari & Gabici, in progress). Another aspect that needs further investigation is the evaluation, in the framework of quasilinear theory, of the self generated magnetic turbulence on

top of which the cosmic rays diffuse after escaping their sources. It is of crucial importance to understand whether the diffusion coefficient can be indeed suppressed (with respect to the average galactic one) as suggested by the analysis of the test-case supernova remnant W28 (Gabici, Marcowith, & Ptuskin, in progress). Moreover, even the validity itself of the diffusion approximation might be not valid at the highest (i.e. $\approx$ PeV) energies, especially on the short propagation distances ($\approx$ 100 pc or so) relevant for these studies. Thus, accurate studies of the generation (cosmic-ray-induced or not) of long wavelength magnetic turbulence seems mandatory to understand the propagation of PeV particles.

On the more experimental side, the capabilities of the Cherenkov Telescope Array (currently in the preparatory phase) needs to be accurately defined, especially for what concerns the observations of extended objects, as supernova remnants and molecular clouds are, with spectra extending possibly up to very high energies ($\approx$ 100 TeV), where only a few photons are expected. An effort to identify the most important physics goals in this field is currently carried out under my leadership within the Cherenkov Telescope Array consortium (Physics Working Package – Task: Cosmic Rays/Supernova Remnants/Molecular Clouds). Such a study will contribute in guiding the choice of the technical specifications that the telescope array will be required to fulfill.

Future perspectives: bridging high and low energy astrophysics

Most of this thesis has been focused on the galactic cosmic rays with energies in the range $\approx$ GeV – PeV, and on their radiative signatures, especially in the gamma ray domain. In the next chapter we will discuss the radiative signatures that one might expect to detect from the sources of the extragalactic cosmic rays, with energies well in excess of the one of the knee, up to the ultra high energy domain: $E_{CR} \approx 10^{20}$eV. However, the most challenging (and thus intriguing) future development in the field of cosmic ray physics probably concerns the study of low energy cosmic rays (well below the GeV range). With this respect, a collaboration is going to be started soon with Thierry Montmerle at the Institut d'AstroPhysique de Paris.

The difficulties of studying the low energy cosmic rays are manifold and mostly connected to our poor knowledge of even the most basic physical quantities characterizing the cosmic ray spectrum in this energy range. First of all, we do not even know with sufficient accuracy which is the *local* cosmic ray spectrum at energies well below the GeV band. This is because of the influence the sun exerts on the intensity of cosmic rays. This phenomenon is called solar modulation and the intrinsic spectrum of cosmic rays with energies up to 1-10 GeV is obtained by de-modulating the observed data (see e.g. Gleeson & Axford 1968). This introduces a very large uncertainty in the determination of the cosmic ray intensity, which can be as large as one order of magnitude at $\approx$ 10 MeV and grows fast at lower energies (see e.g. Padovani et al. 2009). Second, cosmic rays with energy smaller than about 300 MeV are below the threshold of production of neutral pions, and thus their presence cannot be traced by means of observations in the gamma ray domain, as it can be done for higher energy ones. This means that we do not know the local intensity

nor the spatial distribution of low energy cosmic rays throughout the Galaxy.

At such low energies, cosmic rays affect the interstellar matter by mainly ionizing and heating it (e.g. Spitzer & Tomasko 1968; Field et al. 1969; Dalgarno & McCray 1972; Padovani et al. 2009). Though not important under normal galactic conditions, these processes are believed to be the dominant source of ionization and heating in dense molecular cloud cores, where UV ionizing radiation cannot penetrate due to the very high gas column density (for an excellent textbook review of this aspect see Stahler & Palla 2005). Since ionization level and heating regulate the coupling between gas and magnetic field, and the thermal pressure support, respectively, it is evident how low energy cosmic rays play a crucial role in influencing the gravitational collapse of molecular cloud cores that leads to the formation of stars.

Also from the theoretical point of view, very little is known about the way in which low energy cosmic rays are accelerated and propagate in the galactic magnetic field. If, as done for cosmic rays in the GeV energy range and above, we assume that low energy cosmic rays are also accelerated at supernova remnant shocks, we have to face the problem of particle injection into the accelerator. As said in Chapter 2, the way in which particles are injected into the acceleration mechanism is to date very poorly understood. By using a phenomenological approach, we showed in Chapter 2 that particles, in order to be injected, must have a momentum equal to (at least) a few times the average thermal momentum of particles in the shocked gas. This corresponds to a (kinetic) energy of injected particles in the range 10-100 keV or possibly more. Cosmic rays in the MeV range, the ones relevant for ionization and heating of the gas, are thus quite close to the injection energy region, where it is very hard to formulate firm theoretical claims on both the spectrum of the accelerated particles and its normalization (i.e. how many particles are accelerated).

Also the propagation properties of these cosmic rays are very uncertain, and constraining them is difficult due to the absence of clear radiative signatures (e.g. gamma rays) related to particles with energy below $\approx$ 300 MeV. In other words, the gamma ray based approach developed in Chapters 3, 4, and 5 to constrain the cosmic ray diffusion properties do not apply to low energy particles. A comparison can be made with the transport properties of low energy cosmic ray electrons, for which some constraints can be derived from the observation of the electron-positron annihilation line seen as a diffuse emission from the galactic bulge (Prantzos et al. 2010; Jean et al. 2009). However, an analogy between low energy electrons and protons, if possible at all, does not seem straightforward. An additional complication to this (already quite discomforting) scenario comes from the fact that even the most sophisticated and thoughtful theoretical studies on the penetration of low energy cosmic rays into molecular cloud cores (e.g. Cesarsky & Volk 1978; Padoan & Scalo 2005) are still far from a fully self consistent treatment of the problem.

A promising way to study low energy cosmic rays comes from the ever improving studies of interstellar chemistry. This is because some chemical reactions see low energy cosmic rays playing a crucial role. Thus chemical models of the intracloud medium can be used to study indirectly low energy cosmic rays. With this respect, many molecules have been studied (e.g. Caselli et al. 1998), and one of the most

important ones is H_3^+ (Herbst & Klemperer 1973; Watson 1973). This molecule is produced in a simple reaction chain:

$$H_2 + CR \rightarrow H_2^+ + CR + e^-$$

$$H_2^+ + H_2 \rightarrow H_3^+ + H$$

where CR is a cosmic ray proton or electron. The second reaction is very rapid, so that the formation rate of H_3^+ can be expressed as $\zeta\ n(H_2)$, where ζ is the cosmic ray ionization rate (in s^{-1}) and $n(H_2)$ is the number density of H_2. For cosmic ray protons the bulk of ionization is provided by particles with energy in the range 1 MeV - 1 GeV, while for electrons the relevant range is 10 keV - 10 MeV (Padovani et al. 2009). The destruction rate of H_3^+ in diffuse clouds is dominated by the dissociative recombination:

$$H_3^+ + e^- \rightarrow H + H + H$$

or

$$H_3^+ + e^- \rightarrow H_2 + H$$

with a rate $k_e n(e^-) n(H_3^+)$, where k_e is the thermal rate coefficient that depends on temperature and can be derived by laboratory experiments (McCall et al. 2003). In steady state the H_3^+ number density can be written as:

$$n(H_3^+) = \frac{\zeta}{k_e} \times \frac{n(H_2)}{n(e^-)}\ .$$

It is remarkable that the H_3^+ number density does not depend on the cloud density, but on the ratio between the H_2 and electron densities. Thus, if we assume that this ratio is constant throughout the cloud, we can replace it with the ratio between the two column densities N, which are observable quantities. If we further assume $N(H_3^+) = n(H_3^+) * L$, with L the cloud thickness we can write:

$$N(H_3^+) = \frac{(\zeta \times L)}{k_e} \times \frac{N(H_2)}{N(e^-)}\ .$$

The electron fraction $N(e^-)/N(H_2)$ can be determined by ultraviolet observations of molecular hydrogen and ionized carbon, while the H_3^+ column density can be measured directly from infrared absorption spectroscopy of clouds (McCall et al. 2003). It is thus evident how these observations can be used to constrain the cosmic ray ionization rate ζ (protons plus electrons), modulo the uncertainty on the determination of the cloud size. The column density of H_3^+ has been measured towards the direction of diffuse clouds (McCall et al. 2002) and, remarkably, also in the vicinity of a cosmic ray source candidate as the supernova remnant IC 443 (Indriolo et al. 2010). These latter observations seem to suggest that in the vicinity of IC 443 the cosmic ray ionization rate is spatially variable, with peaks that reach values of $\zeta \sim 2 \times 10^{-15} s^{-1}$, about 5 times larger than the standard value. This would be consistent with a localized overdensity of low energy cosmic rays (accelerated

in the supernova remnant?), variable in space possibly due to propagation effects and/or spatial inhomogeneities in the acceleration rate. It is important to stress that, to date, these observations cannot tell us whether the H_3^+ emission comes from upstream or downstream of the shock.

In the light of the above mentioned recent results, it seems that the ever-increasing quality and quantity of data is now at the level of constraining or, better, guiding theoretical and phenomenological studies. Though extremely challenging, measurements of the cosmic ray ionization rate in different diffuse clouds might help to estimate the spatial variation of low energy cosmic rays in the Galaxy, and thus possibly to constrain their diffusion properties. On the other hand, measurement performed in the direction of candidate cosmic ray sources such as supernova remnants might shed light on the injection processes of low energy particles at shocks and on their transport properties in the source environment. The most intriguing aspect of tackling this problem is, in my view, the fact that such a research would constitute an attempt to proceed one step forward towards the solution of one of the longest standing issues in *"traditional"* Astronomy – *how do star forms?* –, by using the methods and the approaches which are extensively used to seek for an answer to the fundamental issue in cosmic ray physics – *where do cosmic rays come from?*

Chapter 8

Addendum: gamma ray astronomy and the origin of *extragalactic* cosmic rays

As described in the previous chapters of this thesis, it is now a widely accepted belief that cosmic rays with energy up to (at least) the knee are accelerated in galactic supernova remnants and that the acceleration mechanism is diffusive shock acceleration. The popularity of this idea relies on the fact that within this scenario many observables (e.g. the total energy in cosmic rays, their spectrum, their chemical composition ...) can be explained fairly well. However, as stressed many times in the previous chapters, a conclusive proof for the fact that supernova remnants are indeed the sources of galactic cosmic rays is still missing.

The situation is even less clear at higher energies. As seen in the introduction, the cosmic ray spectrum extends up to particle energies of the order of $\approx 10^{20}$ eV, where a suppression has been observed (Abbasi et al. 2008; Abraham et al. 2008). The suppression may be either due to the $p\gamma$ interactions of cosmic rays in the ubiquitous cosmic microwave background radiation (and in this case it would be the well known and long-sought GZK feature first predicted by Greisen 1966; Zatsepin & Kuz'min 1966), or it may simply reflect the maximum energy attainable by cosmic rays at their sources. In both cases, since the Galaxy becomes less efficient in confining particles with higher and higher energies, these Ultra High Energy Cosmic Rays (UHECRs) are very likely to have an extragalactic origin (see e.g. Cronin 2005; Olinto 2000) [1]. Understanding the origin of UHECRs constitutes a real challenge for theoretical models, since their acceleration requires extreme conditions, which are hardly fulfilled by known astrophysical objects (Hillas 1984; Norman et al. 1995; Aharonian et al. 2002). Previous studies considered a number of potential sources, including gamma ray bursts, active galactic nuclei, large scale jets and neutron stars, but results are still inconclusive.

For many years, physicists have been pinning their hopes on the feasibility of

[1] However, models in which UHECRs are produced within our Galaxy, though less popular, are not ruled out. For a recent work see e.g. Calvez et al. (2010)

cosmic ray astronomy at the highest energies. The main motivation for this was the fact that at these extreme energies one might expect particles not to be significantly deflected by the (supposedly very weak) intergalactic magnetic field. This would make possible the identification of UHECR sources by looking at the arrival direction of cosmic rays, as it is done with photons in traditional astronomy.

As an illustrative example, consider the most optimistic case (i.e. minimal deflection) in which UHECRs are composed uniquely of protons. Protons lose energy due to $p\gamma$ interactions (both photo-pair and photo-pion production) with soft photons in the cosmic microwave background radiation, and this fact limits the distance they can travel in the intergalactic medium (see e.g. Berezinskii & Grigor'eva 1988). For protons with energy $\approx 10^{20}$ eV the most relevant process is photo-pion production and the loss length is ≈ 100 Mpc. This length constitute a sort of *cosmic ray horizon* and implies that the sources of the UHECRs that we detect must be located within ≈ 100 Mpc from us. If the intergalactic magnetic field has a strength of ≈ 1 nG (this is the maximum value allowed by Faraday rotation measurements of distant quasars, see e.g. Widrow 2002; Vallée 2004) and a coherence length of ≈ 1 Mpc (this is a characteristic distance between galaxies) the deflection of 10^{20} eV protons over 100 Mpc is of a few degrees only (Dolag et al. 2004; Aharonian et al. 2010). Even adding the effect of the galactic magnetic field, which in this case is believed to be roughly comparable to the effect of the extragalactic field (Stanev 1997), the total deflection would remain small enough to allow, in principle, the detection of individual sources in cosmic rays. A smaller value of the intergalactic magnetic field would of course imply a smaller deflection and make even more plausible the feasibility of cosmic ray astronomy.

On the other hand, the most pessimistic situation (i.e. maximal deflection) is represented by the case in which UHECRs are heavy nuclei. In this case, the main energy loss process is photo-disintegration in the cosmic microwave background and the particle horizon is, coincidentally, very close to the one of protons (see e.g. Allard et al. 2005). Thus, the expected deflection in the intergalactic and galactic magnetic field for a nucleus with atomic number Z is simply Z times the one expected for protons. This would result, for example, in a deflection of several tens of degrees for iron nuclei (Z = 26) propagating in a nanoGauss intergalactic field. It is thus clear that cosmic ray astronomy with ultra high energy nuclei is extremely challenging, unless the intergalactic magnetic field is much weaker than the upper limit of 1 nG obtained from Faraday rotations. Moreover, even in that case, the deflection in the galactic magnetic field would be an issue (e.g. Giacinti et al. 2010).

The recent observations performed by the *AUGER* observatory dramatically improved the statistic and the quality of data, and seem to suggest that cosmic ray astronomy is not possible (or, more conservatively, not possible yet). Evidence has been provided for a chemical composition which is not compatible with a pure proton composition (Abraham et al. 2010), which would imply deflections larger than the minimal ones estimated above. Moreover, no clustering of events along any specific direction has been observed. An anisotropy has been reported from the direction of the radio galaxy Centaurus A, but the excess of events is distributed quite broadly

(few tens of degrees in diameter) (The Pierre AUGER Collaboration et al. 2010).

In light of these facts, and in analogy with what has been done for galactic cosmic rays, it seems appropriate to search for indirect ways to identify the sources of UHECRs based on gamma ray observations. Gamma ray telescopes have a much better resolution than AUGER (for Cherenkov telescopes the angular resolutions is as small as a tenth of a degree) and this would greatly help in identifying a source by searching for counterparts in other wavelengths. With this respect, two possibilities have been proposed by various authors: one is to search for the gamma rays produced by the cosmic rays while they are accelerated inside the source (see e.g. Aharonian et al. 2002; Neronov et al. 2005), while the other is to search the gamma rays produced by cosmic rays during the propagation from the source to us (Waxman & Coppi 1996; Rordorf et al. 2004; Ferrigno et al. 2005; Gabici & Aharonian 2005, 2007a; Armengaud et al. 2006; Kotera et al. 2010). While the former of these two possibilities requires to make quite specific assumptions about the nature of the sources of UHECRs (e.g. assumptions on the radiation field inside the source, on the acceleration rate, and on the rate and the way in which particles escape from the source ...), the latter is more model independent, given the fact that the radiation field UHECRs interact with is given by the well known cosmological radiation background. Moreover, as explained below, in this case the only assumptions to be made concern the power of the source in UHECRs, its distance, its steadiness or bursting nature, and the cosmic ray chemical composiiton. The particle spectrum will be shown to have a minor effect on the conclusions, if reasonable assumptions are made on the maximum energy of accelerated particles. For these reasons we focus here on the latter scenario, and we investigate under which conditions gamma ray telescopes will be able to detect the radiation produced by UHECRs during their propagation in the intergalactic medium. Before estimating the detectability condition for a given source, we briefly describe the development of an electromagnetic cascade initiated by an UHECR in the intergalactic medium.

8.1 Development of the electromagnetic cascade initiated by an ultra high energy cosmic ray

In this section we describe the development of the electromagnetic cascade initiated by a UHECR. Consider a proton with energy $E_{p,20} = E_p/10^{20}$ eV. The typical energies of photons and electrons (or positrons) produced in $p\gamma$ interactions are $\sim 10^{19} E_{p,20}$ and $\sim 5\ 10^{18} E_{p,20}$ eV, respectively (Berezinskii & Grigor'eva 1988). In the absence of an intergalactic magnetic field, such electrons and photons interact only via Compton and pair production processes with photons in the cosmic microwave and radio background. In general, this would lead to the development of an electromagnetic cascade, in which the number of electron-positron pairs and photons increases rapidly. In fact, due to the extremely high energy of the particles considered here, each interaction occurs in the limit $\Gamma = \epsilon_b E \gg 1$, where ϵ_b and E are the energies of the background photon and of the energetic electron (photon) respectively, both calculated in units of the electron rest mass energy. Under

this condition the Compton scattering happens in the extreme Klein-Nishina limit, namely, the upscattered photon carries away most of the energy of the incoming electron. The same happens during a pair production event, in which most of the energy goes to one of the two outgoing electrons [2]. The fraction of the energy lost by the energetic particle is approximately $f \sim 1/ln(2\epsilon_b E)$ (Berezinskii et al. 1990), which reduces to only a few percent if we consider a 10^{19}eV electron interacting with a cosmic microwave background photon. Therefore the problem reduces essentially to a single-particle problem, in which a leading particle loses continuously energy and changes state from electron to photon and back : $e^{\pm} \rightarrow \gamma \rightarrow e^{\pm} \ldots$ due to alternate Compton/pair-production interactions. Thus, the effective loss length of an energetic electron can be identified with the loss length of the leading particle (Stecker 1973; Gould & Rephaeli 1978). When the leading particle loses its energy until $\Gamma \approx 1$, the cascade enters the particle multiplication phase, in which the particle energy is roughly divided in half in every collision. This phase ends up with a large number of low energy electrons and photons. Such a cascade would appear to a distant observer as a flux of GeV/TeV photons.

Following this rationale, Ferrigno et al. (2005) suggested to identify the sources of UHECRs by searching for this radiation. Their calculations show that, in an unmagnetized Universe ($B_{IGMF} = 0$ G), a steady source emitting isotropically 2×10^{43} erg/s in form of UHECRs ($E > 10^{19}$ eV) can be detected by a Cherenkov telescope like HESS up to a distance of ~ 100 Mpc. In this case the gamma ray source would be point-like, because in the absence of an intergalactic magnetic field the electromagnetic cascade is one-dimensional and propagates radially away from the accelerator. Unfortunately, the scenario changes dramatically if the more realistic case of a magnetized Universe is considered. This is because low energy electrons produced during the last steps of the cascade are effectively deflected and eventually isotropized if their Larmor radius is smaller or comparable with the Compton cooling length. This condition is satisfied when the intergalactic magnetic field is above:

$$B_{iso} \sim 10^{-12} \left(\frac{E_\gamma}{\mathrm{TeV}} \right) \mathrm{G} \ , \tag{8.1}$$

E_γ being the energy of the Compton photon which is detected at Earth. This implies that *unless the intergalactic magnetic field is extremely weak* ($<< B_{iso}$), electrons emit Compton photons after being fully isotropized. Thus, *an extended halo of emitting pairs forms around UHECR sources.* The radiation from the halo is emitted isotropically, resulting in a *very extended, and thus hard to be detected, gamma ray source* (Aharonian et al. 1994a).

The other effect of an intergalactic magnetic field is to cause electrons to lose energy via synchrotron radiation, and thus to subtract energy to the electromagnetic cascade. In order to investigate this effect, we show in Fig. 8.1 the effective electron loss length for the Compton/pair-production process described above (solid), together with the synchrotron loss length for an intergalactic magnetic field equal to

[2] For the sake of brevity, here and in the following we refer to each member of the electron-positron pair simply as an *electron.*

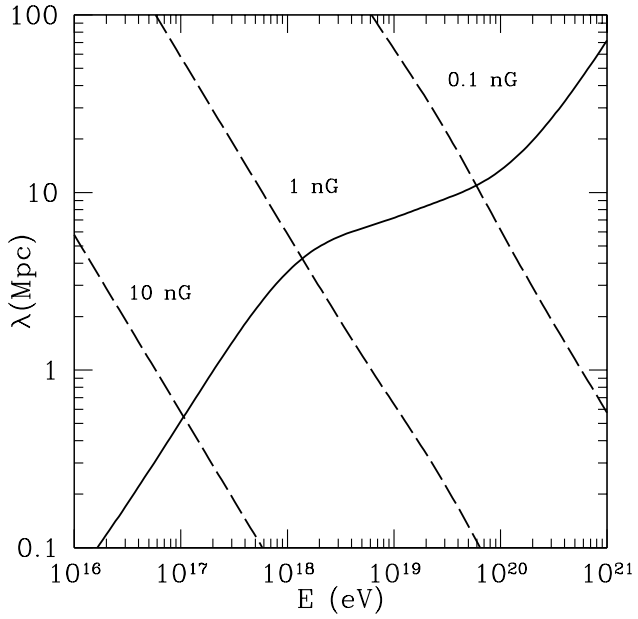

Figure 8.1: Effective loss length for electrons. Solid line refers to Compton and pair production processes in the cosmic microwave background and radio background (assumed to have a low frequency cutoff at 2 $\sim$ MHz, see Clark et al. 1970). Dashed lines refer to synchrotron losses in a magnetic field of 10, 1 and 0.1 nG, respectively.

0.1, 1, and 10 nG (dashed lines). It can be seen that if the magnetic field is at the level of 1 nG or more, all the electrons with energy above $\sim 10^{18}$ eV (namely, the ones produced at the beginning of the cascade initiated by an UHECR) cool fast via synchrotron losses and the development of the cascade is strongly suppressed from its very beginning.

This scenario is of great interest because of the following reasons. Both synchrotron emitting electrons and parent protons are extremely energetic and not appreciably deflected by the intergalactic magnetic field, at least on the first Mpcs distance scale (where the first $p\gamma$ interactions occur). For this reason, *synchrotron photons are emitted basically in the same direction of parent protons.* Thus, they move away from the source almost radially, and *the observed radiation is expected to be point-like*, and thus easily detectable and distinguishable from the extended cascade component. Remarkably, as it will be shown in the following, the spectrum of this radiation would peak in the GeV energy range, and since the Universe is transparent to GeV photons, we might receive this radiation even from powerful UHECR accelerators located outside of the cosmic ray horizon.

Summarizing, three different regimes, corresponding to different values of the intergalactic magnetic field, can be distinguished:

- **Regime I:** $B_{IGMF} \ll B_{iso} \sim 10^{-12}$ G. The electromagnetic cascade is not affected at all by the intergalactic magnetic field.

- **Regime II:** $B_{iso} \leq B_{IGMF} \ll B_{syn} \sim 10^{-9}$ G. No energy is subtracted to the cascade due to synchrotron losses, but low energy electrons are effectively isotropized by the intergalactic magnetic field.
- **Regime III:** $B_{IGMF} \geq B_{syn}$. The development of the electromagnetic cascade is strongly suppressed at its very first steps due to strong synchrotron losses.

These three regimes are described in the following sections.

8.1.1 Regime I: one-dimensional cascade

If the strength of the intergalactic magnetic field is much less than $B_{iso} \sim 10^{-12}$ G, electrons in the cascade do not suffer synchrotron losses, nor are they deflected. Thus, the electromagnetic cascade develops along a straight line. In this case, the calculations by Ferrigno et al. (2005) apply, and nearby and powerful UHECR sources might be detected as point like TeV sources by currently operational Cherenkov telescopes.

In principle, since the strength of the large scale intergalactic magnetic field is basically unknown (Widrow 2002; Vallée 2004), such a low values of the field cannot be ruled out. However, this is probably not a good assumption in the vicinity of UHECR accelerators, where the intergalactic magnetic field is expected to be appreciable, especially if such accelerators are, as it seems reasonable to believe, correlated with the structures in the Universe. The cascade might still be one-dimensional if its last steps develop sufficiently far away from the source, in a region of very low intergalactic magnetic field. Another necessary condition is that the intergalactic magnetic field close to the source must be small enough ($\ll 10^{-9}$ G) to avoid a suppression of the cascade due to synchrotron losses of first generation electrons.

8.1.2 Regime II: extended pair halos

If the intergalactic magnetic field is strong enough to deflect the electrons in the cascade, but not enough to make synchrotron losses relevant (namely, $10^{-12}\text{G} \leq B_{IGMF} \ll 10^{-9}$ G), then the electromagnetic cascade fully develops, low energy electrons are isotropized, and a very extended pair halo forms around the UHECR source. For an isotropic source, the size of the halo can be roughly estimated as follows.

Let E_γ^{obs} be the energy of the gamma ray photons observed from the Earth. Such photons are the cosmic microwave background photons which are Compton-scattered up to the gamma ray domain by electrons with energy:

$$E_e \sim 20 \left(\frac{E_\gamma^{obs}}{\text{TeV}} \right)^{1/2} \text{TeV}. \tag{8.2}$$

These are the electrons forming the pair halo. Since such electrons are rapidly isotropized in the intergalactic magnetic field, one can assume that they do not

propagate away from the sites in which they are created and thus form a halo around the source. Electrons in the halo are in turn produced by parent photons with energy $E_\gamma^{par} \gtrsim E_e$. Since the photon mean free path against pair production in the infrared background λ_{pp} decreases rapidly with increasing energy (Primack et al. 2001), we can safely neglect the contribution to the halo size from older generation (higher energy) photons. Thus, the size of the halo can be roughly estimated as: $l_{halo} \sim \lambda_{pp}(E_\gamma^{par})$ (Aharonian et al. 1994a). For a ~ 20 TeV photon the mean free path is about a few tens of megaparsecs (see e.g. Fig. 2 in Aharonian 2001). In fact, for the situation considered here, the size of the halo is even larger since the parent UHECR protons and the first generation electrons propagate $\sim 10 \div 20$ Mpc before initiating the electromagnetic cascade (see e.g. Berezinskii & Grigor'eva 1988 and Fig. 8.1). Thus, a conservative estimate of the apparent angular size of the halo at 1 TeV can be roughly given by:

$$\vartheta \sim \frac{l_{halo}}{D} \approx 10^\circ \left(\frac{l_{halo}}{20 \text{ Mpc}}\right) \left(\frac{D}{100 \text{ Mpc}}\right)^{-1}, \tag{8.3}$$

where D is the distance of the source. This indicates that *pair halos are extremely extended*, larger than the field of view of Cherenkov telescopes (the field of view of an instrument like *HESS* is $\sim 5^o$) *and thus hard to be detected*. The problem becomes even worse if one considers protons with energy below 10^{20} eV, which have a much larger loss length, namely, up to ~ 1 Gpc for proton energies equal to $\sim 5\ 10^{19}$ eV. For this reason, such protons are likely to contribute only to the TeV flux of very distant sources.

In the recent work by Armengaud et al. (2006) the deflection of electrons in the intergalactic magnetic field has been neglected, even when an intergalactic magnetic field stronger than $B_{iso} \sim 10^{-12}$ G was assumed. On the other hand, the authors considered the deflection of $\sim 10^{20}$ eV protons, which is in fact totally negligible if compared with the full isotropization of electrons. Therefore their claim about the detectability of cascade gamma-rays seems to us over-optimistic.

Finally, as in Regime I, the cascade emission peaks at TeV energies (Ferrigno et al. 2005), and thus Cherenkov telescopes, rather than *FERMI*, seem suited to detect this radiation.

8.1.3 Regime III: synchrotron gamma rays

If the intergalactic magnetic field close to the UHECR accelerator is at the level of 1 nG or above, the development of the cascade is strongly suppressed, because the very high energy electrons produced during $p\gamma$ interactions cool rapidly via synchrotron losses before undergoing Compton scattering. It is evident from Fig. 8.1 that for a $\sim$ nG magnetic field this is true for electron energies well in excess of $E_e \sim 10^{18}$ eV. Such electrons emit synchrotron photons with energy:

$$E_{syn} \approx 2 \left(\frac{B}{\text{nG}}\right) \left(\frac{E}{10^{19}\text{eV}}\right)^2 \text{GeV}, \tag{8.4}$$

which falls in the region of the electromagnetic spectrum investigated by the *FERMI* satellite. It is important to stress that these results are sensitive uniquely to the value of the intergalactic magnetic field *close* to the source, while they are unaffected by the value of the field on much larger scales. This is because synchrotron emitting electrons are produced within a proton interaction length $l_{p\gamma} \approx 10$ Mpc from the accelerator. As a consequence, the only assumption made is that the size of the magnetized region surrounding the accelerator must be greater or comparable with $l_{p\gamma}$. Superclusters of galaxies constitute an example of large and magnetized regions satisfying our requirement (Widrow 2002; Vallée 2004).

Let us now estimate the angular size of the synchrotron emission. After propagating over an interaction length, a proton of energy E_p is deflected by an angle:

$$\vartheta_p \approx 0.8^o \left(\frac{10^{20}\mathrm{eV}}{E_p}\right) \left(\frac{B}{\mathrm{nG}}\right) \sqrt{\frac{l_{p\gamma}}{10\ \mathrm{Mpc}}}\ \sqrt{\frac{l_c}{\mathrm{Mpc}}}\ , \tag{8.5}$$

where l_c is the coherence length of the intergalactic magnetic field (e.g. Waxman & Miralda-Escude 1996). Due to the high energies considered, secondary electrons produced in $p\gamma$ interactions move in the same direction of the parent protons. In a cooling time electrons are deflected by an angle $\vartheta_e \sim \alpha\lambda/R_L$, R_L being the electron Larmor radius, λ the cooling length, and α a number of order unity representing the probability that the leading particle of the cascade is actually an electron (Gould & Rephaeli 1978). Remarkably, if expressed as a function of the synchrotron photon energy, the deflection angle is independent on the magnetic field strength and reads:

$$\vartheta_e \approx 0.5^o \left(\frac{E_{syn}}{10\ \mathrm{GeV}}\right)^{-1}. \tag{8.6}$$

Thus, an observer at a distance $D \gg l_{p\gamma}$ would see a source with angular size:

$$\vartheta_{obs} \approx \sqrt{\vartheta_p^2 + \vartheta_e^2} \left(\frac{l_{p\gamma}}{D}\right) \tag{8.7}$$

that, for $D = 100$ Mpc and for photon energies of $1 \div 10$ GeV is of the order of a fraction of a degree. This is comparable with the angular resolution of *FERMI*, that would classify these sources as point-like if they are located at a distance of ~ 100 Mpc or more. This leads to the important conclusion that, *even if synchrotron photons are produced in an extended region of size* $\sim l_{p\gamma}$ *surrounding the accelerator, the resulting gamma ray source would appear point-like to a distant observer.*

If the proton spectrum extends well above 10^{20} eV, or if the magnetic field strength is significantly larger than 1 nG, these sources might also be detected by Imaging Atmospheric Cherenkov Telescope arrays like, for example, *HESS*, which operate at energies above 100 GeV. The angular resolution of these instruments is a few arcminutes, and thus the sources will appear extended. However, it has been proven that Cherenkov telescope arrays are powerful instruments to image extended gamma ray sources (see e.g. Aharonian et al. 2004), and thus they might still detect and map the synchrotron emission from UHECR sources. Finally, extremely

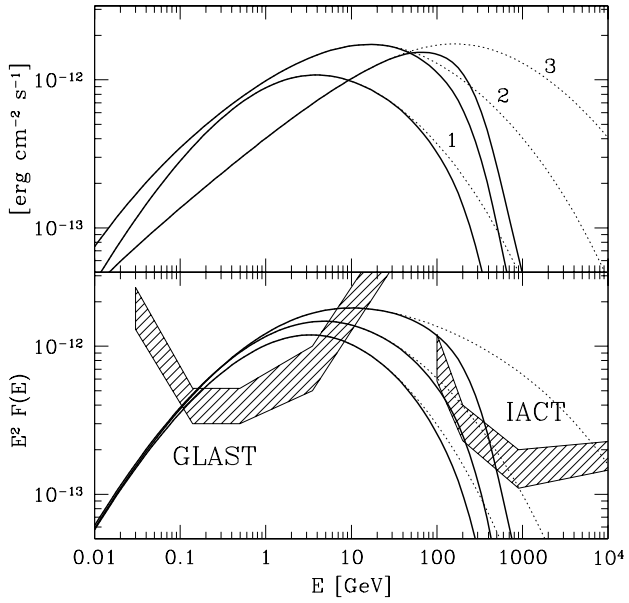

Figure 8.2: Synchrotron spectra for a source at a distance of 1 Gpc in a magnetized region of size 20 Mpc. The luminosity in UHECRs is 10^{46}erg/s, the proton spectral index is $\delta = 2$. TOP: $E_{cut} = 10^{21}$eV, magnetic field 0.5 (curve 1), 5 (2), 50 nG (3). BOTTOM: $E_{cut} = 5 \times 10^{20}$, 10^{21}, 5×10^{21}eV, magnetic field is 1 nG. Dotted lines represent the intrinsic spectra, solid lines show the effect of absorption in the infrared background. The sensitivities of *FERMI* (*GLAST* was its pre-launch name) and of a generic Imaging Atmospheric Cherenkov Telescope (IACT) like *HESS* are shown.

powerful UHECR accelerators located at a distance of 1 Gpc or more would appear as point sources even for Cherenkov telescopes. In the next section we discuss the energy requirement for a detection of this synchrotron radiation.

8.2 Detectability of the synchrotron radiation and total energy requirements

Fig. 8.2 shows synchrotron spectra for an UHECR source at a distance of 1 Gpc. Steady state proton and electron spectra have been calculated taking into account the relevant energy losses (photopion production and Compton/pair-production processes, respectively) and proton escape from the magnetized region with a characteristic time d_p/c. The size of the magnetized region is assumed to be $d_p = 20$ Mpc (roughly the size of a super-cluster of galaxies). Solid lines have been computed taking into account the opacity of the Universe to very high energy photons due to pair production in the cosmic infrared background (Gould & Schréder 1966; Primack et al. 2001) , while dotted lines show the unabsorbed spectra. The total luminosity in UHECRs with energy above 10^{19}eV is $L_{UHE} = 10^{46}$erg/s, with a differential en-

ergy distribution $Q(E) = Q_0 E^{-\delta} \exp(-E/E_{cut})$. We further assume $\delta = 2$, though results are quite insensitive to the slope of the cosmic ray spectrum if the total energy is normalized above a particle energy of 10^{19}eV and the maximum energy of cosmic rays accelerated at the source is not many orders of magnitude larger than that.

In the top panel of Fig. 8.2 we fix $E_{cut} = 10^{21}$eV and we consider three different values for the magnetic field: 0.5, 5 and 50 nG (curves 1, 2 and 3 respectively). If the magnetic field is significantly greater than ~ 50 nG, the peak of the emission falls at TeV energies, where absorption is very strong. The absorbed photons start an electromagnetic cascade that will appear as an extended halo. On the other hand, if the field is well below ~ 0.5 nG, synchrotron emission becomes unimportant and again the cascade contribution dominates (in both cases, the situation becomes the one named Regime II and described in Sec. 8.1.2). However, for the broad interval of values of the magnetic field strength between 0.5 and 50 nG, the formation of a synchrotron point-like gamma ray source seems to be unavoidable.

In the bottom panel of Fig. 8.2, our predictions are compared with the sensitivities of *FERMI* and of a generic Imaging Atmospheric Cherenkov Telescope array such as *HESS*. A magnetic field of 1 nG has been assumed and the three different curves refer to values of the cutoff energy in the proton spectrum equal to $E_{cut} = 5 \times 10^{21}$, 10^{21} and 5×10^{20}eV (top to bottom). For such a magnetic field, the condition for the detectability of a point source by *FERMI* is roughly $L_{UHE} \geq 8\ 10^{43} \div 2\ 10^{44} (D/100\ \mathrm{Mpc})^2 \mathrm{erg/s}$ for δ in the range $2.0 \div 2.6$. In contrast, for Cherenkov telescope arrays the minimum detectable luminosity is about 2 orders of magnitude higher, since the source has to be located at a distance of ~ 1 Gpc in order to appear point-like. However, less powerful accelerators can still be detected as extended sources.

An issue for the detection of these sources in TeV gamma rays is the fact that distant sources might be undetectable above 100 GeV due to the strong absorption in the infrared background. In this case, the maximum energy of UHECRs is very important, since it determines the extension of the (unabsorbed) gamma ray spectrum towards high energies. However, since the peak of the emission falls at ~ 10 GeV, the future Cherenkov telescope arrays operating in the energy range $10 \div 100$ GeV, such as CTA (www.cta-observatory.org) or possibly 5@5 (Aharonian et al. 2001), would be powerful tools to search for these sources.

If the cosmic ray spectrum is a smooth power law with index $\delta = 2$ down to GeV energies, the required total cosmic ray luminosity for a source to be detected by *FERMI* is $L_{CR} \geq 5 \times 10^{44} (D/100\ \mathrm{Mpc})^2 \mathrm{erg/s}$. If cosmic rays are beamed along one axis, the luminosity is reduced by a factor $f_b \sim 0.02(\vartheta_b/10^\circ)$, ϑ_b being the beaming angle. In this case, the detectability condition reads: $L_{CR} \geq 10^{43} (f_b/0.02)(D/100\ \mathrm{Mpc})^2 \mathrm{erg/s}$. This luminosity is small if compared, for example, with the kinetic power of an AGN jet, that can be as high as $\sim 10^{47}$erg/s (e.g. Rawlings & Saunders 1991). Thus, astrophysical object that could in principle satisfy the energy requirement for detectability do exist.

In calculating the spectra shown in Fig. 8.2 we assumed the UHECR accelerator

to be active for a time t_{ON} long enough to reach steady state. This situation is achieved if the accelerator lifetime is greater than the $p\gamma$ interaction time, namely, if $t_{ON} \geq 100$ Myr. Under this assumption, the total energy deposited in CRs during the whole source lifetime is $E_{CR} \geq 3\ 10^{58}(f_b/0.02)(D/100\mathrm{Mpc})^2\mathrm{erg}$. If the UHECR accelerator is located inside a rich cluster of galaxies, then the bulk of this nonthermal energy accumulates in it, due to effective diffusive confinement of CRs with energy up to at least 10^7GeV in the μG intracluster magnetic field (Völk et al. 1996; Berezinsky et al. 1997). Such an amount of energy can be easily stored in a rich cluster, whose total thermal energy can be as high as 10^{64}erg (e.g. Völk et al. 1996).

Of course, if the CR spectrum is much steeper than $\delta = 2$, the problem of energetics could be difficult to circumvent, unless a mechanism is found to limit acceleration to ultra high energy particles only [3].

Thus, calculations show that for objects located within several hundreds of megaparsecs and with jets pointed to the observer, *FERMI* and Cherenkov telescopes like *HESS* should be able to provide meaningful probes of this radiation, if sufficiently powerful sources of UHECRs exist. Distant objects beyond 1 Gpc might be possibly detected only by the next generation instruments with significantly improved sensitivities.

8.2.1 Bursting sources

The results presented above can be qualitatively generalized to the case of a bursting source. Consider a short burst releasing an energy E_{UHE}^{burst} in the form of UHECRs. The deflection of UHECRs in magnetic fields results in a time broadening of the pulse over a time roughly equal to the delay time (Waxman 1995):

$$\delta\tau \sim 5 \times 10^3 \left(\frac{10^{20}\mathrm{eV}}{E}\right)^2 \left(\frac{B}{\mathrm{nG}}\right)^2 \left(\frac{d_p}{20\ \mathrm{Mpc}}\right)^2 \left(\frac{l_c}{\mathrm{Mpc}}\right)\ \mathrm{yr}\ . \tag{8.8}$$

The duration of the synchrotron emission is expected to be roughly the same. If the intrinsic duration of the burst t_b is longer than $\delta\tau$, time broadening is not important. To satisfy the detectability condition, the total energy released in UHECRs must be $E_{UHE}^{burst} \geq L_{UHE}^{ss} t_{obs} \sim 2\ 10^{53}(t_{obs}/\delta\tau)(f_b/0.02)(D/100\mathrm{Mpc})^2\mathrm{erg/s}$ where L_{UHE}^{ss} is the detectability condition for the steady state situation and $t_{obs} \approx \delta\tau + t_b$ is the observed duration of the burst. This is a huge amount of energy to be released in a single explosion, orders of magnitude above the energy $\sim 10^{51}$erg that is believed to be converted into UHECRs during a gamma ray burst (Waxman 1995; Vietri 1995). Thus, if UHECRs are produced during short bursts, the related synchrotron emission is far too faint to be detected. However, if the accelerator remains active for a time $\gg \delta\tau$ the energy requirement is significantly reduced.

[3] If CRs are accelerated only above an energy E_{min} then $L_{CR} \propto E_{min}^{2-\delta}/(\delta - 2)$. For a steep spectrum $\delta = 2.6$ and $E_{min} = 1$GeV the required luminosity is huge $L_{CR} \sim 2.4\ 10^{50}$erg/s

8.2.2 Neutrinos

Muon and electron neutrinos are produced during $p\gamma$ interactions in the ratio 2:1. Due to neutrino oscillation the ratio between the three flavors becomes 1:1:1 at Earth. For the source considered in Fig. 8.2 the total neutrino flux is $E_\nu^2 F_\nu \sim$ 1 EeV/km^2/yr at energy 5 10^{18}eV. These energies are probed by the ANITA and AUGER experiments. The possibility of a detection is challenging and depends on their performances in recognizing steady and point-like sources of neutrinos. The detection of neutrinos could serve as an unequivocal signature of UHECR acceleration.

8.3 Recent developments

The suggestion of searching for the synchrotron point-like gamma ray emission from UHECR sources has been first proposed by Gabici & Aharonian (2005, 2007a). The results presented in these two papers and summarized in the previous sections have been obtained by means of semi-analytic calculations, which necessarily require to adopt simplifying assumptions (e.g. uniform magnetic field, pure proton composition, continuous approximation for energy loss processes ...). Recently, this scenario has been further investigated by Kotera et al. (2010), who made use of numerical simulations to describe the propagation of UHECRs and the related production of secondary particles. Besides confirming all the main conclusions presented in the previous sections, Kotera et al. (2010) extended the analysis to situations which are beyond the capabilities of semi-analytical methods.

They first considered the effect of a structured magnetic field, derived from cosmological simulations, and found that the predicted gamma ray fluxes are robust to changes in the field configuration. They also investigated the role of an enriched chemical composition of UHECRs and showed that gamma ray fluxes are reduced, but in most cases not dramatically, with respect to the pure proton case. For example assuming a pure iron composition would imply a reduction of the expected synchrotron flux of a factor of ≈ 5 (see their Fig. 3). Moreover, they produced simulated maps of the expected emission for sources satisfying the detectability condition derived above, and showed that such sources, if located at a distance of ≈ 1 Gpc, would appear slightly extended (extended) if observed with *FERMI* (*CTA*) in the multi GeV energy domain.

Finally, Kotera et al. (2010) also showed that the detection in synchrotron gamma rays of a source located at ≈ 100 Mpc and with a luminosity in UHECRs of $L_{UHE} \approx 10^{44}$erg/s is already marginally ruled out because it would overshoot the observed diffuse spectrum of UHECRs. A detection in gamma rays seems thus more feasible if rare and extremely powerful ($L_{UHE} \gg 10^{44}$erg/s) sources exist. For example, a source with $L_{UHE} \sim 10^{46}$erg/s located at ~ 1 Gpc (like the one considered in Fig. 8.2) would contribute to only $\sim 10\%$ to the total observed flux of UHECRs at $\sim 10^{19}$eV.

8.4 Conclusions

In this chapter we discussed the possibility to detect the gamma ray emission produced by UHECRs during their propagation from the sources to us. We considered steady sources only, because the deflection of UHECRs in the intergalactic magnetic field would unavoidably induce a time broadening of the short pulse of UHECRs generated in a bursting source. Such broadening would dilute the gamma ray signal and make it hard to be detected (but see Waxman & Coppi 1996 for a more optimistic view). In this case, we showed that the crucial parameter is, besides the source luminosity, the strength of the intergalactic magnetic field. With this respect, we identified three different regimes of propagation that result in very different scenarios of gamma ray production.

The simplest case is the one of an unmagnetized Universe. In such a Universe, the TeV emission resulting from the electromagnetic cascade initiated by UHECRs would be detectable by Cherenkov telescopes of current generation if the source luminosity in form of UHECRs (protons) is $L_{UHE} \gtrsim 10^{43}$erg/s and its distance is within ≈ 100 Mpc (Ferrigno et al. 2005). The advantage of this scenario is that UHECRs are not deflected and thus an observer should receive from the direction of a source *both* cosmic rays and gamma rays. In other words, in this scenario we would know a priori where to search for the gamma ray emission (i.e. the arrival direction of UHECRs). In order for this scenario to be valid, two strict conditions on the strength of the intergalactic magnetic field need to be satisfied: *i)* its value on large cosmic scales has to be much smaller than $\sim 10^{-12}$G in order to avoid the deflection of low energy electrons in the electromagnetic cascade and, *ii)* its value close to the source ($\approx 10 - 20$ Mpc) has to be much smaller than $\sim 10^{-9}$G to avoid electron synchrotron losses that would suppress the cascade. However, even if these conditions are satisfied, another problem has to be faced: in absence of deflection, we would expect to see several UHECRs from the direction of a sources with $L_{UHE} \sim 10^{43}$erg/s, while no clustering of events is seen in *AUGER* data. If one considers future Cherenkov telescope such as *CTA*, then the detectability condition becomes $L_{UHE} \gtrsim 10^{42}$erg/s, which might still be marginally compatible with *AUGER* data (for this luminosity one would expect very roughy 1 UHECR per year for a distance of ≈ 50 Mpc).

The second regime which we investigated is the one of a magnetized universe with field strength in the range $10^{-12}\text{G} \lesssim B_{IGMF} \ll 10^{-9}$G. In this case the low energy electrons in the electromagnetic cascade are strongly deflected and, for an isotropic source of UHECRs, one expects a very extended gamma ray emission (see Eq. 8.3) which is hard to be detected with both current and next generation of instruments (Aharonian et al. 1994a).

The last among the possible scenarios is the one in which the magnetic field *close to the source* (i.e. within 10-20 Mpc) is at the level of a nanoGauss or more. In this case the first generation of electrons produced in the cascade lose all their energy via synchrotron radiation. The resulting synchrotron emission peaks in the multi GeV energy range, where the Universe is transparent. For this reason we might hope to detect this radiation from rare and powerful cosmic ray sources even

if they are located outside of the cosmic ray horizon. Another advantage of this scenario is that, since only extremely high particles ($\gtrsim 10^{19}$eV) are involved in the generation of the multi-GeV photons, and since such photons are produced in the first interaction lengths of UHECRs, the deflection due to the magnetic field is expected to be small, and the emission is thus almost-point-like. Unfortunately, similarly to the first scenario described here, also in this case nearby sources, if detectable in gamma rays, would be inconsistent with *AUGER* data, since they would overshoot the observed diffuse UHECR spectrum. However, the possibility to detect very powerful and rare sources ($L_{UHE} \sim 10^{46}$erg/s) still remains viable. However, in this case, we would not expect to receive UHECRs in spatial coincidence with the multi-GeV flux. The predictions of the spectral shape, with a peak in the multi-GeV range, and of the angular extension (marginally extended for *FERMI*, extended for *CTA*) seem to be very robust against the variation of model parameters. Thus, these characteristics might be used to distinguish such radiation from other contributions (e.g. intrinsic emission from the source, pair halo initiated by gamma rays ...).

Sadly, enriched chemical compositions for UHECRs would lower the expectations in all the scenarios.

To conclude, searching for and finally detecting the gamma ray emission generated during the propagation of UHECRs from their sources to us is quite challenging, but not impossible, both with *FERMI* or future generation of Cherenkov instruments. However, since in the best case the detections will be marginal and/or a meagre number of sources will be detected, an increase in the statistics of cosmic ray data themselves is arguable. With this respect, a key role will be undoubtedly played by future cosmic ray telescopes such as *AUGER North* or *JEM-EUSO*.

The results presented in this chapter have been first published in:

- S. Gabici & F.A. Aharonian, Phys. Rev. Lett. **95**, 251102 (2005)
- S. Gabici & F.A. Aharonian, Astrophys. Space Sci. **309**, 465 (2007)

Appendix A

Curriculum vitae

A.1 Professional experience

- Nov 2009 – present: Chargé de Recherche de 2e classe, Laboratoire AstroParticule et Cosmologie, Paris
- Oct 2007 – Sep 2009: Marie Curie Fellow, Dublin Institute for Advanced Studies
- Nov 2006 – Sep 2007: Postdoc, Max-Planck-Institut für Kernphysik, Heidelberg
- Nov 2004 – Oct 2006: Alexander von Humboldt Fellow, Max-Planck-Institut für Kernphysik, Heidelberg
- October 2004: Short term contract, Department of Astronomy and Space Science, University of Florence
- Apr 2004 – Aug 2004: Short term contract, INAF/Arcetri Astrophysical Observatory

A.2 Education

- June 3rd 2004: PhD in Astronomy, University of Florence
  Particle acceleration and non-thermal activity during large scale structure formation
  Supervisors: P. Blasi and F. Pacini
- October 16th 2000: MSc in Astronomy (cum laude), University of Bologna
  Extended radio sources in clusters of galaxies: pressure balance
  Supervisors: G. Setti, G. Brunetti, L. Feretti

A.3 Grants

- ANR Jeune Chercheur, Dec 2011 - Nov 2013, 140 kEuros
- Marie Curie Reintegration Grant, Sep 2010 - Aug 2013, 45 kEuros

A.4 Teaching and tutoring experience

- Course on "Cosmic rays and gamma rays in the interstellar medium", International winter school on the interstellar medium, Ise-Shima, Mie, Japan, 22-26 February 2010
- Part of the course: "Modern developments in high energy astrophysics" (Prof. F. Aharonian), Trinity College Dublin, February 2008
- Supervision of a M2 student, Pierre Cristofari, 1 March - 31 July 2010, *Gamma ray emission from supernova remnants and the origin of galactic cosmic rays*, M2 Physique Subatomique et Astroparticules, LPSC, Grenoble
- Supervision of a PhD student, Pierre Cristofari, from October 2010, École Doctorale 127 Astronomie et Astrophysique d'Île-de-France
- Co-supervision of:
    1. Giulia Vannoni's MSc thesis, *Self-consistent model for particle injection and acceleration in non-linear shock waves*, 2004, University of Florence (supervisors: C. Chiuderi, P. Blasi)
    2. Giulia Vannoni's PhD thesis, *Diffusive shock acceleration in radiation dominated environments*, 2008, University of Heidelberg (supervisors: W. Hofmann, F.A. Aharonian)
    3. part of Denys Malyshev's PhD thesis, to be submitted, Dublin Institute for Advanced Studies (supervisors: F.A. Aharonian, L. O'C. Drury)

A.5 Memberships

- CTA consortium: task leader for *Cosmic ray origin, supernova remnants, and molecular clouds* within the Astrophysics and Astroparticle Physics Working Package
- Member of the H.E.S.S. collaboration (from 2006 to 2009)
- Member of the Km3NeT consortium (from 2007 to 2009)

A.6 Refereeing

- Referee for: The Astrophysical Journal, Monthly Notices of the Royal Astronomical Society (main journal and letters), Physical Review D, Astronomy and Astrophysics, Astroparticle Physics, Journal of Cosmology and Astroparticle Physics, Astrophysics and Space Science, Advances in Space Research
- Referee for the Irish Research Council for Science, Engineering, and Technology – EMBARK Postgraduate Scholarship Competition
- Referee for the Programme Blancs et Pluridisciplinaires de l'Universit Montpellier 2 Sciences et Techniques

A.7 Talks

- 10 invited talks at international meetings and conferences
- 4 invited talks at French meetings and conferences
- a few tens of contributed talks at international conferences, or collaboration meetings, or research institutes
- 3 participations at invitation-only workshops (2 ISSI meetings, Bern; 1 Lorentz Center meeting, Leiden)

A.7.1 Invited talks at international meetings and conferences

1. "Gamma rays, molecular clouds, and cosmic ray propagation in the Galaxy", Cosmic rays and their interstellar medium environment, Montpellier, 26 Jume - 1 July 2011
2. "How to use molecular clouds to study the propagation of cosmic rays in the Galaxy", ICATPP Conference on Cosmic Rays for Particle and Astroparticle Physics, Villa Olmo, 7-8 October 2010
3. "Non thermal emission from molecular clouds illuminated by cosmic rays from nearby supernova remnants", Exploring supernova remnants and pulsar wind nebulae in X-rays: before and after Astro-H, Tokyo, 18-19 February 2010
4. "Gamma rays from molecular clouds: GeV to TeV connections", Workshop: The GeV to TeV connection, Ringberg, 11-16 January 2010
5. "Cosmic ray propagation and high energy radiation from molecular clouds", Workshop: Molecular clouds as probes of cosmic ray acceleration in supernova remnants, Palavas-les-Flots/Carnon, France, 7-9 September 2009
6. "Cosmic ray propagation in molecular clouds and related gamma ray emission", Workshop on diffuse gamma rays, LPTA, Montpellier, France, 13-14 November 2008

7. "Gamma ray emission associated with Ultra High Energy Cosmic Ray sources", The impact of high-energy-astrophysics experiments on cosmological physics, KICP, Chicago, USA, 27-28 October 2008

8. "GeV and TeV gamma ray Astronomy", 21st European Cosmic Ray Symposium, Kosice, Slovakia, 9-12 September 2008

9. "Molecular clouds with the Cherenkov Telescope Array", CTA meeting, Barcelona, Spain, 24-25 January 2008

10. "Molecular cloud/supernova remnant interactions", Nonthermal hadronic mechanisms in galactic sources, Heidelberg, Germany, 14-16 January 2008

A.7.2 Invited talks at French meetings and conferences

1. "Constraints on the cosmic ray diffusion coefficient in the W28 region from gamma-ray observations", sf2a, Marseille, 21-24 June 2010

2. "Gamma ray emission from supernova remnant/molecular cloud associations", GDR-PCHE meeting, Orsay, 8-9 June 2010

3. "Gamma ray emission from the W28 region", GDR-PCHE meeting, Montpellier, 31 May-1 June 2010

4. "Gamma ray emission from molecular clouds", Atelier Astrophysique avec CTA, Observatoire de Paris, 9 December 2009

A.8 Publications

A.8.1 Publications: summary

- 53 refereed publications (10 as first author, 32 with the HESS collaboration)

- 21 non-refereed publications (12 as first author)

A.8.2 Selected publications

1. S. Gabici, F.A. Aharonian, & S. Casanova, "Broad-band non-thermal emission from molecular clouds illuminated by cosmic rays from nearby supernova remnants", MNRAS **396**, 1629 (2009)

2. HESS collaboration, "Constraints on the multi-TeV particle population in the Coma galaxy cluster with HESS observations", A&A **502**, 437 (2009)

3. S, Gabici, A.M. Taylor, R.J. White, S. Casanova, & F.A. Aharonian, "The diffuse neutrino flux from the inner Galaxy: constraints from very high energy gamma ray observations", Astropart. Phys. **30**, 180 (2008)

4. S. Gabici & F.A. Aharonian, "Searching for Galactic Cosmic-Ray Pevatrons with Multi-TeV Gamma Rays and Neutrinos", ApJ Lett. **665**, L131 (2007)

5. S. Gabici, F.A. Aharonian, & P. Blasi, "Gamma rays from molecular clouds", Astrophys. Space Sci. **309**, 365 (2007)

6. S. Gabici & F.A. Aharonian, "Pointlike Gamma Ray Sources as Signatures of Distant Accelerators of Ultrahigh Energy Cosmic Rays", Phys. Rev. Lett. **95**, 251102 (2005)

7. P. Blasi, S. Gabici, & G. Vannoni, "On the role of injection in kinetic approaches to non-linear particle acceleration at non-relativistic shock waves", MNRAS, **361**, 907 (2005)

8. S. Gabici & P. Blasi, "On the detectability of gamma rays from clusters of galaxies: mergers versus secondary infall", Astropart. Phys. **20**, 579 (2004)

9. S. Gabici & P. Blasi, "The gamma ray background from large scale structure formation", Astropart. Phys. **19**, 679 (2003)

10. S. Gabici & P. Blasi, "Nonthermal Radiation from Clusters of Galaxies: The Role of Merger Shocks in Particle Acceleration", ApJ **583**, 695 (2003)

Bibliography

Abbasi, R. U., Abu-Zayyad, T., Allen, M., et al. 2008, Physical Review Letters, 100, 101101

Abdo, A. A., Ackermann, M., Ajello, M., et al. 2010a, ApJ, 718, 348

Abdo, A. A., Ackermann, M., Ajello, M., et al. 2010b, ApJ, 710, 133

Abraham, J., Abreu, P., Aglietta, M., et al. 2008, Physical Review Letters, 101, 061101

Abraham, J., Abreu, P., Aglietta, M., et al. 2010, Physical Review Letters, 104, 091101

Aharonian, F., Akhperjanian, A. G., Bazer-Bachi, A. R., et al. 2008a, A&A, 481, 401

Aharonian, F., Akhperjanian, A. G., Bazer-Bachi, A. R., et al. 2006a, A&A, 449, 223

Aharonian, F., Akhperjanian, A. G., Bazer-Bachi, A. R., et al. 2006b, Nature, 439, 695

Aharonian, F., Buckley, J., Kifune, T., & Sinnis, G. 2008b, Reports on Progress in Physics, 71, 096901

Aharonian, F. A. 1991, Ap&SS, 180, 305

Aharonian, F. A. 2001, in International Cosmic Ray Conference, Vol. 27, International Cosmic Ray Conference, I250+

Aharonian, F. A., Akhperjanian, A. G., Aye, K., et al. 2004, Nature, 432, 75

Aharonian, F. A. & Atoyan, A. M. 1996, A&A, 309, 917

Aharonian, F. A., Belyanin, A. A., Derishev, E. V., Kocharovsky, V. V., & Kocharovsky, V. V. 2002, Phys. Rev. D, 66, 023005

Aharonian, F. A., Coppi, P. S., & Voelk, H. J. 1994a, ApJ, 423, L5

Aharonian, F. A., Drury, L. O., & Voelk, H. J. 1994b, A&A, 285, 645

Aharonian, F. A., Kelner, S. R., & Prosekin, A. Y. 2010, Phys. Rev. D, 82, 043002

Aharonian, F. A., Konopelko, A. K., Völk, H. J., & Quintana, H. 2001, Astroparticle Physics, 15, 335

Alexandreas, D. E., Berley, D., Biller, S., et al. 1993, Nuclear Instruments and Methods in Physics Research A, 328, 570

Allard, D., Olinto, A. V., & Parizot, E. 2007, A&A, 473, 59

Allard, D., Parizot, E., Olinto, A. V., Khan, E., & Goriely, S. 2005, A&A, 443, L29

Aloisio, R., Berezinsky, V., Blasi, P., & Ostapchenko, S. 2008, Phys. Rev. D, 77, 025007

Amato, E. & Blasi, P. 2005, MNRAS, 364, L76

Amato, E., Blasi, P., & Gabici, S. 2008, MNRAS, 385, 1946

Arimoto, N., Sofue, Y., & Tsujimoto, T. 1996, PASJ, 48, 275

Armengaud, E., Sigl, G., & Miniati, F. 2006, Phys. Rev. D, 73, 083008

Axford, W. I., Leer, E., & Skadron, G. 1977, in International Cosmic Ray Conference, Vol. 11, International Cosmic Ray Conference, 132–137

Baade, W. & Zwicky, F. 1934, Proceedings of the National Academy of Science, 20, 259

Bamba, A., Yamazaki, R., Ueno, M., & Koyama, K. 2003, ApJ, 589, 827

Barr, G., Gaisser, T. K., & Stanev, T. 1989, Phys. Rev. D, 39, 3532

Bell, A. R. 1978, MNRAS, 182, 147

Bell, A. R. 2004, MNRAS, 353, 550

Berezhko, E. G. & Ellison, D. C. 1999, ApJ, 526, 385

Berezhko, E. G., Ksenofontov, L. T., & Völk, H. J. 2003, A&A, 412, L11

Berezhko, E. G. & Völk, H. J. 2006, A&A, 451, 981

Berezhko, E. G., Yelshin, V. K., & Ksenofontov, L. T. 1994, Astroparticle Physics, 2, 215

Berezinskii, V. S., Bulanov, S. V., Dogiel, V. A., & Ptuskin, V. S. 1990, Astrophysics of cosmic rays, ed. Berezinskii, V. S., Bulanov, S. V., Dogiel, V. A., & Ptuskin, V. S.

Berezinskii, V. S. & Grigor'eva, S. I. 1988, A&A, 199, 1

Berezinsky, V. S., Blasi, P., & Ptuskin, V. S. 1997, ApJ, 487, 529

Blandford, R. & Eichler, D. 1987, Phys. Rep., 154, 1

Blandford, R. D. 1980, ApJ, 238, 410

Blandford, R. D. & Ostriker, J. P. 1978, ApJ, 221, L29

Blasi, P. 2002, Astroparticle Physics, 16, 429

Blasi, P., Gabici, S., & Vannoni, G. 2005, MNRAS, 361, 907

Blitz, L., Bloemen, J. B. G. M., Hermsen, W., & Bania, T. M. 1985, A&A, 143, 267

Bloemen, J. B. G. M., Caraveo, P. A., Hermsen, W., et al. 1984, A&A, 139, 37

Bykov, A. M. & Fleishman, G. D. 1992, MNRAS, 255, 269

Bykov, A. M., Uvarov, Y. A., & Ellison, D. C. 2008, ApJ, 689, L133

Calvez, A., Kusenko, A., & Nagataki, S. 2010, Physical Review Letters, 105, 091101

Casanova, S., Aharonian, F. A., Fukui, Y., et al. 2010a, PASJ, 62, 769

Casanova, S., Jones, D. I., Aharonian, F. A., et al. 2010b, PASJ, 62, 1127

Caselli, P., Walmsley, C. M., Terzieva, R., & Herbst, E. 1998, ApJ, 499, 234

Cassam-Chenaï, G., Decourchelle, A., Ballet, J., & Ellison, D. C. 2005, A&A, 443, 955

Cassam-Chenaï, G., Hughes, J. P., Ballet, J., & Decourchelle, A. 2007, ApJ, 665, 315

Casse, M. & Paul, J. A. 1980, ApJ, 237, 236

Cesarsky, C. J. 1980, ARA&A, 18, 289

Cesarsky, C. J. & Volk, H. J. 1978, A&A, 70, 367

Cioffi, D. F., McKee, C. F., & Bertschinger, E. 1988, ApJ, 334, 252

Clark, T. A., Brown, L. W., & Alexander, J. K. 1970, Nature, 228, 847

Costantini, M. L. & Vissani, F. 2005, Astroparticle Physics, 23, 477

Cronin, J. W. 2005, Nuclear Physics B Proceedings Supplements, 138, 465

Crutcher, R. M. 1999, ApJ, 520, 706

Dalgarno, A. & McCray, R. A. 1972, ARA&A, 10, 375

Dame, T. M., Ungerechts, H., Cohen, R. S., et al. 1987, ApJ, 322, 706

Dar, A. & de Rújula, A. 2008, Phys. Rep., 466, 179

Dermer, C. D. 1986, A&A, 157, 223

Dogel', V. A. & Sharov, G. S. 1990, A&A, 229, 259

Dolag, K., Grasso, D., Springel, V., & Tkachev, I. 2004, Soviet Journal of Experimental and Theoretical Physics Letters, 79, 583

Dorfi, E. A. & Bohringer, H. 1993, A&A, 273, 251

Drury, L. O. 1983, Reports on Progress in Physics, 46, 973

Drury, L. O., Aharonian, F. A., Malyshev, D., & Gabici, S. 2009, A&A, 496, 1

Drury, L. O., Aharonian, F. A., & Voelk, H. J. 1994, A&A, 287, 959

Drury, L. O. & Voelk, J. H. 1981, ApJ, 248, 344

Duffy, P. 1992, A&A, 262, 281

Eichler, D. 1979, ApJ, 229, 419

Eichler, D. 1984, ApJ, 277, 429

Ellison, D. C. 2000, in American Institute of Physics Conference Series, Vol. 528, Acceleration and Transport of Energetic Particles Observed in the Heliosphere, ed. R. A. Mewaldt, J. R. Jokipii, M. A. Lee, E. Möbius, & T. H. Zurbuchen , 383–389

Ellison, D. C. & Cassam-Chenaï, G. 2005, ApJ, 632, 920

Ellison, D. C. & Eichler, D. 1984, ApJ, 286, 691

Ellison, D. C., Patnaude, D. J., Slane, P., Blasi, P., & Gabici, S. 2007, ApJ, 661, 879

Ellison, D. C., Patnaude, D. J., Slane, P., & Raymond, J. 2010, ApJ, 712, 287

Erlykin, A. D. & Wolfendale, A. W. 1997, Journal of Physics G Nuclear Physics, 23, 979

Farmer, A. J. & Goldreich, P. 2004, ApJ, 604, 671

Ferrand, G., Downes, T., & Marcowith, A. 2008, MNRAS, 383, 41

Ferrigno, C., Blasi, P., & de Marco, D. 2005, Astroparticle Physics, 23, 211

Field, G. B., Goldsmith, D. W., & Habing, H. J. 1969, ApJ, 155, L149+

Fujita, Y., Ohira, Y., Tanaka, S. J., & Takahara, F. 2009, ApJ, 707, L179

Fukui, Y., Kawamura, A., Minamidani, T., et al. 2008, ApJS, 178, 56

Funk, S. 2007, in American Institute of Physics Conference Series, Vol. 921, The First GLAST Symposium, ed. S. Ritz, P. Michelson, & C. A. Meegan, 393–394

Funk, S., Reimer, O., Torres, D. F., & Hinton, J. A. 2008, ApJ, 679, 1299

Gabici, S. 2008, ArXiv e-prints, arXiv:0811.0836

Gabici, S. 2010, ArXiv e-prints, arXiv:1011.2029

Gabici, S. & Aharonian, F. A. 2005, Physical Review Letters, 95, 251102

Gabici, S. & Aharonian, F. A. 2007a, Ap&SS, 309, 465

Gabici, S. & Aharonian, F. A. 2007b, ApJ, 665, L131

Gabici, S., Aharonian, F. A., & Blasi, P. 2007, Ap&SS, 309, 365

Gabici, S., Aharonian, F. A., & Casanova, S. 2009, MNRAS, 396, 1629

Gabici, S., Blasi, P., & Vannoni, G. 2005, in American Institute of Physics Conference Series, Vol. 801, Astrophysical Sources of High Energy Particles and Radiation, ed. T. Bulik, B. Rudak, & G. Madejski, 369–372

Gabici, S., Casanova, S., Aharonian, F. A., & Rowell, G. 2010, ArXiv e-prints, arXiv:1009.5291

Gabici, S., Taylor, A. M., White, R. J., Casanova, S., & Aharonian, F. A. 2008, Astroparticle Physics, 30, 180

Gaisser, T. K. 1990, Cosmic rays and particle physics, ed. Gaisser, T. K.

Gaisser, T. K. & Stanev, T. 1995, in International Cosmic Ray Conference, Vol. 1, International Cosmic Ray Conference, 694–+

Giacinti, G., Kachelrieß, M., Semikoz, D. V., & Sigl, G. 2010, J. Cosmology Astropart. Phys., 8, 36

Ginzburg, V. L. & Syrovatskii, S. I. 1964, The Origin of Cosmic Rays, ed. Ginzburg, V. L. & Syrovatskii, S. I.

Giuliani, A., Tavani, M., Bulgarelli, A., et al. 2010, A&A, 516, L11+

Gleeson, L. J. & Axford, W. I. 1968, ApJ, 154, 1011

Gould, R. J. & Rephaeli, Y. 1978, ApJ, 225, 318

Gould, R. J. & Schréder, G. 1966, Physical Review Letters, 16, 252

Greisen, K. 1966, Physical Review Letters, 16, 748

Helder, E. A., Kosenko, D., & Vink, J. 2010, ApJ, 719, L140

Helder, E. A., Vink, J., Bassa, C. G., et al. 2009, Science, 325, 719

Herbst, E. & Klemperer, W. 1973, ApJ, 185, 505

Hillas, A. M. 1984, ARA&A, 22, 425

Hillas, A. M. 2005, Journal of Physics G Nuclear Physics, 31, 95

Hinton, J. A. & Hofmann, W. 2009, ARA&A, 47, 523

Honda, M., Kajita, T., Kasahara, K., & Midorikawa, S. 1995, Phys. Rev. D, 52, 4985

Hunter, S. D., Bertsch, D. L., Catelli, J. R., et al. 1997, ApJ, 481, 205

Indriolo, N., Blake, G. A., Goto, M., et al. 2010, ApJ, 724, 1357

Issa, M. R. & Wolfendale, A. W. 1981, Nature, 292, 430

Jean, P., Gillard, W., Marcowith, A., & Ferrière, K. 2009, A&A, 508, 1099

Jones, D. I., Protheroe, R. J., & Crocker, R. M. 2008, PASA, 25, 161

Jones, F. C. & Ellison, D. C. 1991, Space Sci. Rev., 58, 259

Kalberla, P. M. W., Burton, W. B., Hartmann, D., et al. 2005, A&A, 440, 775

Kamae, T., Karlsson, N., Mizuno, T., Abe, T., & Koi, T. 2006, ApJ, 647, 692

Kang, H. & Jones, T. W. 1991, MNRAS, 249, 439

Kang, H. & Jones, T. W. 1995, ApJ, 447, 944

Kang, H., Jones, T. W., & Gieseler, U. D. J. 2002, ApJ, 579, 337

Kappes, A., Hinton, J., Stegmann, C., & Aharonian, F. A. 2007, ApJ, 656, 870

Kelner, S. R., Aharonian, F. A., & Bugayov, V. V. 2006, Phys. Rev. D, 74, 034018

Kobayashi, T., Komori, Y., Yoshida, K., & Nishimura, J. 2004, ApJ, 601, 340

Kotera, K., Allard, D., & Lemoine, M. 2010, ArXiv e-prints

Koyama, K., Petre, R., Gotthelf, E. V., et al. 1995, Nature, 378, 255

Krymskii, G. F. 1977, Akademiia Nauk SSSR Doklady, 234, 1306

Kulsrud, R. & Pearce, W. P. 1969, ApJ, 156, 445

Kulsrud, R. M. & Cesarsky, C. J. 1971, Astrophys. Lett., 8, 189

Lagage, P. O. & Cesarsky, C. J. 1983a, A&A, 118, 223

Lagage, P. O. & Cesarsky, C. J. 1983b, A&A, 125, 249

Lebrun, F. & Paul, J. A. 1978, A&A, 65, 187

Li, H. & Chen, Y. 2010, MNRAS, 409, L35

Malkov, M. A. 1998, Phys. Rev. E, 58, 4911

Malkov, M. A. 1999, ApJ, 511, L53

Malkov, M. A. & O'C Drury, L. 2001, Reports on Progress in Physics, 64, 429

Malkov, M. A. & Voelk, H. J. 1995, A&A, 300, 605

Malyshev, D., Gabici, S., O'C. Drury, L., & Aharonian, F. A. 2010, A&A, 521, A14+

Matthiae, G. 2010, New Journal of Physics, 12, 075009

Maurin, D., Donato, F., Taillet, R., & Salati, P. 2001, ApJ, 555, 585

McCall, B. J., Hinkle, K. H., Geballe, T. R., et al. 2002, ApJ, 567, 391

McCall, B. J., Huneycutt, A. J., Saykally, R. J., et al. 2003, Nature, 422, 500

Mond, M. & O'C. Drury, L. 1998, A&A, 332, 385

Montmerle, T. 1979, ApJ, 231, 95

Mori, M. 1997, ApJ, 478, 225

Mori, M. 2009, Astroparticle Physics, 31, 341

Morlino, G., Amato, E., & Blasi, P. 2009, MNRAS, 392, 240

Morlino, G., Amato, E., Blasi, P., & Caprioli, D. 2010, MNRAS, 405, L21

Nakamura, K. & Particle Data Group. 2010, Journal of Physics G Nuclear Physics, 37, 075021

Neronov, A., Tinyakov, P., & Tkachev, I. 2005, Soviet Journal of Experimental and Theoretical Physics, 100, 656

Norman, C. A., Melrose, D. B., & Achterberg, A. 1995, ApJ, 454, 60

Ohira, Y., Murase, K., & Yamazaki, R. 2010, MNRAS, 1561

Olinto, A. V. 2000, Phys. Rep., 333, 329

Padoan, P. & Scalo, J. 2005, ApJ, 624, L97

Padovani, M., Galli, D., & Glassgold, A. E. 2009, A&A, 501, 619

Parizot, E., Marcowith, A., Ballet, J., & Gallant, Y. A. 2006, A&A, 453, 387

Parizot, E., Marcowith, A., van der Swaluw, E., Bykov, A. M., & Tatischeff, V. 2004, A&A, 424, 747

Parker, E. N. 1969, Space Sci. Rev., 9, 651

Pohl, M., Yan, H., & Lazarian, A. 2005, ApJ, 626, L101

Prantzos, N., Boehm, C., Bykov, A. M., et al. 2010, ArXiv e-prints: arXiv:1009.4620

Primack, J. R., Somerville, R. S., Bullock, J. S., & Devriendt, J. E. G. 2001, in American Institute of Physics Conference Series, Vol. 558, American Institute of Physics Conference Series, ed. F. A. Aharonian & H. J. Völk, 463–478

Protheroe, R. J., Ott, J., Ekers, R. D., Jones, D. I., & Crocker, R. M. 2008, MNRAS, 390, 683

Ptuskin, V., Zirakashvili, V., & Seo, E. 2010, ApJ, 718, 31

Ptuskin, V. S. & Zirakashvili, V. N. 2005, A&A, 429, 755

Ptuskin, V. S., Zirakashvili, V. N., & Plesser, A. A. 2008, Advances in Space Research, 42, 486

Rakowski, C. E. 2005, Advances in Space Research, 35, 1017

Rakowski, C. E., Laming, J. M., & Ghavamian, P. 2008, ApJ, 684, 348

Rawlings, S. & Saunders, R. 1991, Nature, 349, 138

Reynolds, S. P. 2008, ARA&A, 46, 89

Rho, J. & Borkowski, K. J. 2002, ApJ, 575, 201

Rodriguez Marrero, A. Y., Torres, D. F., de Cea del Pozo, E., Reimer, O., & Cillis, A. N. 2008, ApJ, 689, 213

Rordorf, C., Grasso, D., & Dolag, K. 2004, Astroparticle Physics, 22, 167

Rothenflug, R., Ballet, J., Dubner, G., et al. 2004, A&A, 425, 121

Sedov, L. I. 1959, Similarity and Dimensional Methods in Mechanics, ed. Sedov, L. I.

Shu, F. H., Adams, F. C., & Lizano, S. 1987, ARA&A, 25, 23

Skilling, J. & Strong, A. W. 1976, A&A, 53, 253

Spitzer, Jr., L. & Tomasko, M. G. 1968, ApJ, 152, 971

Stage, M. D., Allen, G. E., Houck, J. C., & Davis, J. E. 2006, Nature Physics, 2, 614

Stahler, S. W. & Palla, F. 2005, The Formation of Stars, ed. Stahler, S. W. & Palla, F.

Stanev, T. 1997, ApJ, 479, 290

Stecker, F. W. 1973, Ap&SS, 20, 47

Strong, A. W., Bloemen, J. B. G. M., Dame, T. M., et al. 1988, A&A, 207, 1

Strong, A. W. & Moskalenko, I. V. 1998, ApJ, 509, 212

Strong, A. W., Moskalenko, I. V., & Ptuskin, V. S. 2007, Annual Review of Nuclear and Particle Science, 57, 285

Tanaka, T., Uchiyama, Y., Aharonian, F. A., et al. 2008, ApJ, 685, 988

The Pierre AUGER Collaboration, Abreu, P., Aglietta, M., et al. 2010, Astroparticle Physics, 34, 314

Toptygin, I. N. 1999, Astronomy Letters, 25, 34

Uchiyama, Y. & Aharonian, F. A. 2008, ApJ, 677, L105

Uchiyama, Y., Aharonian, F. A., Tanaka, T., Takahashi, T., & Maeda, Y. 2007, Nature, 449, 576

Vallée, J. P. 2004, New A Rev., 48, 763

Vietri, M. 1995, ApJ, 453, 883

Vink, J. & Laming, J. M. 2003, ApJ, 584, 758

Völk, H. J., Aharonian, F. A., & Breitschwerdt, D. 1996, Space Sci. Rev., 75, 279

Völk, H. J., Berezhko, E. G., & Ksenofontov, L. T. 2005, A&A, 433, 229

Volkova, L. V. 1980, Soviet Journal of Nuclear Physics, 31, 784

Wang, Z. R., Qu, Q., & Chen, Y. 1997, A&A, 318, L59

Warren, J. S., Hughes, J. P., Badenes, C., et al. 2005, ApJ, 634, 376

Watson, W. D. 1973, ApJ, 183, L17+

Waxman, E. 1995, Physical Review Letters, 75, 386

Waxman, E. & Coppi, P. 1996, ApJ, 464, L75+

Waxman, E. & Miralda-Escude, J. 1996, ApJ, 472, L89+

Wentzel, D. G. 1974, ARA&A, 12, 71

Widrow, L. M. 2002, Reviews of Modern Physics, 74, 775

Williams, J. P. & McKee, C. F. 1997, ApJ, 476, 166

Zatsepin, G. T. & Kuz'min, V. A. 1966, Soviet Journal of Experimental and Theoretical Physics Letters, 4, 78

Zirakashvili, V. N. & Aharonian, F. 2007, A&A, 465, 695

Zirakashvili, V. N. & Aharonian, F. A. 2010, ApJ, 708, 965